FINAL REPORT

Vortex Lattice UXO Mobility Model for Reef-Type Range Environments

ESTCP Project MR-201003

JULY 2012

Scott Jenkins
Gerald D'Spain
Joseph Wasyl
Scripps Institution of Oceanography,
Marine Physical Laboratory

This document has been cleared for public release

REPORT DOCUMENTATION PAGE

Form Approved
OMB No. 0704-0188

The public reporting burden for this collection of information is estimated to average 1 hour per response, including the time for reviewing instructions, searching existing data sources, gathering and maintaining the data needed, and completing and reviewing the collection of information. Send comments regarding this burden estimate or any other aspect of this collection of information, including suggestions for reducing the burden, to the Department of Defense, Executive Services and Communications Directorate (0704-0188). Respondents should be aware that notwithstanding any other provision of law, no person shall be subject to any penalty for failing to comply with a collection of information if it does not display a currently valid OMB control number.

PLEASE DO NOT RETURN YOUR FORM TO THE ABOVE ORGANIZATION.

1. REPORT DATE *(DD-MM-YYYY)* 12-08-2011	**2. REPORT TYPE** Final Report Army Corps of Engineers	**3. DATES COVERED** *(From - To)* May-Dec, 2010; Jun-Aug, 2011

4. TITLE AND SUBTITLE Vortex Lattice UXO Mobility Model for Reef-Type Range Environments	**5a. CONTRACT NUMBER** W912HQ-10-0037 **5b. GRANT NUMBER** **5c. PROGRAM ELEMENT NUMBER**
6. AUTHOR(S) Scott Jenkins, Gerald D'Spain and Joseph Wasyl	**5d. PROJECT NUMBER** ESTCP Project MR-201003 **5e. TASK NUMBER** **5f. WORK UNIT NUMBER**
7. PERFORMING ORGANIZATION NAME(S) AND ADDRESS(ES) Scripps Institution of Oceanography, Marine Physical Laboratory 291 Rosecrans Street San Diego, CA 92106	**8. PERFORMING ORGANIZATION REPORT NUMBER**
9. SPONSORING/MONITORING AGENCY NAME(S) AND ADDRESS(ES) Environmental Security Technology Certification Program 901 North Stuart Street, Suite 303 Arlington, VA 22203	**10. SPONSOR/MONITOR'S ACRONYM(S)** ESTCP **11. SPONSOR/MONITOR'S REPORT NUMBER(S)** MR-201003

12. DISTRIBUTION/AVAILABILITY STATEMENT

Distribution Statement A. Approved for public release; distribution is unlimited.

13. SUPPLEMENTARY NOTES

14. ABSTRACT Reef platform micro-bathymetry was constructed from spatial Fourier transforms of LIDAR data from the reef platform at PMRF, Kauai as a geomorphic proxy of other island reef systems. A discrete arrangement of these awa control cells allowed numerically stable computations of erosion and transport of large UXO fields across reefs that surround an entire island. We constructed probability density functions of migration and burial magnitudes predicted by the awa cell model, and compared them with probability density functions assembled from observed outcomes of the experiment. We also computed predictive skill factors from the mean squared error between the awa cell prediction and measured outcomes for migration distance, and burial depth. After validating software revisions using the previous ESTCP funded field data at PMRF, we tested and proved the hypothesis (through long-term, extreme-event simulations at Vieques Island) that the UXO eventually concentrate in the reef awa channels where the UXO are amenable to recovery by conventional sand dredging methods.

15. SUBJECT TERMS

UXO Mobility Model, PMRF, Kauai, Vieques Island, South Impact Area

16. SECURITY CLASSIFICATION OF:			**17. LIMITATION OF ABSTRACT**	**18. NUMBER OF PAGES**	**19a. NAME OF RESPONSIBLE PERSON**
a. REPORT	**b. ABSTRACT**	**c. THIS PAGE**			**19b. TELEPHONE NUMBER** *(Include area code)*

Standard Form 298 (Rev. 8/98)
Prescribed by ANSI Std. Z39.18

TABLE OF CONTENTS

List of Figures.....5
List of Tables.....6
Acronyms.....8
Acknowledgements.....10
Executive Summary.....11

1.0 INTRODUCTION.....14
1.1 BACKGROUND.....14
1.2 OBJECTIVE OF THE DEMONSTRATION.....16
1.3 REGULATORY DRIVERS.....17

2.0 TECHNOLOGY.....17
2.1 TECHNOLOGY DESCRIPTION.....17
2.2 TECHNOLOGY DEVELOMENT.....27
2.2 ADVANTAGES AND LIMITATIONS OF THE TECHNOLOGY.....30

3.0 PERFORMANCE OBJECTIVES.....31

4.0 SITE DESCRIPTION.....32
4.1 SITE SELECTION.....33
4.2 SITE HISTORY.....34
4.3 SITE GEOLOGY.....34
4.4 MUNITIONS CONTAMINATION.....34

5.0 TEST DESIGN.....34
5.1 CONCEPTUAL EXPERIMENTAL DESIGN.....35
5.2 SITE PREPARATION.....35
5.3 SYSTEM SPECIFICATION.....35
5.4 CALIBRATION ACTIVITIES.....37
5.5 DATA COLLECTION PROCEDURES.....37
5.6 VALIDATION.....37

6.0 DATA ANALYSIS AND PRODUCTS.....38
6.1 PREPROCESSING.....40
6.2 TARGET SELECTION FOR DETECTION.....49
6.3 PARAMETER ESTIMATION.....49
6.4 CLASSIFICATION.....50
6.5 TRAINING.....50
6.6 DATA PRODUCT SPECIFICATION.....50

7.0 PERFORMANCEASSESSMENT.....59

8.0 COST ASSESSMENT.....63

9.0 IMPLEMENTATION ISSUES…….....73

10.0 REFERENCES.....94

APPENDICES……100

LIST OF FIGURES

Figure 1. Site Conceptual Model for UXO
Figure 2: Architecture to the Vortex Lattice UXO Mobility Model (MM)
Figure 3: Schematic diagram of awa control cells along a fringing reef coast
Figure 4**:** Mechanics of far-field burial
Figure 5. Vortex Lattice Method
Figure 6. a) Image method of trailing vortex induced velocity; b) trailing vortex pair in cross-wake plane; c) Moment balance for threshold of UXO movement.
Figure 7: Longshore auto spectra of departure from mean depth of reef platform
Figure 8**:** Multiple Awa Control Cell Reconstructed Bathymetry Grid
Figure 9. PMRF, Barking Sands, is located on the west coast of Kauai, Hawaii.
Figure 10. PMRF Field Demonstration configuration.
Figure 11. Surrogate 5”/38 projectiles used in UXO Mobility Model field demonstrations
Figure 12. Wave gauge installed in the Deep Field.
Figure 13. Composite bathymetry (meters below MSL) derived from NOS database and equilibrium profiles ([Jenkins and Inman, 2006) for February–May 2007 wave conditions.
Figure 14. Sample density of LIDAR high resolution bathymetry data (green dots) over the PMRF demonstration site, including a fringing reef section.
Figure 15. a) PMRF Demonstration Site and b) LIDAR-derived, high-resolution bathymetry of awa channel with current magnitude scaled to color (upper left corner).
Figure 16. Refraction/Diffraction pattern at PMRF site for highest waves occurring during the duration of the demonstration; yellow stars indicate the inshore and offshore fields.
Figure 17. Wave height (upper) and current magnitude (lower) measured with an RD Instruments wave gauge and current profiling ADCP during the demonstration.
Figure 18. Current speed (upper) and current direction (lower) measured with an RD Instruments wave gauge and current profiling ADCP during the demonstration.
Figure 19. Grain size distribution of sediment, PMRF Field Demonstration Site, Kauai, May 2007; data provided by Sea Engineering, Inc.
Figure 20. A simulation of the vortex and scour field in the nearfield grid shows 55% of the 5”/38 UXO surrogate buried in a coarse sand bottom.
Figure 21. The awa channel’s sidewall intersects the carbonate seabed at the PMRF site; note the wall surface roughness and curvature of the lithified reef structures, photo: Sea Engineering Inc. (SEI).
Figure 22. A simulation of vertical divergence and secondary flows induced by the curvature of the awa axis in the vicinity of the demonstration site at PMRF, Kauai.
Figure 23. A simulation of the large-scale eddies induced over UXO by the encroaching shoulders of the awa sidewalls in the vicinity of the demonstration site at PMRF, Kauai.
Figure 24. Upgraded awa-cell MM simulation of migration and burial rates of 5”/38 UXO surrogates at the inshore site at 8.3m depth as a function of measured wave height
Figure 25. Modeled probability density functions for UXO migration versus (a) the measured probability density function and (b) all surrogates during the demonstration.

Figure 26. Upgraded awa-cell MM simulation of migration and burial rates of 5”/38 UXO surrogates at the offshore site at 16.6m depth as a function of measured wave heights
Figure 27. Comparing Upgraded awa-cell MM modeled probability density functions for UXO burial versus (a) the measured probability density function and (b) for all surrogates during the demonstration
Figure 28 Regression analysis of Mode 2 Fourier micro-bathymetric technique v. Mode 3 high resolution LIDAR supported predictions for 5’’/38 rounds, PMRF, HI
Figure 29. Vieques Island and Ordance Reef, Waianae UXO remediation area comparisons.
Figure 30: Vieques Island Aerial Photograph
Figure 31: Vieques Island UXO Demonstration Areas
Figure 32: Vieques Island North Impact Area Awa Channels
Figure 33: Vieques Island South Impact Area Awa Channels
Figure 34: Long-term Wave Climate for UXO Migration and Sorting Simulation at Vieques Island South Impact Area
Figure 35: Vieques Island Wave Refraction/Diffraction Pattern. Bathymetry contours (white), m MSL; Deep water wave height, 2 m; period, 12 sec; direction, 225 degrees.
Figure 36: Multiple Awa Control Cell Reconstructed Bathymetry Grid with Initial UXO Distribution, Vieques Island, South Impact Area.
Figure 37: Streamlines over Multiple Awa Control Cell Reconstructed Bathymetry Grid with Initial UXO Distribution, Vieques Island, South Impact Area.
Figure 38: Velocity Profiles over Multiple Awa Control Cell Reconstructed Bathymetry Grid with Initial UXO Distribution, Vieques Island, South Impact Area.
Figure 39: Multiple Awa Control Cell Reconstructed Bathymetry Grid with UXO Distribution at t = +10 years, Vieques Island, South Impact Area.
Figure 40: Multiple Awa Control Cell Reconstructed Bathymetry Grid with UXO Distribution at t = + 20 years, Vieques Island, South Impact Area.
Figure 41: Multiple Awa Control Cell Reconstructed Bathymetry Grid with UXO Distribution at t = +30 years, Vieques Island, South Impact Area.
Figure 42: Streamlines over multiple Awa Control Cell Reconstructed Bathymetry Grid with UXO Distribution at t = +30 years, Vieques Island, South Impact Area.
Figure 43: Velocity Profiles over multiple Awa Control Cell Reconstructed Bathymetry Grid with UXO Distribution at t = +30 years, Vieques Island, South Impact Area.
Figure 44: Upgraded MM simulation of local flow field around a UXO resting on hard substrate
Figure 45: Mechanics of UXO Downslope Migration Progression.

LIST OF TABLES

Table 1. Performance Objectives
Table 2. UXO Mobility Model Farfield Input Parameters.
Table 3. UXO Mobility Model Nearfield Input Parameters.
Table 4. UXO Mobility Model program cost summary
Table 5. Nominal cost of Mode 1 screening analysis of a single UXO site
Table 6. Estimated cost of Mode 2 Detailed Analysis

Table 7. Mode 3 Enhanced Analysis cost estimate

ACRONYMS

Acronym	Definition
ADCP	Acoustic Doppler Current Profiler
AGD	Applications Guidance Document
ArcGIS	Global Information System (Esri)
CNO	Chief of Naval Operations
DoD	U.S. Department of Defense
EPA	U.S. Environmental Protection Agency
DMA	Defense Mapping Agency
DRI	Benthos Diver Range Interrogator
ESTCP	Environmental Security Technology Certification Program
FRTR	Federal Remediation Technologies Roundtable
GIS	Geographic Information System
GPS	Global Positioning System
LIDAR	Light Detection and Ranging
MBBS	MultiBeam BackScatter
MCC/3	Maritime Capability Group 3
MSL	Mean Sea Level
MM	UXO Mobility Model
MMFT	Measurement Method Field Test
NAVFAC	Naval Facilities Engineering Command
NF SEC	Naval Facilities Engineering Service Center
NESDI	Navy Environmental Sustainability Development to Integration
NOAA	National Oceanic and Atmospheric Administration
NOS	National Ocean Service
PDF	Probability Density Function

PMRF	Pacific Missile Range Facility
ROI	Return on Investment
ROV	Remotely Operated Vehicle
RDI	Teledyne RD Instruments
SCM	Site Conceptual Model
SEI	Sea Engineering, Inc.
SSe	residual sum of squares
SSr	regression sum of squares
SST	Sound and Sea Technology
UDR	Sonotronics Underwater Diver Receiver
USGS	United States Geological Survey
UXO	unexploded ordnance
WAA	Wide Area Assessment

Acknowledgements

The work reported in this final report builds on extensive previous work in model development and field validation. In 2003 The Naval Facilities Engineering Service Center (NAVFAC ESC) Point Hueneme began a UXO Mobility Model program effort that leveraged model development begun under ONR's Mine Burial Program. NAVFAC ESC proceeded to fund new algorithm development for the Vortex Lattice Model (one of three models to emerge from the Mine Burial Program) and the new software was called the UXO Mobility Model (MM). The MM was developed under Chief of Naval Operation's (CNO) Navy Environmental Sustainability Development to Integration (NESDI) program. The NESDI program is managed for CNO-N45 by the Naval Facilities Engineering Command (NAVFAC).

Subsequently, NAVFAC ESC was awarded a three-year project by The Environmental Security Technology Certification Program (ESTCP) called "The Unexploded Ordnance (UXO) Mobility Model Demonstration/Validation Program" (DeVisser, 2004). Ms. Barbara Sugiyama and Ms. Alexandra DeVisser, with NAVFAC ESC, were the Co-Principle Investigators for this effort with support from Sound & Sea Technology, Inc. (SST). The SST program was led by Mr. Jeffrey Wilson. The UXO Mobility Model was developed by Dr. Scott Jenkins and Mr. Joe Wasyl of the Scripps Institution of Oceanography. The Model was tested and evaluated by Mr. Dennis Garrood, Mrs. Chanda Daly, and Mr. Eugene Keam of SST. The field work was directed by Mr. William Daly and Mr. Ian McKissick of SST. Model refinements that were developed in this report were validated by field data collected on previous ESTCP funding at the Pacific Missile Range Facility (PMRF) at Barking Sands, Kauai, Hawaii. On-site field test demonstration support at PMRF was provided by Mr. Dan Momohara and the PMRF staff.

Executive Summary

This one-year project leverages previous ESTCP investments in the development of a UXO Mobility Model (MM) to assess probable UXO fate and transport at the Waianae dump site and at the Vieques Islands firing and bombing exercise ranges (with focus on the South Impact Area). The objective of this work is to develop modifications to the UXO Mobility Model software to implement reef geomorphology in the model grid building scheme. This feature allows the model to predict UXO migration and burial in a reef environment without relying on dense LIDAR bathymetric grids that limit the model's computational domain, thereby increasing its computational efficiency in complex reef environments. This refinement uses geomorphic control cells consisting of a reef platform bounded by awa channels. An assemblage of these cells creates a digital representation of the fringing reef system around Vieques island.

The reef platform micro-bathymetry is constructed from spatial Fourier transforms of the LIDAR data using the reef platform at PMRF, Kauai as a geomorphic proxy of other island reef systems. The Fourier transforms allow the billions of discrete LIDAR data points to be compressed into a workable number of Fourier coefficients that represent the roughness details of the reef platforms of the awa control cells. With these discrete control cells, the vortex lattice algorithms can rapidly calculate ambient flow features such as bathymetric divergence over a UXO field. A discrete arrangement of these awa control cells allows numerically stable computations of erosion and transport of large UXO fields over reefs that surround an entire island.

This new awa cell computational approach using synthetic micro-bathymetry of reef platform roughness was validated in hindcast against the PMRF data base from ESTCP-funded UXO field experiments, using the same predictive skill measures detailed in NFESC (2008). We applied two approaches to assessing the skill of the awa cell predictions of the magnitude of migration and burial of UXO surrogates at PMRF. In the first approach, we constructed probability density functions (PDF's) of migration and burial magnitudes predicted by the awa cell model and compared them with the probability density functions assembled from the observed outcomes of the experiment. Because the experimental outcomes involve small ensemble statistics, we merge the results of all 24 surrogates from the inshore and offshore test sites into a single set of probability density functions. In the second approach, we a compute predictive skill factor R from the mean squared error between the awa cell prediction and measured outcomes for migration distance, ξ, and burial depth, h. The peak, spread, and shape of the predicted and measured probability density functions of migration were quite similar to each other. The upgraded awa-cell MM predicted a mean migration distance of 1.25 m as compared to a measured mean migration of 1.45 m from the ensemble of 24 UXO surrogates. For the extremes, both the measured and modeled minimum migration distance was 0 m, occurring at the offshore site, while the predicted maximum migration distance was 3.0 m as compared to a measured maximum migration of 4.0 m occurring at the inshore cluster of 12 UXO surrogates. In both the predicted and observed outcomes, migration almost exclusively occurred along the major axis of the awa channel. The peak of the measured burial probability distribution, its spread, and shape all closely resemble the modeled distribution. The upgraded awa-cell MM predicted a mean burial depth of 17.5 cm as compared to a measured mean burial depth of 20.5 cm from the ensemble of 24 UXO surrogates. For the extremes, both the measured and modeled

minimum burial depths were on the order of 8 cm, occurring at the offshore site, while the model predictions indicated a maximum burial depth of 50.0 cm as compared to a measured maximum burial depth of 40.0 cm occurring at the inshore cluster of 12 UXO surrogates.

The skill factor, R_ξ, for the awa-model at PMRF was $R_\xi =$ 0.88 for migration and $R_h =$ 0.90 for burial. For modeling of coastal processes and mine burial prediction in particular, a skill factor in excess of 0.8 is considered to be a good result (Gallagher et al., 1998; Jenkins and Inman, 2006). The predictive skill factors achieved by upgraded awa-cell MM at PMRF using the synthetic micro-bathymetry are comparable to the predictive skill previously achieved using the high resolution LIDAR data directly on a relatively smaller area of reef (cf, Wilson et al., 2008b). Alternatively, the accuracy of predictions from upgraded awa-cell MM based the Fourier reconstructed reef platform roughness (mode-2) versus the earlier approach using the high resolution LIDAR bathymetry after Wilson et al., 2008 can be quantified by the coefficient of determination, r^2. The numerically efficient Fourier-based mode-2 can replicate the mode-3 simulations of migration (based on high resolution LIDAR inputs) with an $r^2 = 0.93$, and the burial predictions within an $r^2 = 0.86$. Because the upgraded awa-cell MM can do better than R > 0.8 or $r^2 > 0.8$, it performs with an accuracy comparable to the present ESTCP certified MM, while the cost savings derived from its reduced input rigor makes it attractive for remediation planning. The upgraded MM is able to achieve this comparable performance at significantly greater numerical efficiency and stability, allowing it to model the fate and transport of significantly greater numbers of UXO over larger UXO fields. Whereas the earlier generation MM code reported in Wilson et al, 2008b modeled fate and transport of only 24 UXO surrogates, the upgraded awa-cell MM is capable of modeling the simultaneous migration and burial of as many as 500 UXO.

After validating software revisions using the ESTCP-funded field data at PMRF, we tested and proved the hypothesis (through long-term, extreme-event simulations at Vieques Island) that the UXO eventually concentrate in the reef awa channels. Here, UXO are amenable to recovery by conventional sand dredging methods, while presenting a persistent danger, if not recovered, of becoming transported to the beach during storms. Concentration of UXO in the awa channels over time results from higher mobility on the reef platform due to two primary mechanisms 1) higher ambient wave-induced velocity over the locally shallower reef platform, and 2) reduced rolling resistance of UXO on the hard substrate of the reef platform. However, lithification effects acting to cement UXO in place on the reef platform were not explicitly treated by the model physics.

The UXO sorting mechanism that we have demonstrated at biogenic reef environments has important cost savings and remediation planning implications. It is generally infeasible to search 100% of a known underwater UXO field with 100% probability of detection using present platform and sensor technology. Therefore, it is advantageous and cost effective to integrate these numerical models at the outset of a survey with detection systems to guide those assets into the most problematic areas of a given underwater UXO field. By using the upgraded UXO MM to develop an initial Wide Area Assessment (WAA), that subdivides a UXO field into stable and unstable areas, one can avoid wasting deployment of detection resources in areas where UXO populations are either depleted by sorting, or remain permanently entombed beneath a stable seabed.

Predictive fate and transport models can be used to conduct an analysis of the risk and cost impact of UXO at a coastal site. Given an area of UXO locations and the required input data, the model output can be used to clearly define: a) areas outside of human contact and b) areas where UXO are fully stabilized and pose little risk to humans. Further consideration of the risks presented by the UXO can lead range management to make recommendations for site remediation and assessment of the hazard presented to humans and wildlife. Substantial benefits to remediation planners can be obtained from using these models to:

- Determine (and minimize) the scope of any required remediation efforts, minimize both survey and removal efforts, and thus realize potential savings of millions of dollars.
- Ensure that any remediation effort covers enough distance that UXO will not move back into areas of concern (to avoid recurring clean-up efforts).
- Aid in planning the sampling survey by predicting (a) the conditions under which the most UXO would be unburied (visible) and (b) the effective *half-life of the survey data*. This predictive capability enables survey and/or remediation efforts to be scheduled, with respect to making a determination of how long UXO will remain where they are found. Often, considerable mobilization time is required for UXO clearance efforts. Post survey model predictions can provide guidance to remediation planners of the effects of intervening storms on already located UXO positions during the period between UXO surveys and site mobilization of clearance assets.
- Provide an inexpensive, rapidly implemented method of demonstrating good-faith effort to assess risk to public health from UXO.

The long-term goal is to include the UXO mobility and burial model output in forthcoming risk evaluation models specifically configured to support munitions response programs. The operational costs of using the UXO MM vary from $100,000 for a Mode 1 “desktop” analysis to approximately $1,000,000 for a detailed Mode-3 analysis of a large site, which would include bathymetric surveys, UXO distribution baseline surveys, etc. The primary cost driver at any level of analysis is the acquisition of site environmental data (i.e., waves, currents, seafloor sediments, and initial UXO distributions), and the conversion of those data into input files that are consistent with the UXO MM code formats.

1.0 INTRODUCTION

This is a one-year project to leverage field data collected in 2007 (under ESTCP-200417) and to develop additional refinements to the UXO Mobility Model (MM). Results of upgrades to the MM are compared against field data published in "Predicting the Mobility and Burial of Underwater Unexploded Ordnance (UXO) Using the *UXO Mobility Model"* (PMRF Barking Sands, Kauai, Hawaii).

The UXO Mobility Model is a processes-based software model that uses vortex lattice computational methods to generate 3-d simulations of subsequent burial, exposure and migration of complex UXO shapes. These simulations account for effects of large scale erosion or accretion of the seabed (far-field processes) and fine scale vortex shedding, scour and bedform evolution around the UXO shape (nearfield processes).

1.1 BACKGROUND

In January 2002, the Navy through its Pollution Abatement Ashore Program (now referred to as the Navy Environmental Sustainability Development to Integration Program, NESDI) published a study "Environmental effects of underwater ordinance" (Johnson et al., 2002). A site conceptual model (SCM) was developed under this program and is shown schematically in Figure 1. After evaluating the SCM against existing scientific data and models, various data gaps were identified. One of these data gaps was the inability to predict the mobility and burial of UXO underwater. To meet this need, the Naval Facilities Engineering Service Center (NAVFAC ESC) Point Hueneme began a UXO Mobility Model program effort that was based on the schematic outlined in dark blue on the lower left side of Figure 1. The initial focus of this effort was to explore the feasibility of leveraging model development begun under ONR's Mine Burial Program. In October 2002, Professor Douglas Inman and Dr. Scott Jenkins gave a briefing at NAVFAC ESC Point Hueneme, Code ESC51, on the Vortex Lattice Mine Burial Model, one of three predictive models being developed and field validated under the Mine Burial Program (Inman and Jenkins, 2002; Jenkins and Inman, 2002; Jenkins et al., 2007). The other two were a simple rational parameterized model formulated by Professor Carl T. Friedrichs, Virginia Institute of Marine Science (Friedrichs, 2001 & 2007, Richardson et al., 2004; Elmore et al., 2005; Trembalis et al., 2007) and a probabilistic Mine Burial Expert System (MBES) being developed by Dr. Alan Brandt and Dr. Sarah E. Rennie at Johns Hopkins University Applied Physics Laboratory (Rennie and Brandt, 2002; Rennie et al., 2007; Almquist et al., 2007).

While the mine burial models were well advanced in predicting the scour and burial processes and the general vertical movement of mines on a sedimentary seabed, there were a number of aspects of underwater UXO behaviors that these models could not account for, notably UXO mobility associated with horizontal displacement of the UXO target. In addition, the prediction of UXO mobility often begins with an initial state of complete burial due to high velocity ballistic impact, in contrast to the mine burial prediction problem that generally begins with an initial state of partial burial due to relatively low velocity impacts with the seabed during the mine planting operations. Many UXO targets are considerably smaller and lighter than mines

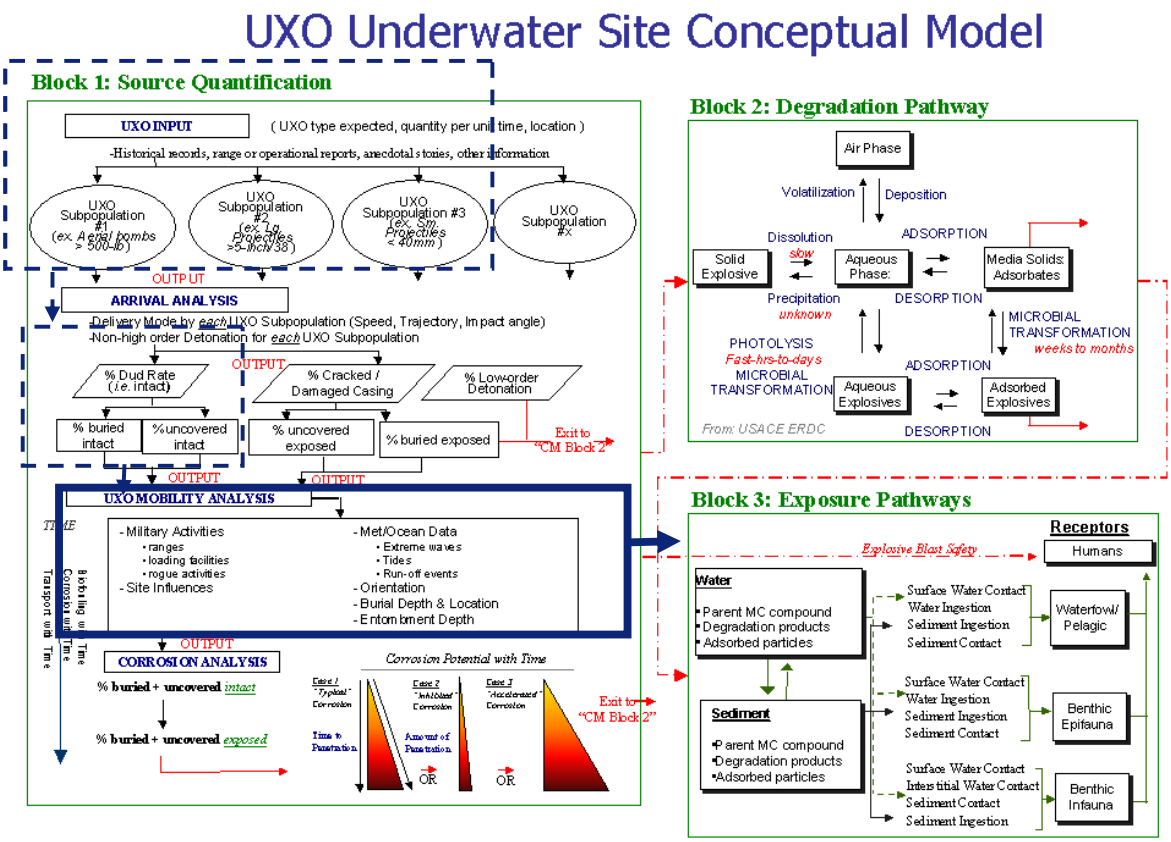

Figure 1. Site Conceptual Model for UXO showing the UXO Mobility Model Analysis (lower left) as part of source quantification efforts (from Johnson et al., 2002).

with tapered and often complex shapes due to fragmentation of the UXO round on impact. Therefore, it was apparent at the outset that evolving a UXO mobility model from the existing mine burial models would require additional algorithm development and validation. NAVFAC ESC proceeded to fund new algorithm development for the Vortex Lattice Model and the new software was called the UXO Mobility Model (MM). The MM was developed under Chief of Naval Operation's (CNO) Navy Environmental Sustainability Development to Integration (NESDI) program. The NESDI program is managed for CNO-N45 by the Naval Facilities Engineering Command (NAVFAC).

The MM was initially field validated using 20mm UXO surrogates at Pt Mugu, CA (Wilson 2004) and 5"/38 naval round surrogates at Pacific Beach, WA (Wilson and Jenkins, 2005). Subsequently, NAVFAC ESC was awarded a three-year project by The Environmental Security Technology Certification Program (ESTCP) called "The Unexploded Ordnance (UXO) Mobility Model Demonstration/Validation Program" (DeVisser, 2004). This program was managed by Ms. Barbara Sugiyama and Ms. Alex DeVisser, of NAVFAC ESC, with support from Sound & Sea Technology, Inc. (SST). The SST effort was lead by Mr. Jeffrey Wilson. The ESTCP funded certification program developed a detailed software User's Manual for the MM (Garood, 2008) and attempted to test the MM in a greater range of coastal environments than had been

attempted previously, and environments that were specifically selected to be proxies for known UXO sites.

In the present project we have developed UXO Mobility Model software that will allow the model to predict UXO migration and burial in reef environments without reliance on dense LIDAR bathymetric grids that limit the model's computational domain. This revised model software is built on the concept of interconnected geomorphic control cells consisting of a reef platform bounded by awa channels, which when assembled together, form a digital representation of the fringing reef system around an island.

1.2 OBJECTIVE OF THE DEMONSTRATION

Calibrate and validate changes in the predictive skill of the UXO Mobility Model by matching observed migration patterns of instrumented surrogate UXO samples allowed to move freely under the influence of the local conditions in the seafloor environment at PMRF Barking Sands, Kauai, Hawaii.

We apply two approaches to validation. By the first approach, we construct probability density functions of migration and burial magnitudes predicted by the awa cell model and compare them with the probability density functions assembled from the observed outcomes of the experiment. Because the experimental outcomes involve small ensemble statistics, we merge the results of all 24 surrogates from the inshore and offshore test sites into a single set of probability density functions.

By the second approach, we compute a predictive skill factor R from the mean squared error between the awa cell prediction and measured outcomes for migration distance, ξ, and burial depth h. For burial depth the skill factor has the following form originally adapted from Gallagher et al. 1997 and later implemented by Jenkins et. al., 2007:

$$R_h = 1 - \frac{1}{N\hat{\sigma}_i}\left\{\sum_{1}^{i=N}\left[\hat{h}(i) - h(i)\right]^2\right\}^{1/2} \qquad (1)$$

where $\hat{h}(i)$ is the measured burial depth for i = 1, 2...N observations, $h(i)$ is the predicted burial depth for the ith observation, and σ_i is the standard deviation of all observations over the period of record. For migration distance the skill factor would has the form:

$$R_\xi = 1 - \frac{1}{N\hat{\sigma}_i}\left\{\sum_{1}^{i=N}\left[\hat{\xi}(i) - \xi(i)\right]^2\right\}^{1/2} \qquad (2)$$

where $\hat{\xi}(i)$ is the measured migration distance for i = 1, 2...N observations, $\xi(i)$ is the predicted migration distance for the ith observation.

1.3 REGULATORY DRIVERS

Navy requirements: 1.I.2.b *Improved Marine Sediment/Dredge Spoil Remediation and Decontamination,* 1.I.1.g *Improved Methods for Removal of Unexploded Ordnance (UXO),* and 1.III.2.n *Improved Characterization and Monitoring Techniques for Sediments*; (Johnson, et al, 2002).

Army requirements: A(1.6.a) *Unexploded Ordnance (UXO) Screening, Detection and Discrimination,* and A(1.6.b) *Soil/Sediment Unexploded Ordnance (UXO) Neutralization/Removal/Remediation;* (Johnson, et al, 2002).

2.0 TECHNOLOGY

The Vortex Lattice MM is a 3-dimensional, time-stepped, process-based model for the prediction of exhumation, migration, and subsequent burial of UXO by general bed erosion and local vortex scour. Details of the MM and the model code are provided in Wilson, J.V. et al., (2008).

2.1 TECHNOLOGY DESCRIPTION

The UXO Mobility Model (MM) is a processes-based model that uses vortex lattice computational methods to generate 3-d simulations of subsequent burial, exposure and migration of complex UXO shapes. In these simulations it accounts for effects of large scale erosion or accretion of the seabed (far-field processes) and fine scale vortex shedding, scour and bedform evolution around the UXO shape (nearfield processes). Farfield processes are those that alter the seabed elevation over length scales that are comparatively large with respect to the size of an individual UXO round. Nearfield processes are due to the flow disturbance caused by the UXO and affect the seabed elevation by local scour, as well as induce hydrodynamic forces that cause the UXO to move. The present MM software was validated in two ESTCP funded field tests, where it correctly predicted all the basic behaviors of UXO test surrogates with high quantitative predictive skill factors.

Migration and burial processes consist of two distinct types: nearfield and farfield (Jenkins et al., 2007). These operate on significantly different length and time scales. Nearfield processes occur over length scales the order of the body dimensions and on time scales of a wave period, primarily governed by scour mechanics. In contrast, farfield processes involve changes in the elevation of the seabed with cross-shore distances of hundreds of meters that may extend along the coast for kilometers. Farfield time scales are typically seasonal with longer periods due to variations in climate and travel time of longshore sediment fluxes associated with accretion/erosion waves. These processes are coupled together in an architecture diagrammed by the flow chart shown in Figure 2 and referred to as the *Vortex Lattice (VORTEX) Scour and Burial Model* (Jenkins et al., 2007). The farfield processes and inputs are found above the orange line in Figure 2, while the nearfield processes and inputs are below the green line.

As with any boundary value problem, the solution follows from specifying initial conditions, forcing functions and the boundary conditions, from which the response is computed using a set of process-based algorithms. This computational sequence proceeds in Figure 2 from the top

down, with the set of forcing functions and initial conditions bundled together in a *module* shown by the pink shaded box at the top of the flow chart, while boundary conditions (beige box) and response (blue box) modules of the farfield are found in the pathways below that. The farfield response modules are upstream of the nearfield modules in the computational flow chart because the farfield processes determine the fluid forcing and elevation of the sand bed around the object, essential to specifying the nearfield boundary value problem.

Farfield processes provide the broad-scale forcing leading to general seabed erosion and/or accretion. Seabed erosion can exhume buried UXO, while seabed accretion can result in deeper entombment of buried UXO, or can lead to the subsequent re-burial of exhumed UXO. These farfield processes involve changes in the elevation of the seabed with cross-shore distances of hundreds of meters that may extend along the coast for kilometers. The domain of such regional scale variation is the littoral cell. Farfield time scales are typically seasonal with longer periods due to variations in climate. Farfield exhumation and burial mechanics are associated with large scale processes including changes in beach profile, deposition from rivers, sediment loss by turbidity currents, and bottom modification by ice push. These processes vary with many time scales, including diurnal oscillations associated with tides and sea breeze, inter-annual oscillations associated with summer/winter seasonal change, multi-annual variability associated with short-term global climate oscillations such as the El Nino-Southern Oscillation and multi-decadal differences due to long term climate variability associated with the Pacific Decadal and North Atlantic Oscillations. Because the farfield processes determine the elevation and slope of the seabed on which the nearfield processes operate, the farfield exerts a controlling influence on the nearfield. Hence, farfield processes form the basis of the model and are shown as the top half of the MM architecture in Figure 2.

Farfield processes are controlled by the balance between the amount of sediment entering the farfield and the amount leaving. This balance, known as the sediment budget, requires the identification of sediment sources and sinks, which will vary with the type of coastline. Some basic types of coastlines have been identified. The Geomorphic Coastal Classification module in Figure 2 (highlighted in red) is used to select the relative scaling and assigns the sediment sources and sinks to which a particular UXO site belongs. The classification includes three general tectonic types of coasts with their morphologic equivalents and two types associated with latitudinal extremes: 1) collision coasts with narrow shelves and steep coastal topography resulting from collisions between two or more tectonic plates, 2) trailing edge coasts that are on the stable, passive margins of continents with broad shelves and low inland relief, 3) marginal sea coasts that are semi-enclosed by island arcs and thereby fetch limited, and, 4) biogenic coasts that are formed by fringing coral reefs or mangroves.

Although the relative importance of transport processes varies among coastal type, two processes are always important to UXO exhumation and burial. These are seasonal changes in the beach profile (Figure 4a) and fluxes of sediment into and out of the UXO environment by accretion/erosion waves.

The forcing functions that drive the far field processes are developed by the module indicated by the pink box in Figure 2 and provide time series of waves (#2), currents (#3) and sediment flux (#4). Waves and currents are derived from direct observations by means of Datawell directional

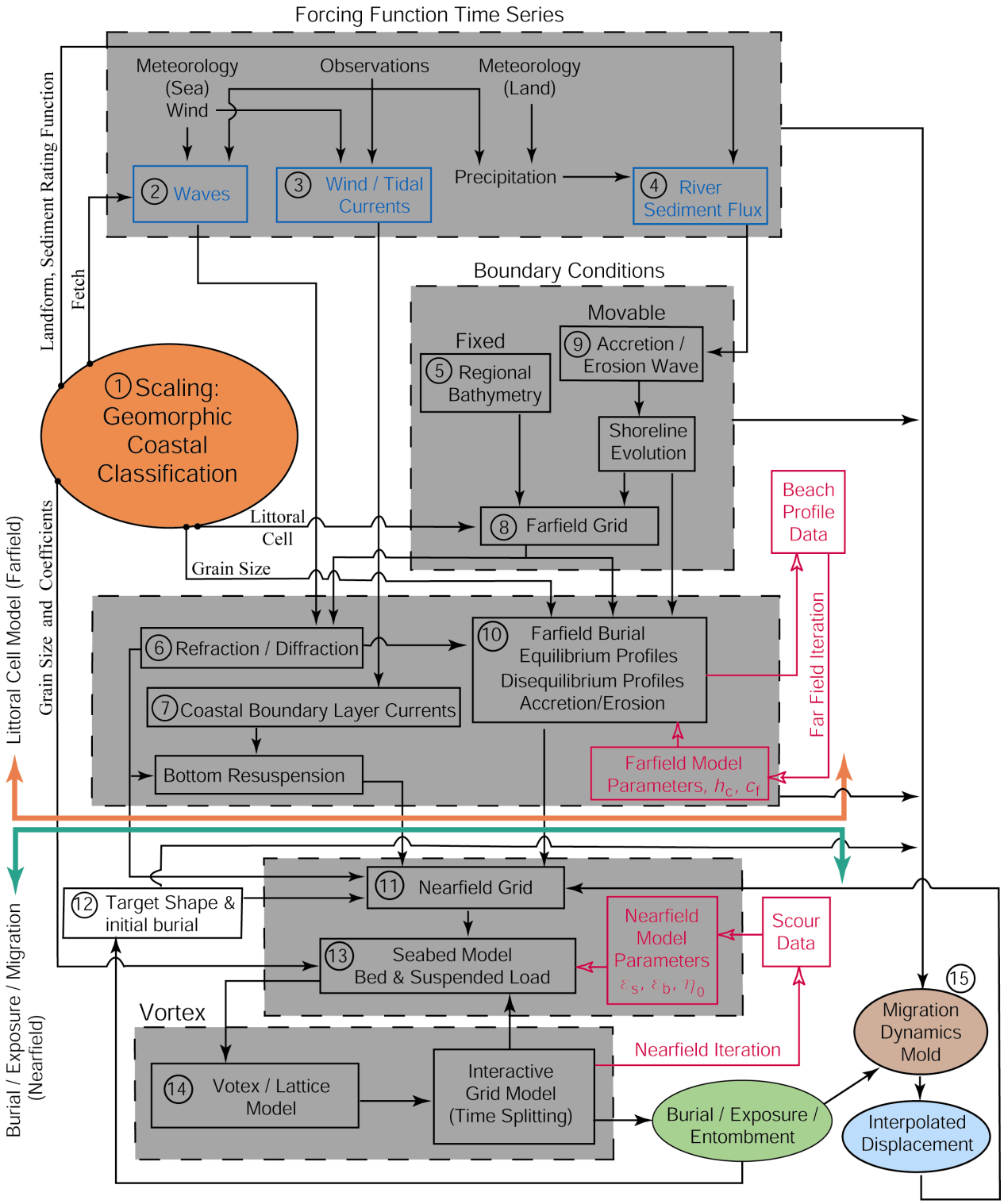

Figure 2: Architecture to the Vortex Lattice UXO Mobility Model (MM). Code revisions for the awa-control cell far field gridding system developed under this project are made to Module #8.

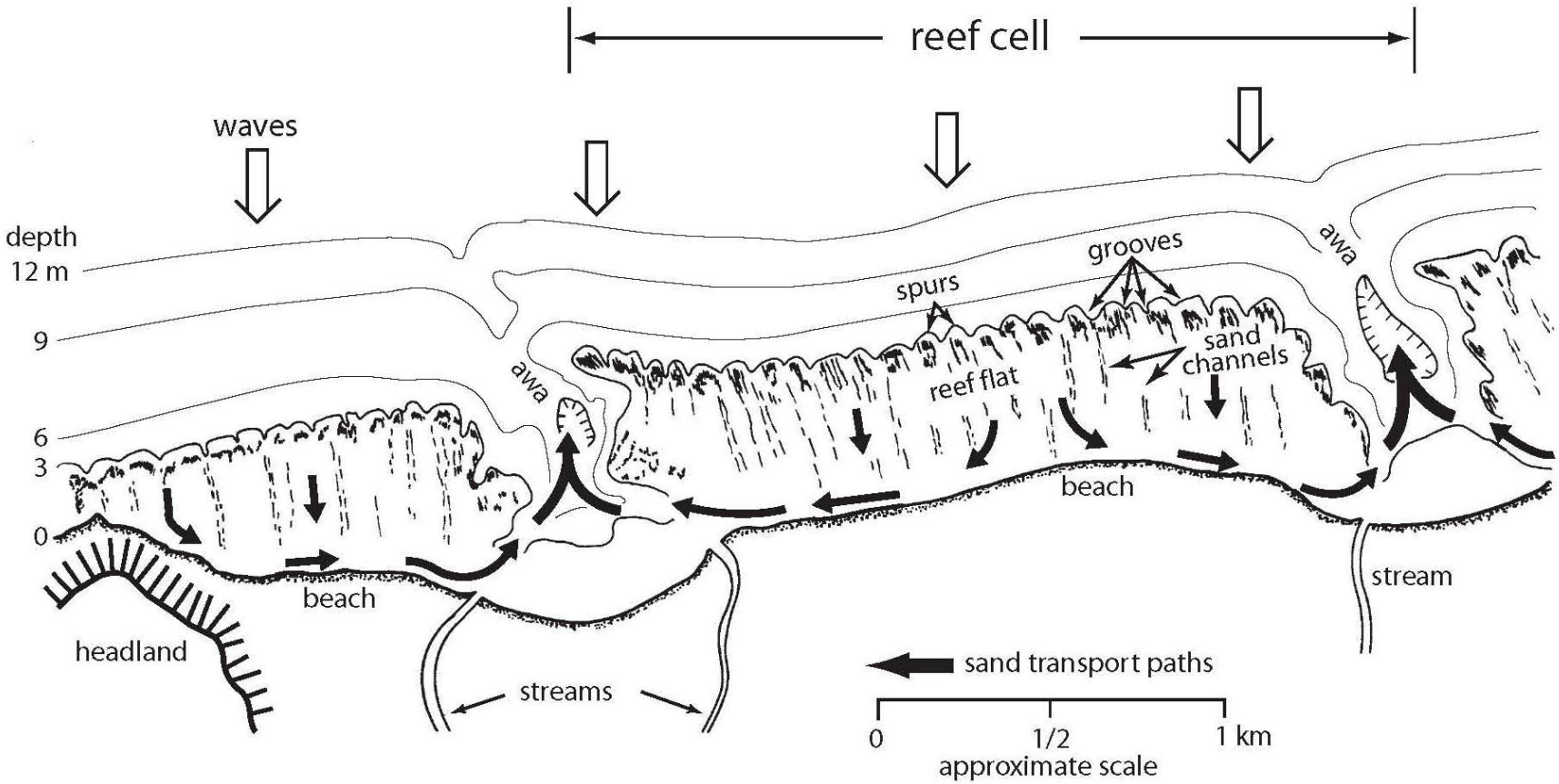

Figure 3. Schematic diagram of control cells along a fringing reef coast (after Inman, 1994).

wave buoys and Acoustic Doppler Current Profilers (ADCP), to validate model velocity algorithms. Fluxes of river sediment are neglected as explicit boundary conditions, but the presence of those sediments are accounted for in the grain size distributions of the offshore sediments. The wave and current forcing provides excitation applied to the deep water boundary of the farfield computational domain. These boundaries are specified in the boundary conditions module (beige box) in Figure 2, where the farfield computational domain is assembled from a series of boundary-conforming control cells [Figure 3], using a combination of bathymetric data obtained from National Ocean Survey (NOS) and United States Geological Survey (USGS) as by the National Geophysical Data Center to assemble the gross morphology of the fringing reef ; and LIDAR data to construct bathymetric details of local awa channels (at 1m grid cell resolution) in which the UXO fields were placed.

With these forcing functions and boundary conditions, the farfield response module (blue box) computes the spatial and temporal evolution of the fluid forcing and bottom elevation along cross-shore profiles of a control cell representing the gross morphology of a fringing reef system [Figure 3]. These control cells are bounded in the cross shore by the walls of sand and awa channels cut cross-shore through the lithofied reef structures. Predominately carbonate sediments accumulate in these channels along bottom gradients that can be specified by profiles having three matching segments: 1) the stationary profile that extends from the deep water boundary inshore to closure depth h_c, where profile changes become vanishingly small; 2) the shorerise profile that continues from closure depth to the wave break point; and, 3) the bar-berm profile that begins at the break point and ends at the berm crest. The stationary profile is invariant with time and is given by the regional bathymetry. Bottom elevation changes along the non-stationary profiles of the shorerise and bar-berm (Figure 4a) are computed by (#10) in the farfield response module (blue box) using equilibrium profile algorithms Jenkins and Inman, (2006). The stationary and non-stationary profiles are interpolated to create a Cartesian depth grid within each control cell on which simultaneous refraction and diffraction patterns are computed by (#6) using algorithms from Kirby (1986) and Dalrymple et al., (1983) to specify fluid forcing by shoaling waves. Fluid forcing by currents in the farfield are computed in (#7) where wave induced streaming and mass transport are based on algorithms and shallow water tidal currents follow from algorithms.

Fluid forcing time series and bottom elevations computed in the farfield response module are through-put to the nearfield response modules shown below the green line in Figure 2. Nearfield processes occur over length scales on the order of the UXO dimensions and on time scales of a few seconds to hours, primarily governed by local hydrodynamic forces and scour mechanics arising from the disturbance which the UXO creates in the flow.

The UXO and adjacent seabed is subdivided into a set of panels to form a lattice (Figure 5a). The vortex field induced by the UXO is constructed from an assemblage of horseshoe vortices, with a horseshoe vortex prescribed for each panel. This computational technique is known as the vortex lattice method and has been widely used in aerodynamics and naval architecture. The strength of the vortices is derived from the pressure change over each panel associated with the local wave and current velocity. The release of trailing vortex filaments from each panel causes scour of the neighboring seabed. This action is portrayed in Nature in Figure 5b and schematically in Figure 6. When viewed in any cross-wake plane, (Figure 6b), each pair of

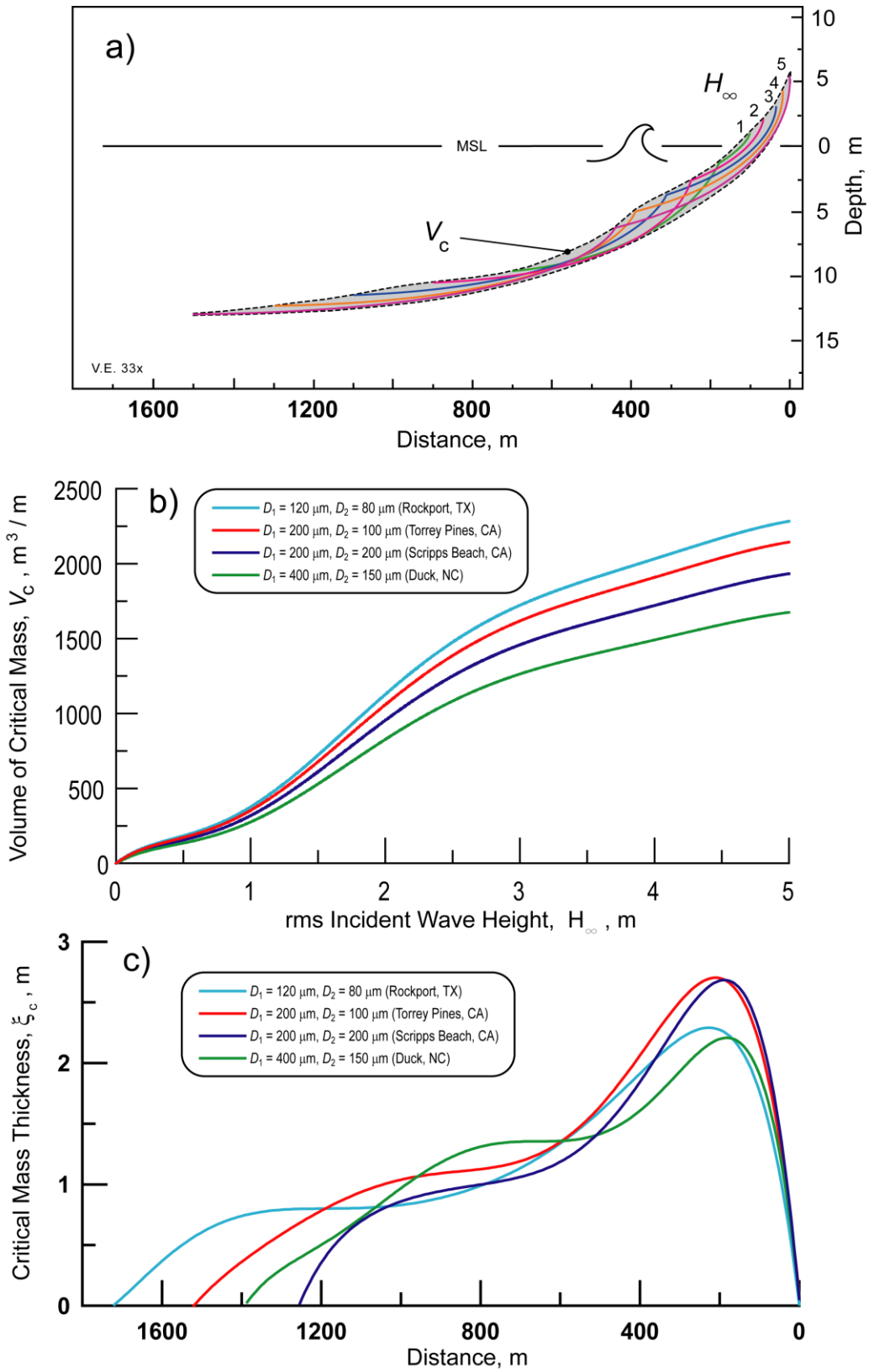

Figure 4. Mechanics of farfield burial: a) envelope of profile change gives critical mass; b) volume of critical mass from elliptic cycloids; c) cross-shore variation in thickness.

a)

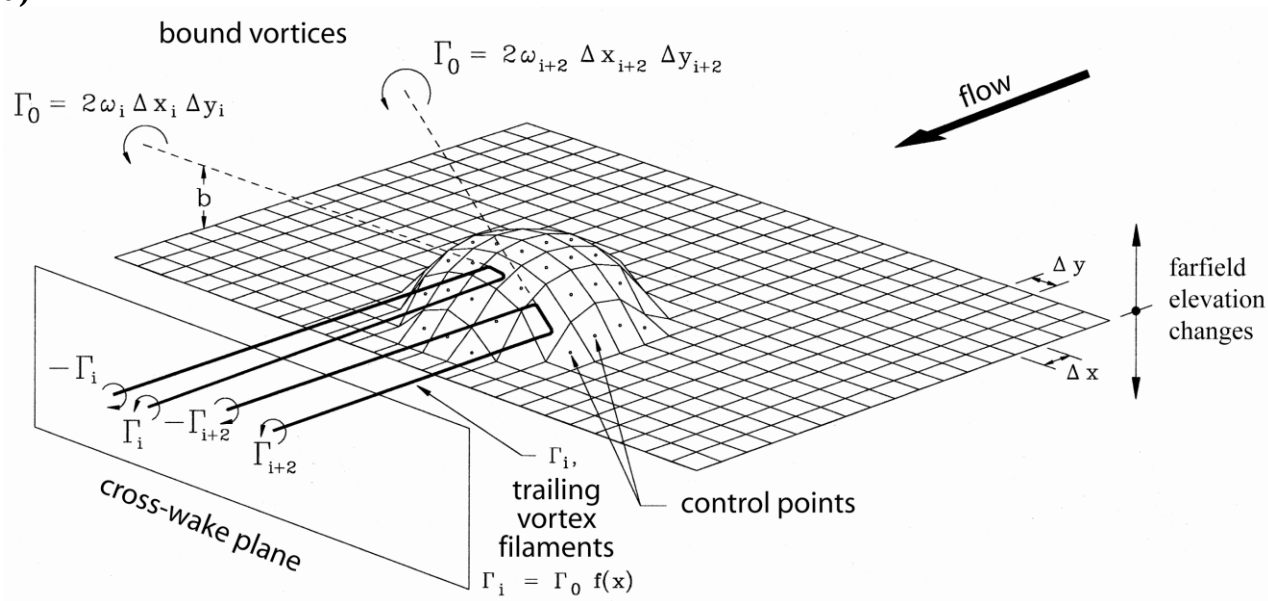

b)

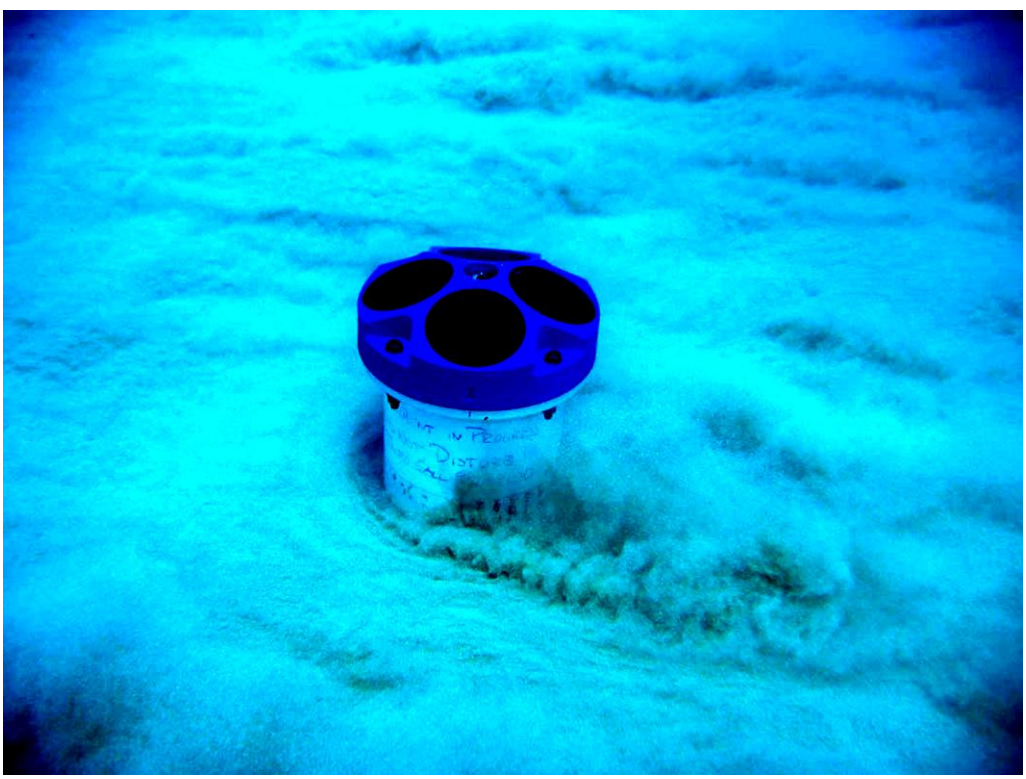

Figure 5. Vortex lattice method: a)lattice and horsehoe vortex system; b) horsehoe vortices inducing sediment transport in nature [photo courtesy of Kimball Millikan].

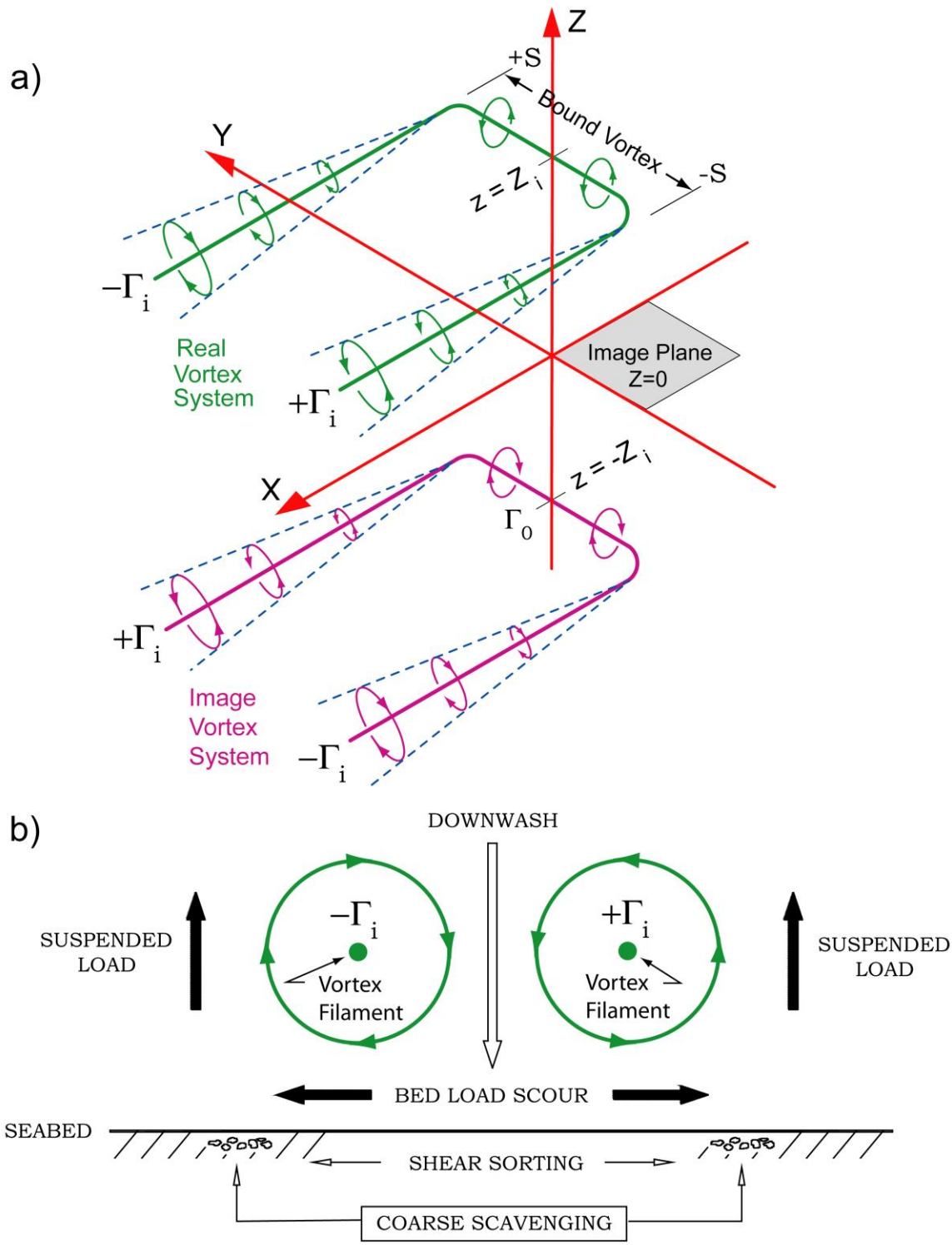

Figure 6. a) Image method for vortex induced velocity at any point near the bed (image plane) due to the horseshoe vortex system of an arbitrary lattice panel (Figure 5a). The real vortex of the lattice panel is diagrammed in magenta, the image vortex is in green. b) Schematic in the cross-wake plane of a pair of vortex filaments trailing out of the page, (Figure 5a).

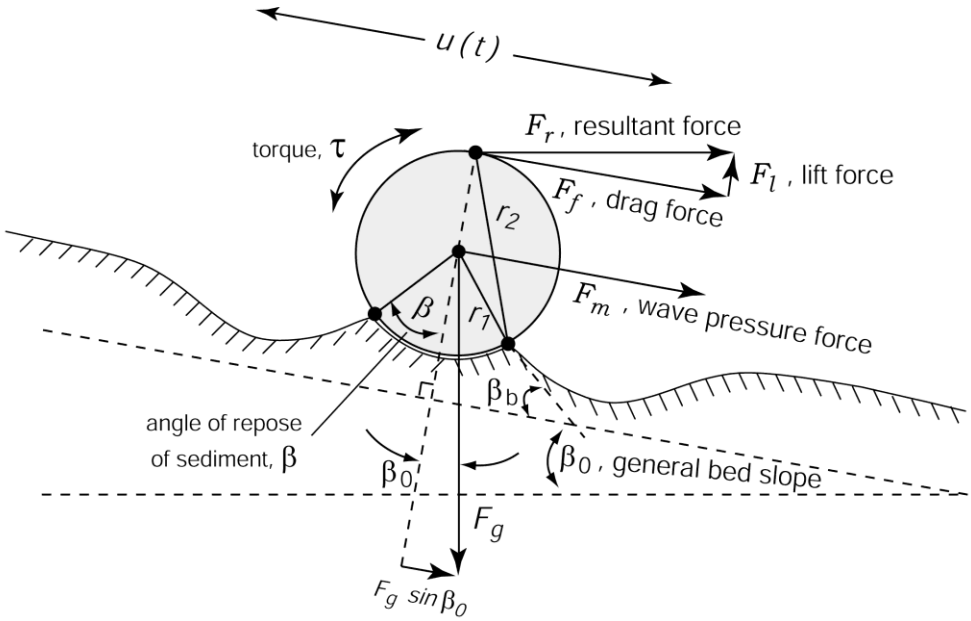

Threshold of migration criteria: Σ moments = 0

$$\vec{F}_g \times \vec{r}_1 = \vec{F}_m \times \vec{r}_1 + \vec{F}_r \times \vec{r}_2 + \vec{\tau}$$

Figure 6c. Moment balance for threshold of UXO movement in response to reaction forces generated by trailing vortex filaments in Figure 6b.

filaments induces a flow across the seabed that results in scour proportional to the cube of the vortex strength and inversely proportional to the cube of the sediment grain size. This sensitivity of scour to grain size selectively removes the finer grained fraction of the bed material and leaves behind the coarser grained fraction in the scour depression. The coarse material that remains in the scour hole armors the bed against further scour thereby slowing the rate of scour burial.

The farfield throughput to the nearfield process modules is initially applied to the local seabed boundary conditions module (gray box in Figure 2. These local boundary conditions include two types: 1) the slope and elevation of the seabed plane around the object base derived by (#11) from location in the farfield control cell; and 2) the shape file of the body in question (#12). These two local boundary conditions are used to generate lattice panels by (#13) that define the object and bedform of the surrounding seabed (Figure5a). The lattice is the computational domain of the nearfield scour-burial processes in which the method of embedded vortex singularities (vortex lattice method) is applied in (#14) using algorithms after Jenkins and Wasyl (1990) and Jenkins et al., 2007. This method employs horseshoe vortices embedded in the near-bottom potential wave oscillation to drive local sediment transport in (#13) based on ideal granular bed load and suspended load equations after Bagnold (1956 &1963). A horseshoe vortex is specified by (#14) for each lattice panel during every half-cycle of the wave oscillation as shown schematically in Figure 5a. The horseshoe vortices release trailing pairs of vortex filaments into the local potential flow field that induce downwash on the neighboring seabed

(Figure 6b), causing scour with associated bed and suspended load transport as computed by (#13). This scour action by trailing vortex filaments can be seen occurring in nature in Figure 5b. The trailing vortex filaments also produce reaction forces on the UXO, that induce movement at the instant the moments from these forces balance the moments of gravity associated with the immersed weight of the UXO, as shown schematically in Figure 6c,

The lattice generation in (#14), horseshoe vortex generation in (#14) and sediment transport computations in (#13) and UXO threshold movement and migration (#15) are implemented as a leap-frog iteration in a time-stepped loop shown by the red and blue pathway arrows at the bottom of Figure 2. The leading time step (red arrow) computes the strength of the horseshoe vortex filaments generated by the pressure gradients and shear setup over the lattice panels of the combined body-bedform geometry of the previous (lagging) time step. The bed and suspended load transport induced by these filaments results in an erosion flux from certain neighboring lattice panels on the seabed and a deposition flux on others, based on image lifting line theory (Figure 6a) as first applied in Jenkins and Wasyl (1990) to a mobile sedimentary boundary. The erosion and deposition fluxes of the leading time step are returned in the computational loop to the lattice generator (blue arrow) where those fluxes are superimposed on the lattice geometry of the lagging time step. That superposition produces a new lattice geometry for implementing the next leading time step. By this leap-frog iterative technique, an interactive bedform response is achieved whereby the flow field of the leading time step modifies the bedform of the lagging time step; and that modified bedform in turn alters the flow field of the next leading time step. This lead and lag arrangement is based on the fact that the inertial forces of granular bed near incipient motion are large compared to those of the fluid, hence the flow field responds faster to a change in bedform than the bedform can respond to a change in flow field.

Because most UXO are bodies of revolution, the burial mechanism proceeds by a series of scour and roll events on a fine sand bottom, whereby the UXO successively scours a depression and then rolls into that depression. In contrast, a flat bottom mine-like objects (e.g., MANTA, ROCKAN, etc.) or UXO resting flat-side down bury by scour and slip sequences involving episodic shear failures (avalanches) of the slopes of the scoured depression, Jenkins & Inman (2002). During these shear failures, the UXO is in a state of sliding friction with the bed and is easily moved by the hydrodynamic forces of waves and currents.

Both of these mechanisms (scour and roll or scour and slip) may be arrested by large scale changes in the bed elevation due to either seasonal profile changes or influx of material by accretion/erosion waves. Both of these mechanisms (scour and roll, and scour and slip) involve movement of the UXO during the burial sequence. Over erosion-resistant beds, waves and currents may cause UXOs to migrate large distances before scour and burial arrests further UXO migration. During lower energy summer condition, sand moves onshore from the shorerise, shifting the bottom profile shoreward, exposing the UXOs and inducing migration. On muddy seabeds during storms, both the UXO and seabed may move as a unit.

2.2 TECHNOLOGY DEVELOPMENT

The MM is adapted from a modification of the Vortex Lattice UXO Scour/Burial Model originally developed under ONR's Mine Burial Program (Jenkins, et. al., 2007). Several important modifications to the previous basic VORTEX lattice model were made:

- Algorithms for calculating the near-field effects on UXO were modified to address the complex and tapered shapes of small size (relative to mines).

- The overall algorithm for calculating the far-field effects that drive sediment movement was modified. The sediment movement determines when the UXO is and is not buried, which has a major impact on overall UXO migration. The algorithm for calculating the total shape and size of the critical volume of sediment that is active along a given beach was re-created using thermodynamic balance as the basis rather than the past methods based on Dean's models.

- To support the critical volume analysis, an improved method of calculating the closure depth (the depth beyond which there is no net movement of sediment) was developed and incorporated in the MM.

Under the present project, the MM has been upgraded to more efficiently compute fate and transport of UXO in biogenic reef environments. We have developed code revisions to Module #8 in the architecture of the MM (Figure 2) in order to model the Vieques Island UXO fields using geomorphic computational (control) cells bounded by the walls of awa channels cut cross-shore through the lithofied reef structures at the mouths of island streams. The awa channels set natural boundaries on the reef control cells based on land features of streambeds identified with Google Earth satellite imagery. Each control cell thus becomes a reef platform bounded by awa channels, and an assemblage of these cells fit together forming a fringing reef system around the island. The reef platform micro-bathymetry is constructed from spatial Fourier transforms of the LIDAR data for the reef platforms at PMRF, Kauai. We can one-dimensionalize this technique by taking the local depth , $z\ (\eta)$, variation about the mean depth $z_0\ (\eta)$ along any given bathymetric contour, η, as a sum of $N/2$ sine- and cosinsoids. Here N is the number of local depth measurements (typically from LIDAR) along any segment of isobath of length , $L = N\Delta s$, giving the Fourier decomposition of the local depth variation as:

$$\frac{\left[z(\eta) - z_0(\eta)\right]}{L} = \sum_{n=1}^{n=N/2} a_n \sin(n\sigma s) + \sum_{n=1}^{n=N/2} b_n \cos(n\sigma s) \qquad (3)$$

Where s is the curvilinear coordinate tangential to the isobath, Δs is the sampling interval of the LIDAR data, $\sigma = 2\pi / s$ is the radian distance frequency of the reef roughness and

$$a_n = \frac{\sigma}{\pi} \int_0^{2\pi} \frac{[z(\eta) - z_0(\eta)]}{L} \sin(n\sigma s)\, ds \tag{4}$$

$$b_n = \frac{\sigma}{\pi} \int_0^{2\pi} \frac{[z(\eta) - z_0(\eta)]}{L} \cos(n\sigma s)\, ds \tag{5}$$

The Fourier coefficients (a_n, b_n), are evaluated using a digital Fast Fourier transform (FFT) of digital LIDAR data. In general, the sampling interval of the LIDAR data is $\Delta s = 1$ m, and the FFT requires a particular number N of these depth samples that are some power of the integer 2. Typically, we maximize the number of samples input to the FFT in order to resolve the lowest possible distance frequencies (longest length scales). In our applications herein we choose an N that spans the distance $L = \Delta s N$ along a given bathymetric contour between two adjacent awa channels. However our FFT software permits Fourier decomposition involving as many as N = 16, 384 depth samples, allowing 16.4 km of bathymetric contour to be decomposed by FFT into 8,192 pairs Fourier coefficients, each with a frequency resolution of $2\pi s$ = 6.1 X 10^{-5} m^{-1} . Figure 7 gives an example of this approach of compressing depth data on the reef platform at

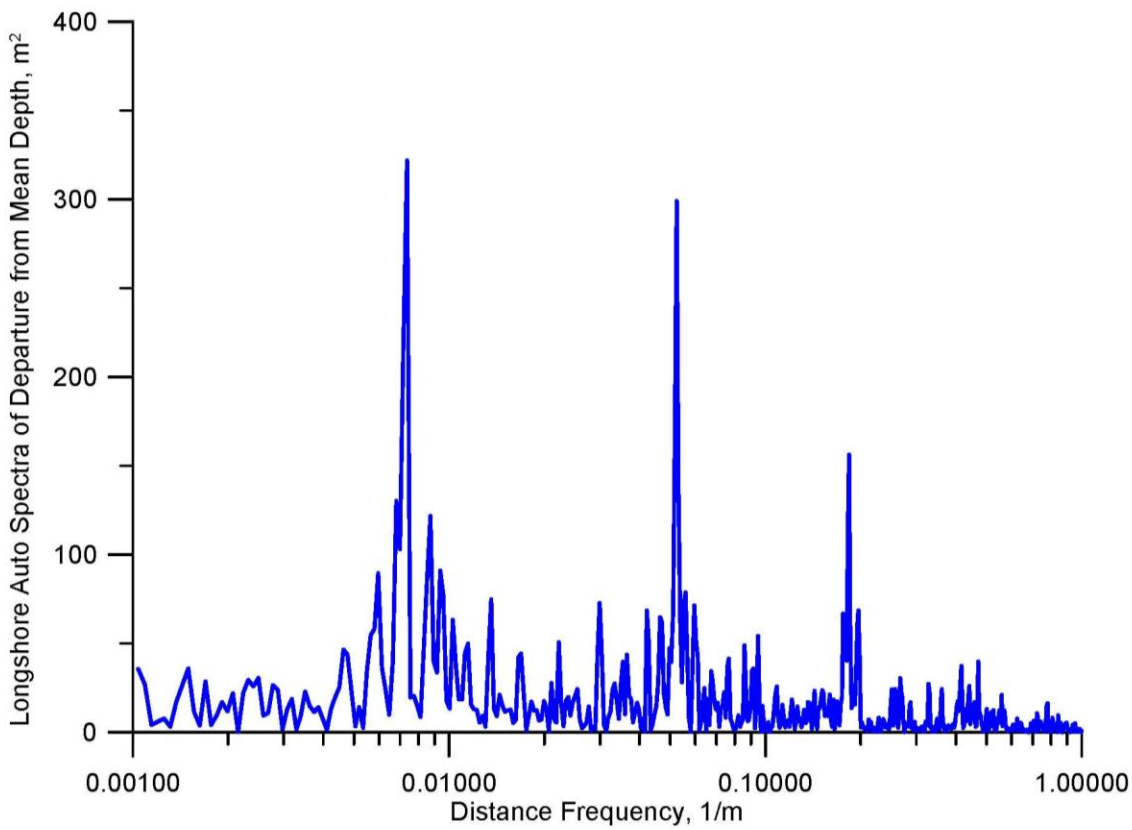

Longshore auto spectra of departure from mean depth of reef platform, from LIDAR bathymetry data at PMRF, Kauai, HI.

Figure 7: Longshore auto spectra of departure from 30 m mean depth of reef platform, from LIDAR bathymetry data at PMRF, Kauai, HI.

PMRF, Kauai using the auto-spectra along the 30m depth contour.The Fourier transforms allow the billions of discrete LIDAR data points to be compressed into a workable number of Fourier coefficients that represent the roughness details of the reef platforms of the awa control cells (Figure 8). Here awa channels are 2 km apart and the FFT's of the LIDAR data involved N = 2048 depth samples along bathymetric contours at 2m intervals, where each bathymetric contour is represented by 1024 pairs Fourier coefficients. With these discrete control cells, the vortex lattice algorithms can rapidly calculate ambient flow features such as bathymetric divergence over a UXO field. A discrete arrangement of these awa control cells allow numerically stable computations of erosion and transport of large UXO reef fields that surround an entire island (cf. Section 9).

The new awa cell computational approach is validated in hindcast in Section 5.6 against the PMRF data base from prior ESTCP funded UXO field experiments, using the same predictive skill measures detailed in NFESC (2008). With the validated up-graded UXO Mobility Model (MM), we predict the fate of UXO over the broad expanse of reef environments at Vieques Island (Figure 8). We test the hypothesis (through long-term, extreme-event simulations) that the UXO at these sites eventually concentrate in the reef awa channels. Here, UXO are amenable to recovery by conventional sand dredging methods, while presenting a persistent danger (if not recovered) of becoming transported to the beach during storms.

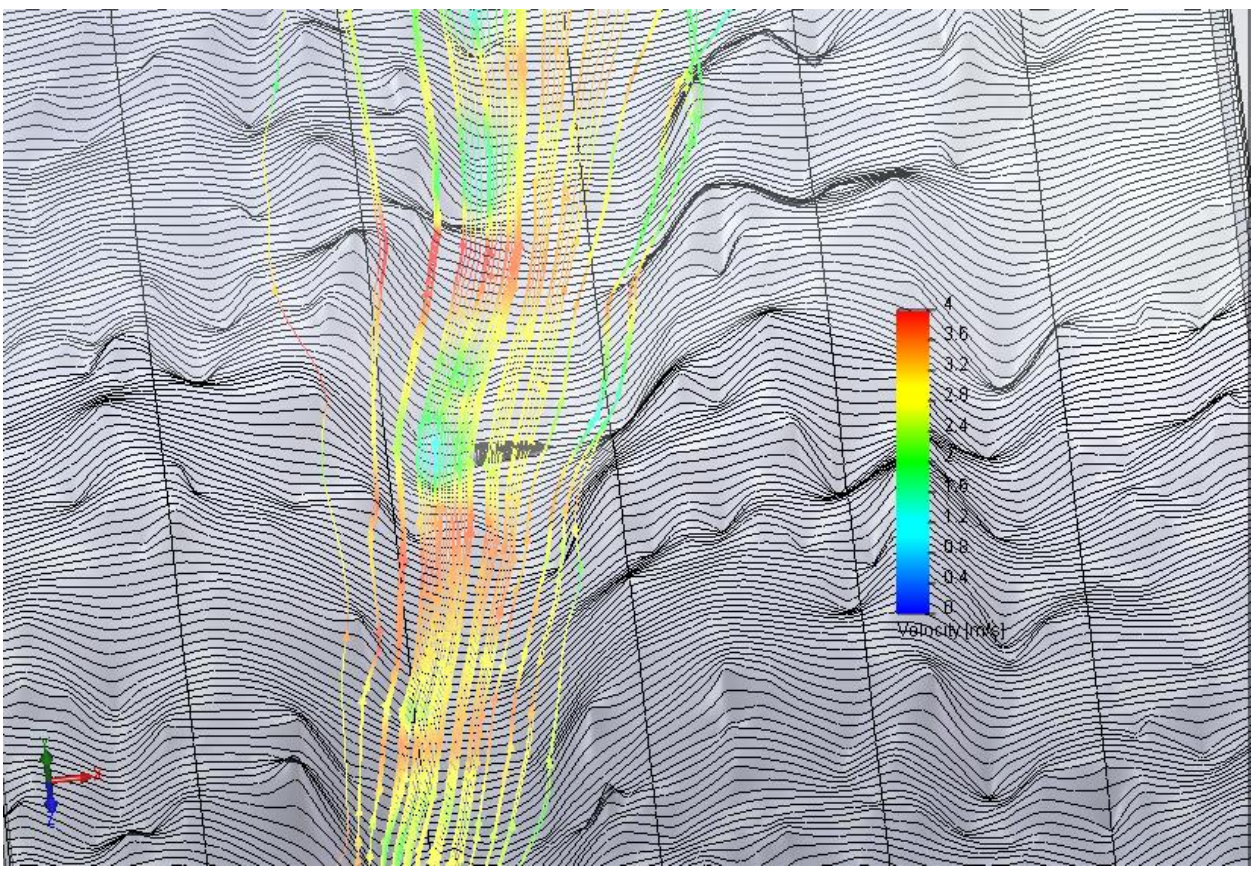

Figure 8: Awa channel and reef platform at PMRF, Kauai, constructed from lofting of Fourier decomposition of high resolution LIDAR bathymetry. Rip current simulated from 5 m incident shoaling wave with 15 second wave period.

2.3 ADVANTAGES AND LIMITATIONS OF THE TECHNOLOGY

The advantages of using the MM to assess the fate of UXO are as follows: 1) Areas in which UXO are buried and will remain so can be positively identified – which can substantially reduce areas of required remediation. 2) In areas of intermittent or sustained exposure, it is possible to predict the percent of the time that UXO are exposed to human contact, or to other hazardous processes such as corrosion, damage, etc. 3) Where UXO are exposed, it is possible to predict the rate and direction of net movement as a function of weather and other local conditions. These calculations help to determine the probability of UXO appearing in adjacent areas outside of initial impact zones. 4) After obtaining *in situ* survey of UXO, the MM allows munitions response managers to determine whether the UXO will remain where originally found, and thereby guide the speed of remediation efforts.

The primary limitations of the MM, as with all computer models, are the quantity and quality of the input data. In general, the MM output statistics are driven by the statistics of (a) the estimates of original UXO distributions (type, location, burial depth) and (b) the data on past weather conditions (waves, currents). Data on the sediment type and local bathymetry are also critical to the MM accuracy, but they tend to be more deterministic in nature.

The MM does not include a module for calculating the initial condition of the UXO (e.g., state of impact burial our special distribution of UXO population immediately after impact). That state is derived from a combination of historical data and other hydrodynamic models of projectile impact processes (through the water column, initial burial, etc.). Absent those calculations or other assumptions, the MM starts with the assumption that the UXO were initially deposited on the seafloor intact and unburied. The MM only deals with intact rounds (not fragments). Fragments are sharp and cannot roll, so in general they tend to move much less than the smoothly contoured and intact projectiles. The MM does not specifically address UXO populations consisting of boxes or intact pallets, although it could be modified to do so. The MM does not take into account the degradation of UXO rounds by corrosion, dispersion of dissolved chemicals. Explosives are unique environmental contaminants, solid at room temperature, and subject to slow dissolution in an aqueous medium. Explosives have slower degradation rates and tend to be less mobile than other anthropogenic water contaminants such as oil and metals. However, since the MM does predict the time sequence of burial, exposure, movement, and reburial, that information is an important input to other software programs that estimate corrosion rates and the release of chemicals.

3.0 PERFORMANCE OBJECTIVES

The performance objectives shown in Table 1 provide the basis for evaluating the performance and costs of using the modified MM.

Table 1. Performance Objectives

Performance Objective	Metric	Data Required	Success Criteria
MM provides credible prediction of movement in support of test planning, ops.	Predictions check against general engineering theory and observations at similar sites.	Graphic presentations of predicted and measured movement of surrogates from the field demo site.	Differences between predicted values and measurements are consistent, and can be reduced to within 20% or less by calibration
Field Demonstration collection of sufficient quality data to allow validation of MM	Tracking movement of surrogates with accuracy consistent with input data and MM computational resolution	Measured position of the surrogates v. time at the field test (location and depth of burial)	> 50% of surrogates are tracked successfully at the test site. Movements are measured within +/- 10%.
Match between predictions and measurements, with coefficients correctable to positive match.	Model skill factor (ability to correctly predict surrogate movements and burial)	Measured position of the surrogates v. time at the field test (location and depth of burial)	R > 0.8

It is very easy to create hundreds or even thousands of data points with the UXO MM simulations by modeling the given UXO type at various locations at a site, with various subsets of historical wave data inputs. In order to provide reasonable statistics from the field demonstrations measurements it was necessary to have at least a 50 to 100 measured data points for the given UXO type (5”/38 round). It was anticipated that there would be at least 3 to 6 rounds of measurements during the tests, so a minimum of around 16 surrogates were required. Because it was expected that some of the surrogates would either be lost, have their acoustic beacons fail or otherwise not provide a full set of data, 24 surrogates were used at each field test site.

Also, it was necessary that the measurements of location be accurate within about 10% of the actual movement distance, or about 1 meter (whichever was larger). That level of accuracy is consistent with the expected error bounds on the basic environmental parameter measurements (sediment grain sized, wave velocities, etc.). Data collection at the PMRF field tests exceeded the requirements. While there are certainly other locations and conditions under which the MM could be further validated, the fact that not only these two field demonstrations but also both of

the prior limited Navy field tests all required very minor calibration of the MM suggests that the basic fluid theory and mathematical modeling methods in the MM are very sound and could be extrapolated to other sites with confidence.

When the predictions of the calibrated MM were compared to the measured UXO surrogate movements using the basic least-squares skill evaluations criterion, it was found with the un-modified MM that: $R_{\xi} = 0.88$ for movement and $R_h = 0.90$ for burial.

4.0 SITE DESCRIPTION

The Pacific Missile Range Facility (PMRF), Kauai, Hawaii, site is located on the southwestern coast of Kauai, HI. Figure 9 gives an aerial perspective on the test site relative to the active runway at PMRF.

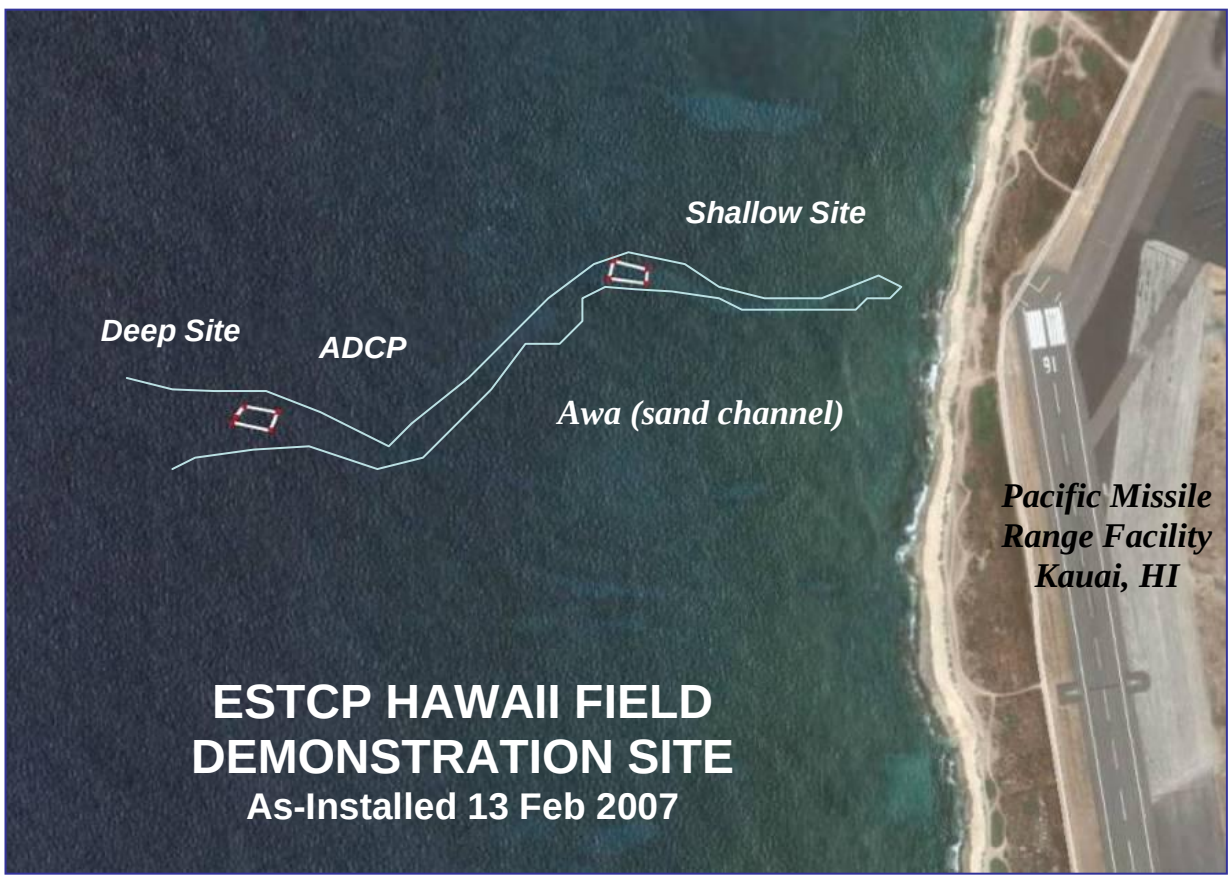

Figure 9. PMRF, Barking Sands, is located on the west coast of Kauai, Hawaii.

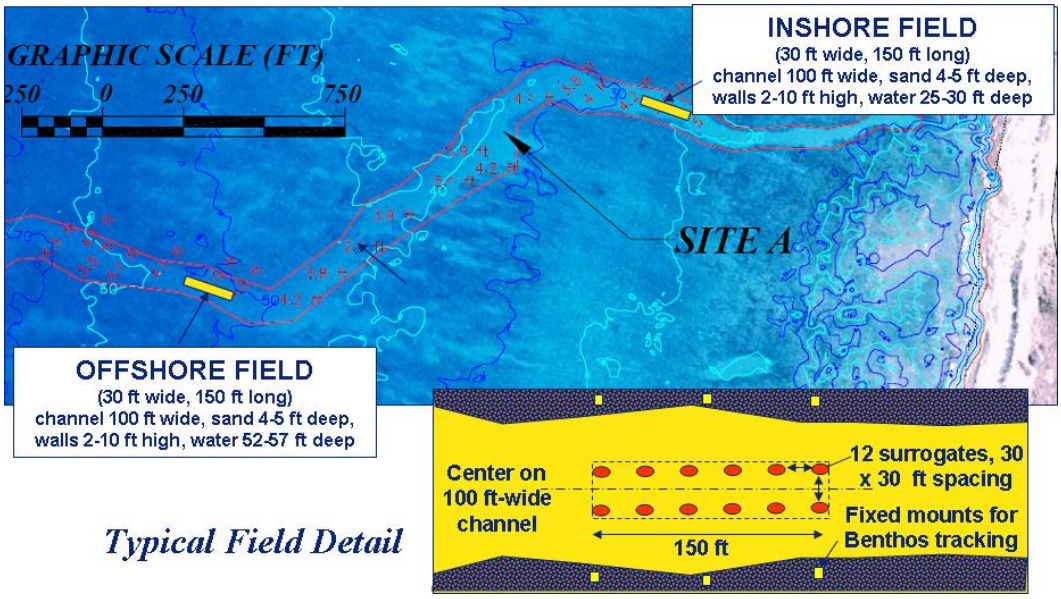

Figure 10. PMRF field demonstration configuration.

The deployment area selected for the Hawaii field demonstration is an awa channel oriented in an approximately east-west direction that bisects a limestone and coral reef bottom off the Pacific Missile Range Facility on the west coast of the island of Kauai (Figures 9 & 10). The awa extends from approximately the 5.5 m to the 24.5 m water depth, where it opens up into a larger offshore sand deposit. The distance from the 9.25 m depth to the 18.5 m depth is approximately 600 m. At the 15 m water depth there are vessel remnants in the middle of the awa that appear to be the remains of a small sail boat. At the 13 m water depth the sand channel narrows to a width of only approximately 3 m, but it is at least 18.5 m wide between the 6.2 m to 12.5 m depths and the 15 m to 25 m depths. This entire awa is bounded by reef and/or limestone on three sides. It ends abruptly inshore at a 1.5m reef escarpment in 4m of water. The escarpment walls on the north and south sides of the channel are typically 0.6 to 3.0 m high. The awa's sand thickness at the 13 m depth (the location of the narrow bottleneck) is 0.7 m, but the thickness throughout the remaining channel varies between 1.1 to 1.6m. All surrogates were installed in the sandy part of the awa, rather than on the coral sides, to (a) ensure minimal chance of actual loss of the surrogates and (b) to minimize any possible damage to the coral reefs.

4.1 SITE SELECTION

The PMRF/Barking Sands site was chosen as an example of a Biogenic reef coastal morphology, typically exhibiting more irregular seafloor shapes crossed by channels and limited sediment covers of detrital carbonate sands. The following additional criteria were used to select the demonstration site:

a. Representative of a major coastal classification. The PMRF site is geomorphically similar to the impact ranges at Vieques Isalnd that are chosen for subsequent numerical sensitivity analysis of the modified MM.
b. Controlled access. The PMRF Dem/Val areas have limited public access which are favored in order to minimize disturbance.

c. High frequency of high-energy weather events. Areas which experience frequent storms are conducive to measuring surrogate movement.
d. Environmental permits. The ability to meet environmental permitting requirements is necessary.

4.2 SITE HISTORY

Details of the PMRF, Barking Sands field experiment can be found in "Predicting the Mobility and Burial of Underwater Unexploded Ordnance (UXO) using the *UXO Mobility Model",* ESTCP Project 200417, J.V. Wilson, A. De Visser, and B. Sugiyama

4.3 SITE GEOLOGY

The PMRF site is situated in a narrow, meandering sand channel (*awa*) that bisects a limestone and coral reef bottom (Figure 10). This awa extends from approximately the 5.5-meter to the 24.4-meter water depth, where it opens up into a larger offshore sand deposit. The distance from the 9.1-meter depth to the 18.3-meter depth is approximately 579.1 meters, a slope of less than 1:600. The sand channel varies in width from 3.0 meters to more than 30.5 meters. The entire channel is bounded by reef and/or limestone on both sides and bottom. The channel ends abruptly inshore at a 1.5 meter reef escarpment at the 3.7-meter water depth. The escarpment walls on the north and south sides of the channel are typically 0.6 to 3.0 meters high.

4.4 MUNITIONS CONTAMINATION

The experiment involved the deployment of surrogates in order to generate as experimental baseline for the processes involved in movement/burial. No munitions were involved.

5.0 TEST DESIGN

Our demonstration/validation exercise of the upgraded awa-cell MM uses field data collected in 2007, ESTCP Project 200417. At PMRF, a series of UXO surrogates were placed on the seafloor in various water depths. Their location and depth of burial (whenever possible) were then monitored by diver inspections at intervals determined by the occurrence of high-energy environmental events (e.g., storms or large, local wave events). The surrogates were left in place through the 2007 spring season, with some overlap into winter and summer at the end of each measurement round.

The 5"/38 surrogates were installed at pre-planned distances from the shoreline from the closure depth to just seaward of the low tide line. By then plotting the actual movements of each individual surrogate it was possible to examine trends as a function of location with respect to such meteorological/oceanographic parameters as surf zone characteristics, weather forcing function conditions, local sediment properties, etc. Only the 5"/38 surrogates were used during the field efforts at the PMRF site.

The locations of the 5"/38 surrogates were tracked by a variety of methods. The surrogates were each composed of a large metal core and equipped with an acoustic pinger. Divers used hand-

held receivers, as well as a Benthos fixed acoustic tracking system to track the surrogates. Metal detectors were used to further locate the surrogates in conditions of poor visibility or when they were buried. Each location was measured with respect to fixed references by employing acoustical methods, Global Positioning System (GPS) to surface floats, and tape measures, depending on the local conditions at the time. Those range data were then intersected to obtain fixes on surrogate locations by using the method of triangulation.

5.1 CONCEPTUAL EXPERIMENTAL DESIGN

Field data was collected on the movement of all or most of the UXO surrogates and to document the environmental conditions that caused those movements (e.g., currents, tides, waves, and seafloor properties).

The primary metric for defining a successful UXO MM software refinement/upgrade is that the observed movement matches the predicted movement well enough to allow final adjustment of the model parameters to match the observations within the basic structure of the revised model (i.e., assumptions of basic forces and interactions would remain unchanged).

5.2 SITE PREPARATION

The support diving team made two preliminary dives at the site to photograph the bottom conditions, confirm the awa configuration, and obtain samples of the sediment (sand) in the awa at the two sites selected for the inshore and offshore fields. There were some delays in locating, obtaining, and then gridding the detailed LIDAR data. To make up for lost time, the hardware and surrogates were installed as soon as the permits allowed, which precluded running the MM for this site prior to deployment. However, analyses of the height of the awa walls were performed to confirm that even in the worst possible storm the surrogates would not move out of the awa and onto the beach; they would remain in the demonstration area so they would not damage local coral, and so they could be closely monitored.

5.3 SYSTEM SPECIFICATION

The main hardware for the UXO Field Demonstrations was the surrogate 5”/38 projectiles. They were cast from plastic with a steel core so they represented the correct shape and weight. They were equipped with small Sonotronics acoustic pingers in the nose to facilitate locating them even when buried. Sonotronics underwater acoustic receivers were used to guide divers to the location of the surrogates during each round of measurements. When the surrogates were buried, hand-held metal detectors were used to refine the diver’s position within less than 1 meter. The diver’s location in the test field was then determined by ranges from two or more Benthos acoustic transponders located at fixed points in or near the field.

The surrogates are shown in 1. The details of the test hardware are provided in the two Field Demonstration Reports Wilson, et al, 2008a-d.

Figure 11. Surrogate 5”/38 projectiles used in UXO Mobility Model field demonstrations.

To provide a systematic and manageable set of inputs for shape specific calibration parameters we concentrated our model simulations on the 5”/38 Naval projectile shown in Figure 11. These rounds were approximated by an elliptic frustrum revolved about the major axis of the round, say the *y*-axis, taken for example as the transverse axis to the mean flow as shown in Figure 5a. For this orientation the generalized shape of the round can be represented by the analytic expression:

$$R(y) = a - a\left(\frac{y}{S}\right)^{\beta} \qquad (6)$$

Here $a = D/2$ is the basal radius and D is the basal diameter of the round; $R(y)$ is the local radius at any arbitrary location y along the major axis of the round; S is the total length of the round as measured along the *y*-axis; and β is a constant that adjusts the pointedness of the round. A best fit of equation (6) to the 5”/38 rounds shown in Figure 11 was found to be β =3.5. To accommodate these dimensions and the small radius curves of the shape, the VORTEX shape lattice file was gridded for 3mm grid cells. The dry bulk mass of the 5”/38 surrogate rounds was nominally $\rho_s V_0 = 22.8$ kg.

5.4 CALIBRATION ACTIVITIES

The locations of UXO surrogates was computed from the Benthos tracking units were compared against hand-held tape measurements from multiple points. In all cases, the tape measured locations (typically accurate to +/- 6 inches) fell in the center of the acoustic error bounds (+/- 1 meter).

5.5 DATA COLLECTION PROCEDURES

The surrogates were installed in two groups of twelve each. The surrogates labeled 1 through 12 were installed in the offshore field in approximately 18.3 m of water (Offshore Field, Figure 10). The surrogates labeled 13 through 24 were deployed along the inshore field in approximately 9.1 meters of water (Inshore Field, Figure 10). An RDI Workhorse Acoustic Doppler Current Profiler (ADCP) wave gauge was anchored to the seafloor on the northern side of the deep field at 16.8 meter water depth (Figure 12).

Figure 12. RD Instruments ADCP installed in the Offshore Field**.**

5.6 VALIDATION

During the April 2007 site visit, the wave gauge was retrieved and the battery and memory card replaced. From this date on, the metal detectors were the primary means of determining surrogate location, and the Sonotronics Underwater Diver Receiver (UDR)s were only used occasionally. After the deep field was located, the positions were measured using the Benthos Diver Range Interrogator (DRI). Measurements were also obtained with tape measures for comparison. During the 9 May 2007 site visit, all surrogates in the deep and shallow fields were located using the metal detectors. An attempt was made to identify the surrogates using the UDRs, but the results were inconsistent. The positions for the deep field were obtained with the

Benthos DRI while the positions for the shallow field were obtained with the DRI and then verified with a tape measure. All surrogates were located using the metal detectors and positions were measured using the Benthos DRI. Sea Engineering, Inc. (SEI) also probed for the surrogates to determine burial depth using a 0.3 cm diameter fiberglass instrument. The search process was carefully conducted, so no surrogates were displaced or disturbed during the probing activities. SEI located the deep and shallow fields using the metal detector and retrieved the Acoustic Doppler Current Profiler (ADCP) for maintenance and redeployment.

The MM will be used to predict migration and burial behavior of UXO surrogates of 5”/38 projectiles when grounded on the seafloor in the near shore of a biogenic reef environment.

6.0 DATA ANALYSIS AND PRODUCTS

The MM can be operated in three distinct modes depending on the data that are available for making a burial prediction and the user’s desire to make site specific adaptations to the model’s configuration. When little more than the general coastal setting and the time frame of UXO introduction and initial depth are known, the MM is run in Mode 1. Mode 1 predictions use pre-configured gridding systems, forcing functions, boundary conditions and calibration factors based on the coastal classification system. The 7 input parameters required for Mode 1 operation are indicated by the *italicized* entries in Table 2 & 3.

When information is known about the gross site specific details of a suspected UXO field, then the MM can be run in Mode 2. Mode 2 operation makes burial predictions using pre-configured gridding systems and calibration parameters with user supplied bathymetry, wave and sediment data. The Mode 2 input parameters are the 7 *italicized* and 13 <u>underlined</u> entries for parameters listed in Table 2 & 3.

The MM is run in its most detail intensive configuration as Mode 3. This operational mode is for applications in which contemporary, high-resolution, site-specific information is known about the UXO field. This operational mode was used in field experiments at Ocean Shores in August 2003 and for both of the ESTCP field tests. And Mode 3 is intended for experienced modelers, and allows for customized configurations of all gridding systems, calibration factors and file structures of forcing functions and boundary conditions. Mode 3 input parameters include all 40 parameters listed below in Tables 2 & 3.

Table 2. UXO Mobility Model Farfield Input Parameters.

<u>Farfield Littoral Cell Model Parameters</u>

1 *Coastal Type: Collision, Trailing Edge, Marginal Sea/Narrow-Shelf Mountainous, Marginal Sea/Wide-Shelf Plains, Marginal Sea/Deltaic-Tideless, Marginal Sea/Deltaic-Tidal, Arctic Form of Cryogenic, Coral Reef Form of Biogenic*
2 *Estimated time when UXO entered the environment*
3 *Time period of prediction*
<u>4</u> <u>Deep water directional wave spectra or discrete height, period and direction estimates of principal band</u>
<u>5</u> <u>Deep water wave height of antecedent extreme event</u>

6 Wind speed
7 Precipitation or river flow rate data, Q
8 Coefficients (a, b) of sediment rating curve (R = aQb)
9 Grid cell dimension x-axis (Longitude)
10 Grid cell dimension y-axis (Latitude)
11 Number of grid cells along the x-axis (Longitude)
12 Number of grid cells along the y-axis (Latitude)
13 Latitude/longitude of upper left hand corner of farfield grid (Raster formatted grid)
14 Stationary bathymetry file at start of simulation
15 Position of mean shoreline (0.0 m MSL) at start of simulation
16 Distance offshore to closure depth
17 Median grain size of shelf sediments (seaward of closure depth)
18 Grain size distribution of shorerise and bar-berm sediments (as many as 9 size bins)
19 Volume concentration of seabed sediment
20 Tidal harmonic constituents
21 Longshore transport efficiency coefficient
22 Shorerise bottom friction coefficient
23 Breaker dissipation coefficient
24 Angle of internal friction

Table 3. UXO Mobility Model Nearfield Input Parameters.

Nearfield Scour and Burial Model Parameters

25 UXO type
26 User selected grid cell(s) from farfield grid corresponding to UXO sweep area
27 Estimated time of UXO deployment
28 Time period of prediction
29 Degree of impact burial
30 Grain size distribution of seabed sediments (as many as 9 size bins)
31 Local seabed elevation and slope from user selected grid cell of farfield model
32 Local orbital velocity from user selected grid cell of farfield model
33 Local tidal velocity from user selected grid cell of farfield model
34 Bed roughness
35 Seabed drag coefficient
36 Bedload transport efficiency
37 Suspended local transport efficiency
38 Angle of internal friction
39 Volume concentration of seabed sediment
40 User selected grid cell dimension for unregistered UXO type

Note that these parameters are all measurable by, or derivable from, conventional ocean environmental measurement technology. Existing Defense Mapping Agency (DMA) charts, commercial surveys with multi-beam bathymetry/imagery, and a few selected sub-bottom profiles, a series of core samples, and hindcast coastal wave, tide and current measurements are all sources for the data needed for useful MM operation. The MM is very complete in the parameters it considers, but does not demand new technology or great expense to collect the

required data. The inputs allow deterministic simulations of UXO behavior. The MM simulations then allow long-range predictions based on stochastic application of site-specific climatic conditions. The accuracy of the MM predictions is limited almost entirely by the statistics of the inputs.

6.1 PREPROCESSING

The stationary farfield bathymetry was derived from the National Ocean Service (NOS) digital database as contoured in Figure 13, seaward of the 0 m mean sea level (MSL) depth contour. This coarse-scale bathymetry defines the basic morphology of the fringing reef system at PMRF along the west coast of Kauai. The mesh is defined by latitude and longitude with a 3 x 3 arc-second grid cell resolution yielding a computational domain of 15.4 km x 18.5 km. Grid cell dimensions along the x-axis (longitude) are 77.2 m and 92.6 m along the y-axis (latitude). This small amount of grid distortion is converted internally to Cartesian coordinates, using a Mercator projection of the latitude-longitude grid centered on PMRF air field. The convention for Cartesian coordinates uses x-grid spacings for longitude and y-grid spacings for latitude. For the non-stationary bathymetry data inshore of closure depth (<12 m MSL), equilibrium beach algorithms were used, see Jenkins and Inman (2006) Depth contours generated from these algorithms vary with wave height, period, and grain size landward of the 12m depth contour for the typical seasonal range of wave parameters of the PMRF site during the time frame of February through June 2007.

While Figure 13 defines the gross morphology of the reef platform, the micro-bathymetry of the specific awa in which the UXO were placed was first resolved with high resolution LIDAR data, which was subsequently subjected to spatial Fourier transform decomposition to reassemble the micro bathymetry in terms of a relatively small number Fourier coefficients in the awa-cell restructuring of the MM far field grid . Figure 14 gives a co-registration of the LIDAR data with the coarse-scale NOS bathymetry, and shows the sample density of the LIDAR data over that portion of the PMRF reef where the UXO fields were placed. Sample density of the LIDAR data was typically on the order of 1m, allowing for considerable detail of the awa to be resolved around the offshore and inshore UXO sites (Figure 14). The reef platform micro-bathymetry in Figure 14 is then reconstructed from spatial Fourier transforms of the LIDAR data expressed in terms of departures about mean depth contours at 2 meter depth intervals across the reef platform at PMRF, Kauai (Figure 7). The example in Figure 7 gives the auto spectra of these departures from the 30 m depth contour (cf. Figure 13). This procedure was repeated at 2 m depth increments between the 0 and 50 m depth contours, and the ensemble of the Fourier coefficients of these departures from the local mean depth were then lofted into a complete awa cell. The Fourier transforms allow the billions of discrete LIDAR data points to be compressed into a workable number of Fourier coefficients that represent the roughness details of the reef platforms of the awa control cells (Figure 3). With these discrete control cells, the vortex lattice algorithms can rapidly calculate ambient flow features such as bathymetric divergence over a UXO field. A discrete arrangement of these awa control cells allow numerically stable computations of erosion and transport of large UXO reef fields that surround an entire island (Figure 8).

Coordinates for the offshore and inshore UXO sites are given in Figure 15a. The inshore site is located in local water depths of 7.6 m -9.1 m (~8.4 m MSL), while the offshore site is at depths

of 15.9 m – 17.4 m (~16.6 m MSL). The channel takes several bends and curves in the cross shore direction between the offshore and inshore sites, resulting in vertical convergence and divergence of surge currents flowing over the reef top as is apparent in Figure 15b where the instantaneous current magnitude ranges from 0.9 to 1.1 m/sec; the current forcing is computed by using the coastal boundary layer currents.. This reef-induced divergence tends to make UXO mobility and more sensitive to specific location than is otherwise found on the planar beaches of collision and trailing edge coastlines.

Spatial variation in wave forcing over the reef platform and channel system is derived from refraction/diffraction analysis of directional wave measurements interpolated from an RD Instruments ADCP (Appendix B) installation at 22° 1.782'N; 159° 47.732'W near the offshore (deep) UXO site. The ADCP data were back refracted to deep water and forward refracted over the PMRF site (Figure 16). The broad-scale refraction/diffraction plot in Figure 16 was computed for the largest waves measured by the ADCP during the duration of the demonstration, February through May 2007, with a deep water wave height of 3 m, a 12 sec period, and approaching the coast from 270°, which is indicative of a swell from the post-frontal side of a distant cold front dropping south from the Gulf of Alaska. Considering that 10m high waves are not uncommon in winter months along the windward coast of Kauai, the measured wave climate at 22° 1.782'N; 159° 47.732'W near the offshore (deep) site at a depth of 16.6 m MSL must be considered unusually benign (Figure 17). This observation is enforced by the fact that the summer portion of the wave record in Figure 17 produced wave heights comparable to all but the first few weeks of winter waves. The benign wave climate during the experiment combined with the vertical divergence in the flow field over the awa (Figure 15b) produced fluid forcing that was generally insufficient to cause large displacements in the 5"/38 UXO surrogates.

While the reef produces bright spots in the refraction pattern along the west coast of Kauai at several locations north of the PMRF demonstration (Figure 16), the refracted waves display small alongshore variation around the UXO sites. The absence of local alongshore gradients in shoaling wave heights indicate very small longshore currents produced from the current prediction algorithms of the model. That assures that the predominant motion over the UXO fields will be up/down channel along the cross-shore axis of the awa. This observation is confirmed by the measured current directions given in Figure 18, which on a daily basis are from the west and south west, directed onshore along the axis of the awa (cf. Figure 15b). These currents were measured at a location of 22° 1.782'N; 159° 47.732'W near the offshore site at a depth of 16.6 m MSL. Nearfield initialization involves data base constructions and model parameterizations for nearfield model inputs. A detailed listing of these inputs can be found in

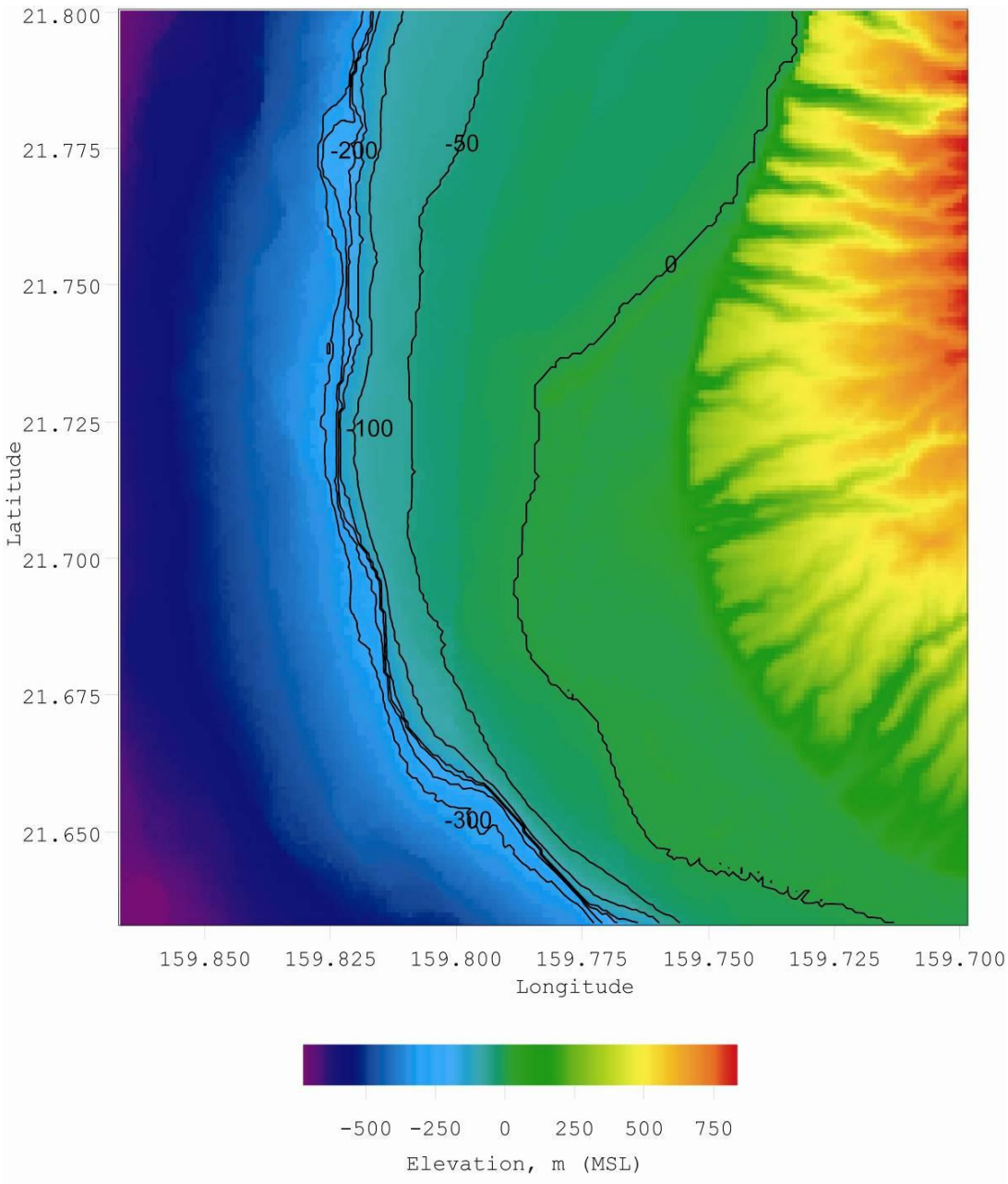

Figure 13. Composite bathymetry (meters below MSL) derived from NOS database and equilibrium profiles (Jenkins and Inman, 2006) for February–May 2007 wave conditions.

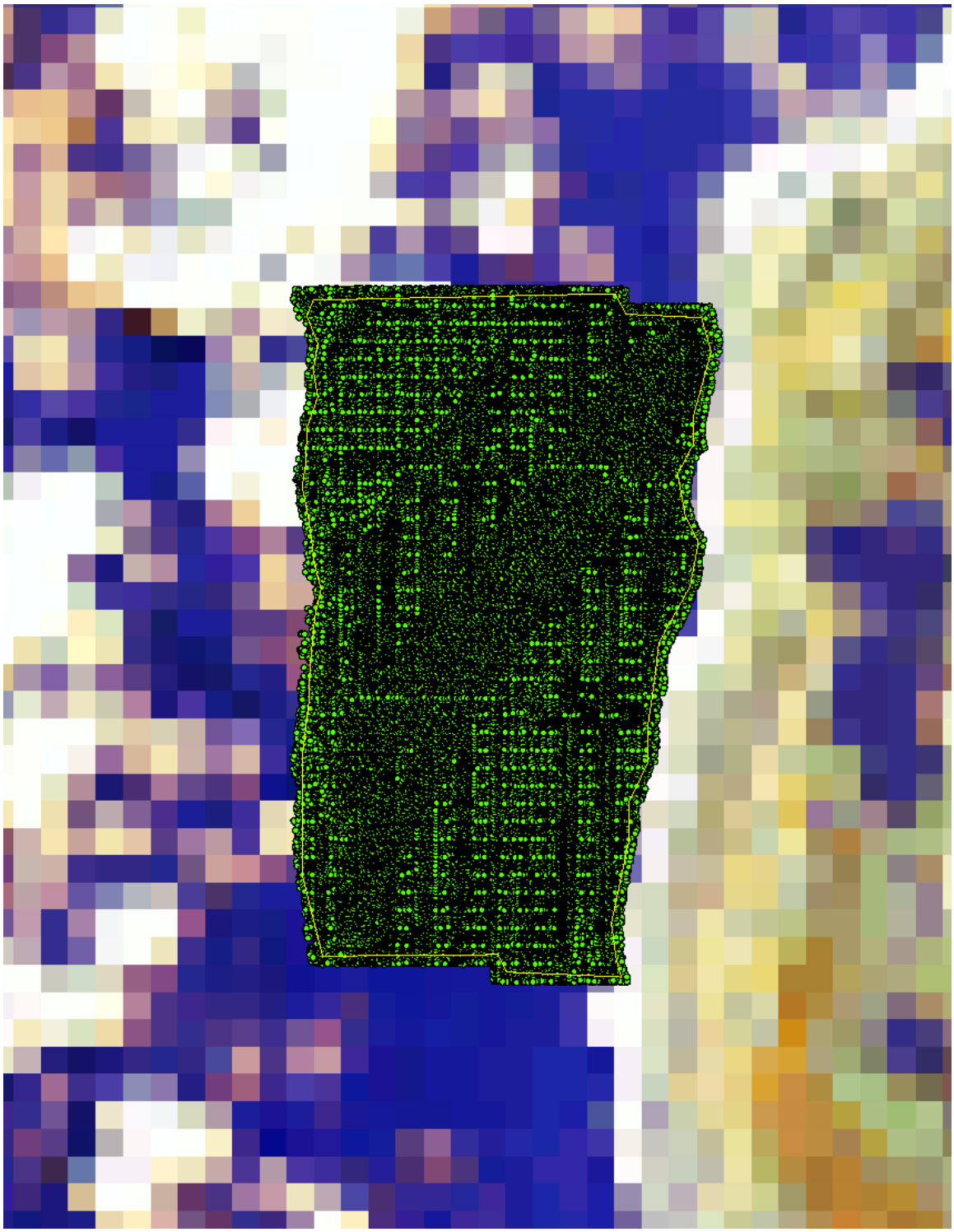

Figure 14. Sample density of LIDAR high resolution bathymetry data (green dots) over the PMRF demonstration site, including a fringing reef section.

a)

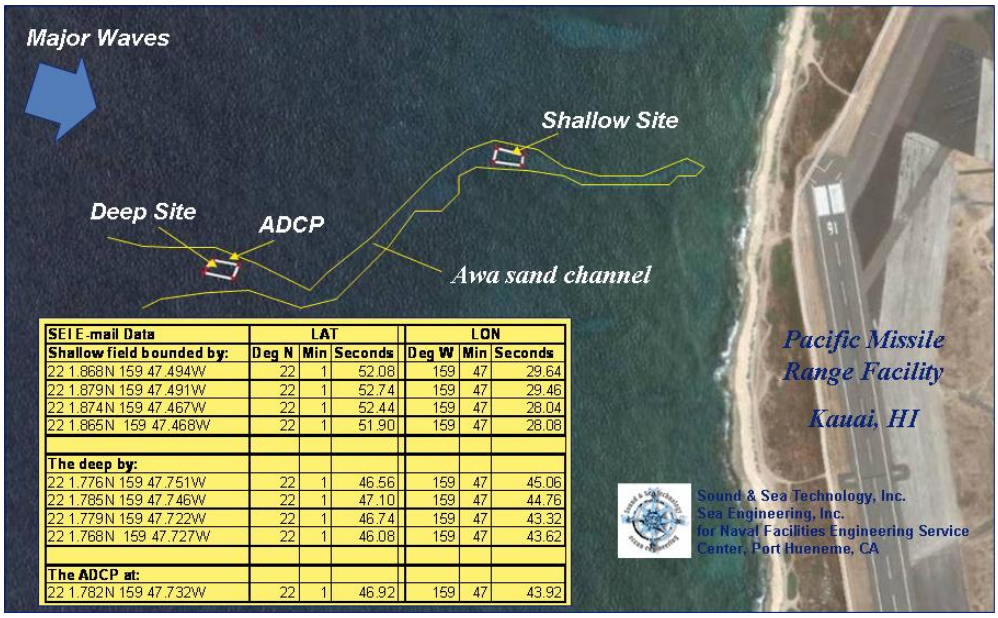

SEI E-mail Data	LAT			LON		
Shallow field bounded by:	**Deg N**	**Min**	**Seconds**	**Deg W**	**Min**	**Seconds**
22 1.868N 159 47.494W	22	1	52.08	159	47	29.64
22 1.879N 159 47.491W	22	1	52.74	159	47	29.46
22 1.874N 159 47.467W	22	1	52.44	159	47	28.04
22 1.865N 159 47.468W	22	1	51.90	159	47	28.08
The deep by:						
22 1.776N 159 47.751W	22	1	46.56	159	47	45.06
22 1.785N 159 47.746W	22	1	47.10	159	47	44.76
22 1.779N 159 47.722W	22	1	46.74	159	47	43.32
22 1.768N 159 47.727W	22	1	46.08	159	47	43.62
The ADCP at:						
22 1.782N 159 47.732W	22	1	46.92	159	47	43.92

b)

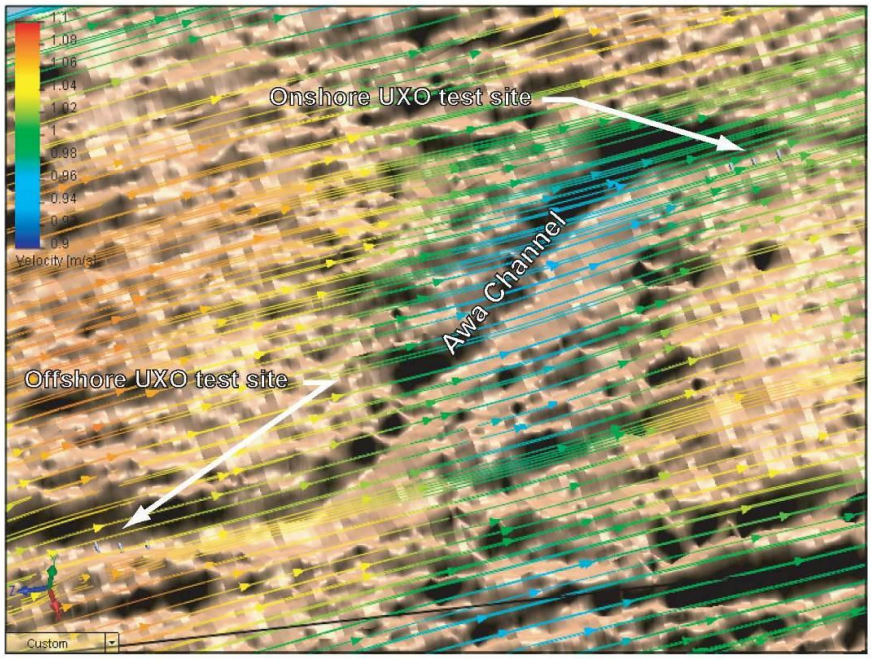

Figure 15. a) PMRF demonstration site and b) general flow over micro-bathymetry derived from Fourier decomposition of high-resolution LIDAR bathymetry showing awa channel with current magnitude scaled to color (upper left corner).

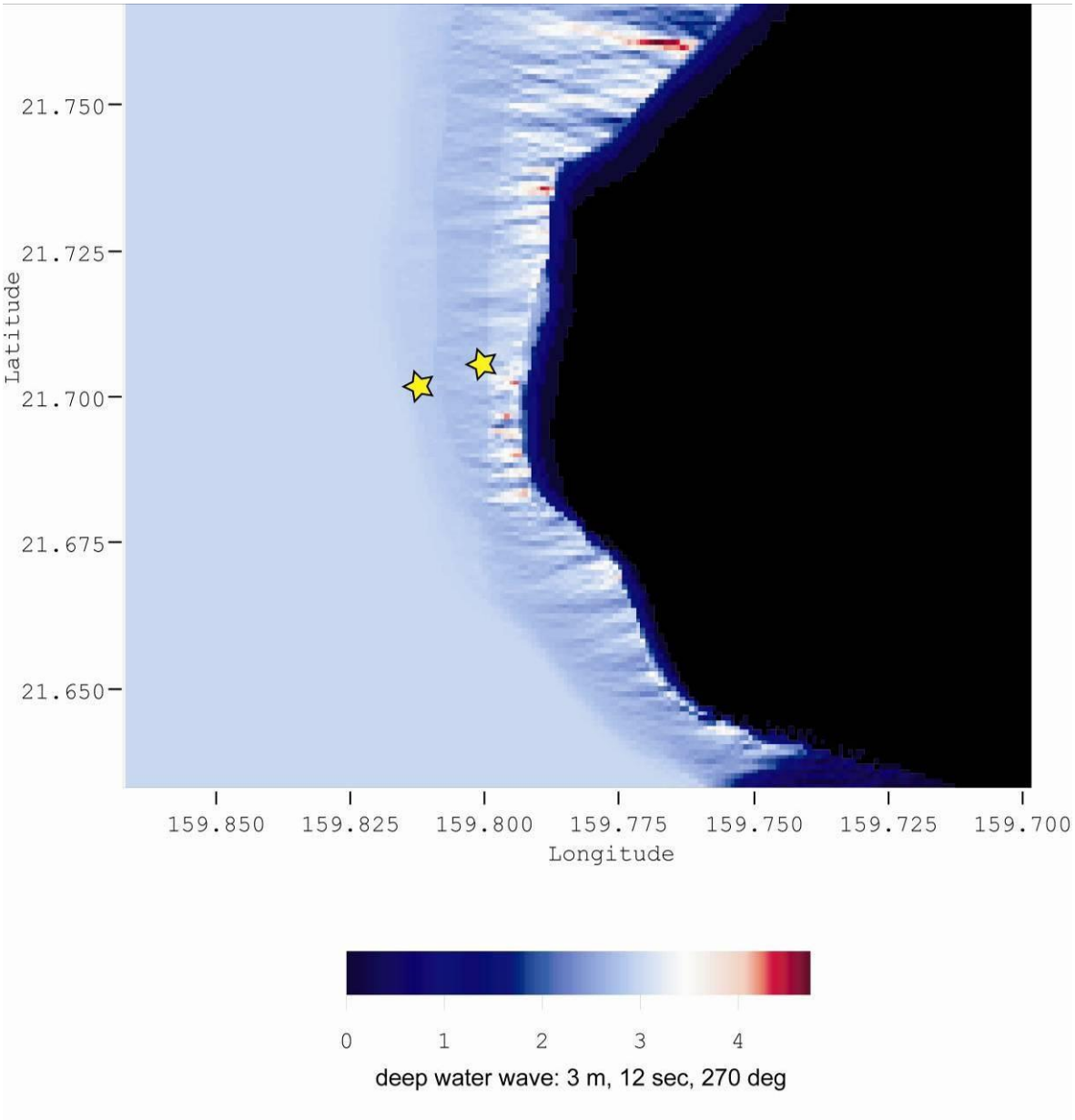

Figure 16. Refraction/Diffraction pattern at PMRF site for highest waves occurring during the duration of the demonstration; yellow stars indicate the inshore and offshore fields. Wave heights are contoured in meters according to the color bar scale.

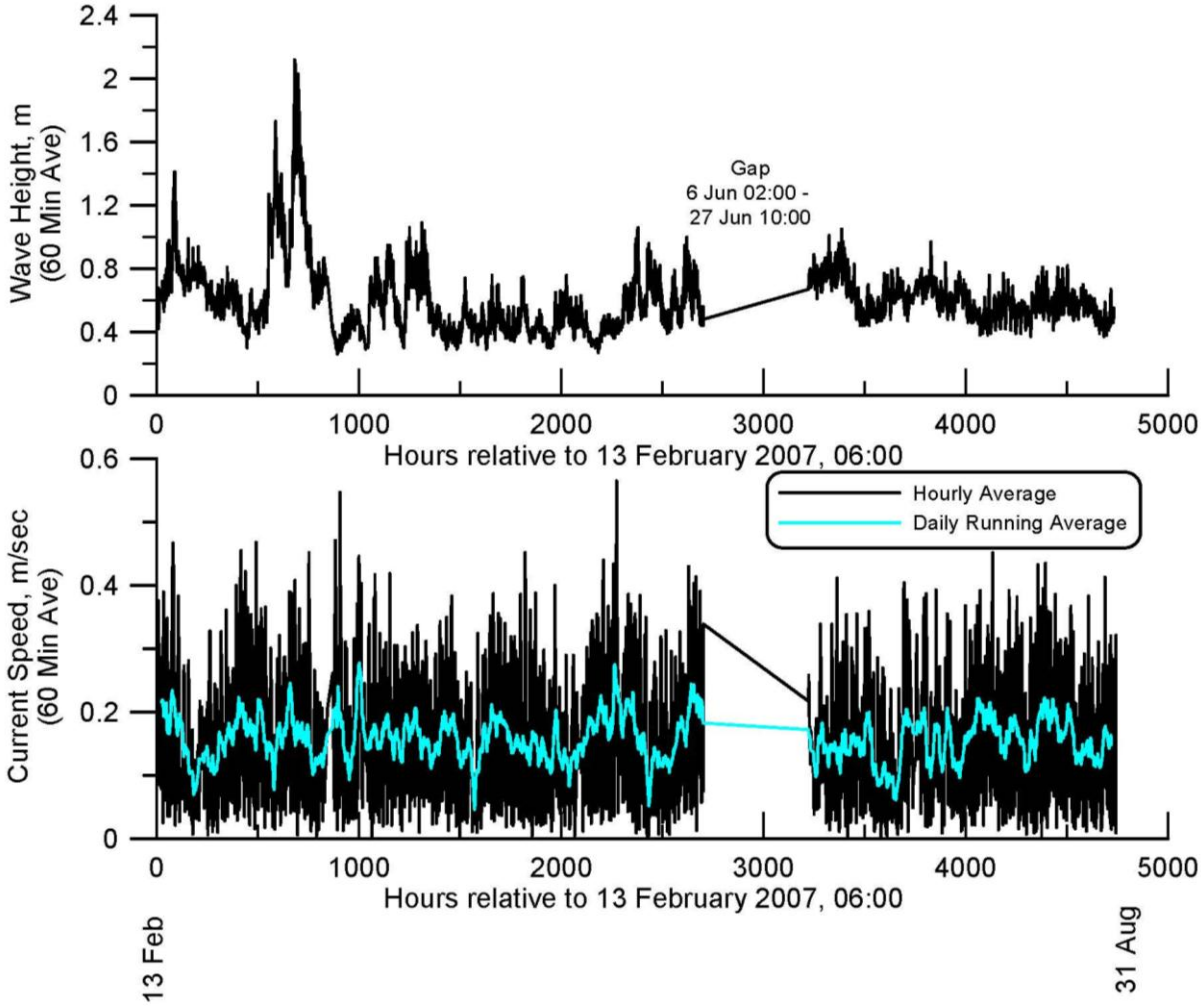

Figure 17. Wave height (upper) and current magnitude (lower) measured with an RD Instruments wave gauge and current profiling ADCP during the demonstration.

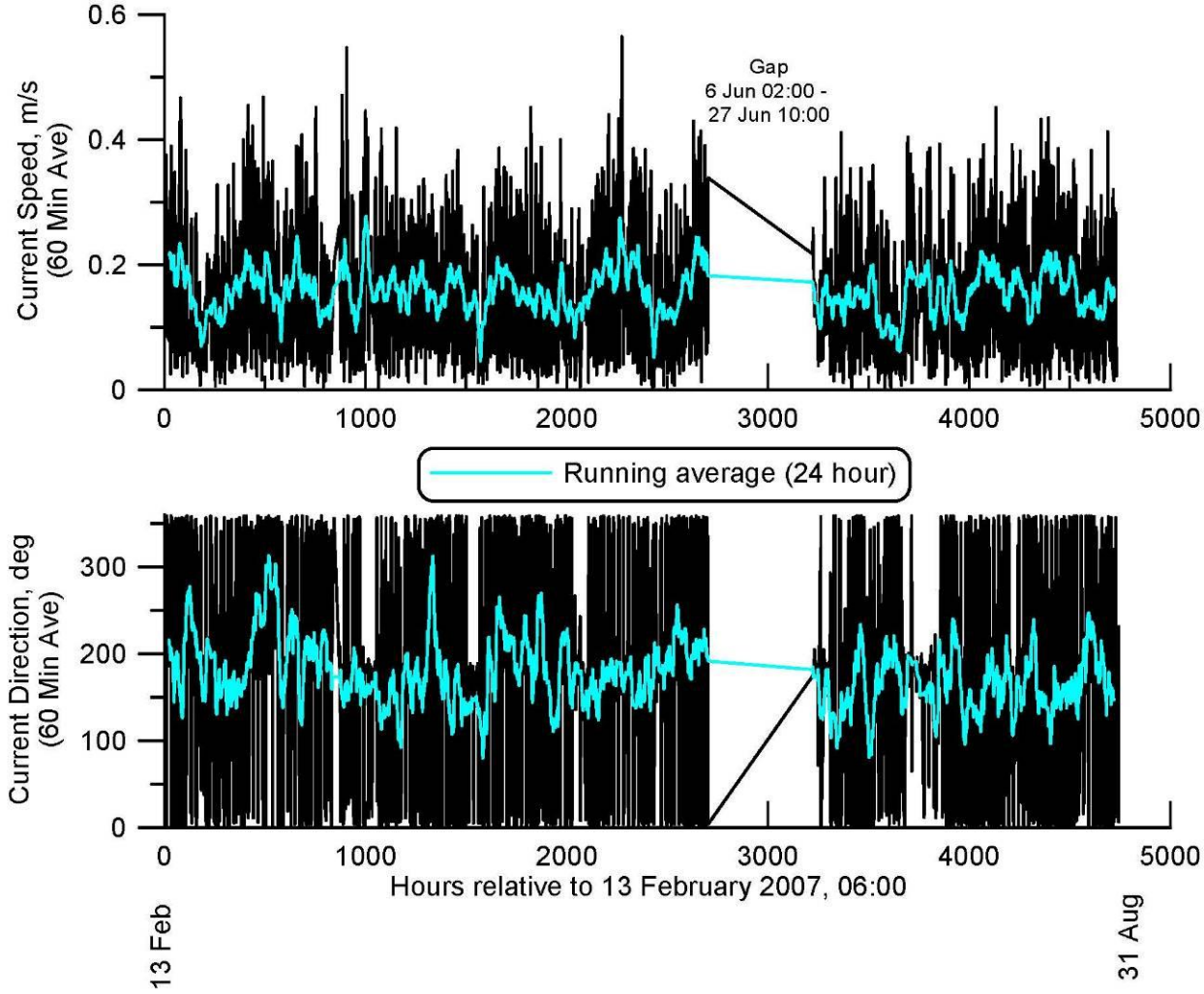

Figure 18. Current speed (upper) and current direction (lower) measured with an RD Instruments wave gauge and current profiling ADCP during the demonstration.

Wilson et al., (2008) and are reviewed here with respect to those that are either in context specific or unique to the PMRF site.

The model's nearfield grid was defined for a coarse sand bottom in the awa channel defined by 14 grain size bins according to the grain size distribution shown in Figure 19. The pie chart reveals that 70% of these channel sediments are carbonate, derived from biogenic processes and reef fragments. The carbonate sediments comprise the majority of the coarser size bins shown. The finer fractions are predominately sediments of terrigenous origin and make up about 27% of the awa sediments. Generally, mean grain sizes of sandy sediments from streams draining the leeward sides of Kauai are smaller than those of streams draining the windward sides, and the PMRF site is a leeward location. Most of the terrigenous sands along the PMRF beaches,

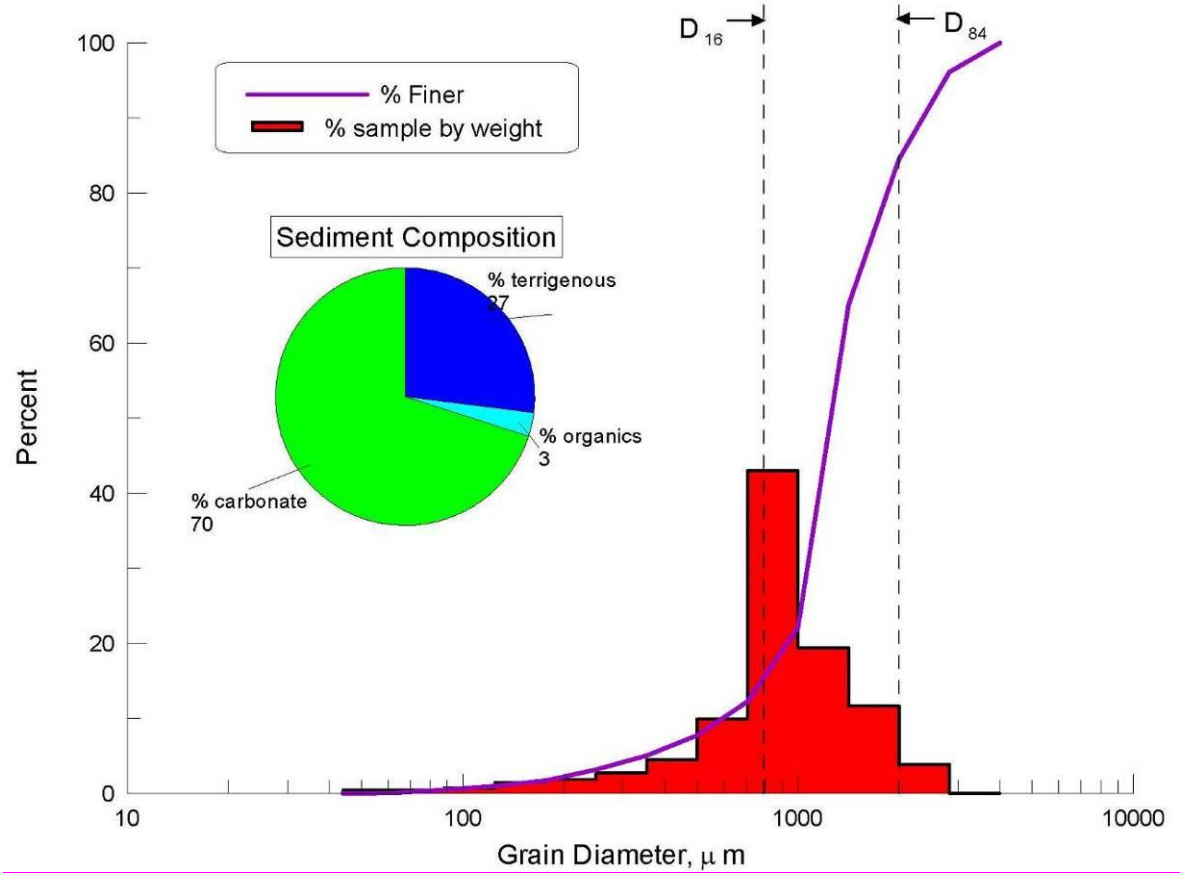

Figure 19. Grain size distribution of sediment, PMRF Field Demonstration Site, Kauai, May 2007; data provided by Sea Engineering, Inc.

stretching from the Napali Coast, south through Polihale State Park to Barking Sands, are composed of material eroded from the Kokee Highlands, remnant of a shield volcano that is dissected on its western side by numerous small intermittent streams and outwash areas. Drainage basins under erosion on the leeward side drain older geomorphic surfaces, which when combined with smaller amounts of leeward rainfall, results in a longer duration of weathering, predominantly chemical in nature, with greater fining and rounding of eroded sand-sized fractions. The small percentage of organics in the PMRF sand sample is another characteristic of the terrigenous sediment yield of the lee-side watersheds. Conversely, the sediments discharged from drainage basins on the windward side are eroded from younger, more vegetated geomorphic surfaces having steeper gradients exposed to higher rainfall, which result in larger sand-sized fractions with higher organic content. Therefore, a windward/leeward segregation of grain size parameters is probably necessary when initializing the model for generic biogenic reef environments.

Of course for this particular demonstration season, which covers the time period of late winter through spring, the dominant winds and waves are from the west, so the hydrodynamic forcing functions are typical of a windward shore.

In general, the sediment properties of the biogenic reef environment of the Kauai site presents a composite of coarse-grained carbonate and fine-grained volcanic sediments that is less well sorted and contains a higher percentage of organics (although not enough to produce granular cohesion). The lithified side walls of the channels in the biogenic reef also introduce longshore barriers to sediment transport, analogous to what is found in densely packed groin fields along well developed coastlines, Inman and Dolan (1989). These obstructions to longshore transport tend to compartmentalize the sediment transport to the along channel axis of the awas, Figure 15b.

6.2 TARGET SELECTION FOR DETECTION

Our demonstration plan used field data collected in a 2007 field experiment. Because the surrogates all became buried during the experiment, the primary method for locating the surrogates was an acoustic ranging technique utilizing embedded pingers and four transponders mounted about the perimeter of each test site. Because of reverberation concerns from the awa sidewalls at PMRF, the accuracy of this acoustic ranging technique was verified during the 13 April 2007 survey, when the acoustic range data was compared against tape measurements between each of the four transponders and the UXO specimens. The acoustic measurements showed a consistent underestimation of the range to the surrogates. This error averaged 2.5 cm and had a standard deviation of 2.0 cm. The acoustic range data was subsequently corrected for this systematic error.

Burial depths were measured by penetration probes that were inserted into the sand bed at the surrogate locations indicated by the acoustic range data. Probes were hand driven by divers and refusal depths recorded manually. All refusal depths were substantially less than the known thickness of the sediment cover in the awa, which averaged 4-5 ft (~140 cm). Consequently refusal depth was taken as equivalent to burial depth.

6.3 PARAMETER ESTIMATION

Migration and burial of each of the 24 UXO in the inshore and offshore demonstration sites at PMRF will be simulated by the VORTEX model for the wave and current forcing measured by the ADCP (Figures 17 & 18), and the grain size distribution in Figure 19. Wave forcing measured at the offshore site by the ADCP will be corrected to the inshore site using refraction/diffraction analysis like that shown in Figure 16.

Using the analytical statistical approach to error assessment, we compute the predictive skill factor, R, of the UXO migration distance, ξ, and burial depth, h, as quantified by an estimator adapted from the mean squared error. For burial depth the skill factor, R_{h}, is given in Equation 1 in Section 1.2, while the migration distance, skill factor, R_{ξ}, is given in Equation 2 in Section 1.2

6.4 CLASSIFIER : unclassified

6.5 TRAINING:

The technical lead for the overall analysis must be an engineer whose technical background includes a familiarity with ocean processes and the general principles of computer modeling, as well as the general principles of data collection on the types and amounts of human activity in coastal areas. This lead engineer also needs to be experienced in basic project management and be a liaison with the site UXO manager as well. In order to conduct the entire risk analysis, the lead engineer must be able to use ESRI ArcGIS software and the Microsoft Excel spreadsheet program, and be familiar with the overall processes described in the AGD [7].

The lead oceanographer/coastal scientist must be skilled in locating the sources of environmental data (e.g., waves, currents, bottom types, etc.), acquiring those data sets for the time periods of interest, and formatting those data to serve as inputs to the MM. The lead scientist also needs a general understanding of coastal processes, basic hydrodynamics, and related ocean engineering technologies in order to assist in setting up the model inputs and understanding its outputs.

Finally, the MM itself needs to be run by a person skilled in the using basic FORTRAN programs for computer modeling purposes. The MM is a FORTRAN program than will run on a variety of professional-grade laptop or desktop computers, so the user must be capable of compiling and running FORTRAN programs.

Of course the above list of skills and abilities may be provided by various possible combinations of individuals. During various stages of the MM development effort, the analysis work was conducted by as few as two and as many as four to six persons.

The detailed requirements for software, computer hardware, and user skills are described in the User's Manual by Garood, (2008).

6.6 DATA PRODUCTS

Prior to considering the nearfield influence of the channel walls on the burial migration response of the UXO at PMRF, we test the performance of the shape lattice files using the coarse-grained carbonate sediment distribution from Figure 19 on a planar sedimentary bed typical of the floor of an awa channel, (with no extraneous irregularities in either the stream-wise or cross stream directions). Figure 20 presents the modeled instantaneous vortex and scour field produced from an initially planar bed with the surrogate's major axis aligned transverse to a train of monochromatic waves with 12 sec period propagating from right to left. The wave oscillatory velocity amplitude at the top of the bottom boundary layer is 96 cm/sec, which corresponds to the super-critical transport regime for the grain size distribution in Figure 19. In this regime, flow separation with a basal vortex is observed on the down-wave (shoreward) side of the round, inducing formation of a scour hole. As the scour hole deepens, the round slips or rolls into the

hole, resulting in migration and burial through what is known either as a *scour and slip* or *scour and roll* burial sequence. At the instant the flow field in Figure 20 was calculated, the burial/ migration progression of the UXO had advanced to a state of 64% burial in the upper panel and 67% burial in the lower panel.

At an advanced stage in the burial/migration progression referred to as *lock-down*, burial becomes sufficiently extensive that migration is no longer possible, see Jenkins and Wasyl (2005), Conner and Wang (1973), and Jenkins and Wasyl (1990). For excitation by monochromatic waves of various periods and heights, the distance a UXO migrates before lock-down sets up has a monotonic dependence on a parameter of dynamic similitude referred to as the Shield's parameter. This parameter, which combined with the grain Reynolds number, is now recognized as a reliable predictor of whether or not a grain will erode, is a measure of the intensity of environmental forcing relative to the inertia of the UXO. Explicitly, the Shields parameter, Θ, or dimensionless shear stress, represents a ratio between the hydrodynamic forces (i.e., drag and lift) acting to move the UXO and the gravitational forces acting to restrain and bury the UXO:

$$\Theta = \frac{u^2}{g'D} \qquad (7)$$

where u is the oscillatory wave velocity amplitude at the top of the bottom boundary layer, D is the basal diameter of the UXO, g is the acceleration of gravity, $g' = g\,\Delta\rho / \rho$ is the reduced gravity, and $\Delta\rho$ is the density difference between the UXO and seawater density, ρ. Planar bed simulations of the type shown in Figure 20 indicate that UXO mobility increases with increasing wave velocity (proportional to wave height and inversely proportional to wave period), with decreasing caliber of the UXO, or with decreasing density (specific gravity) of the UXO. Planar bed simulations using the wave velocities measured at PMRF (Figure 18) reveal that with the exception of a few storms early in the deployment, the Shields parameter was predominantly in the sub-critical range of $\Theta \leq 7$; see Jenkins and Wasyl (2005), Conner and Wang (1973), and Jenkins and Wasyl (1990) for more detailed references on sub- and super-critical transport regimes. As an indicator of the stability of a particle, sub-critical values of the Shield's

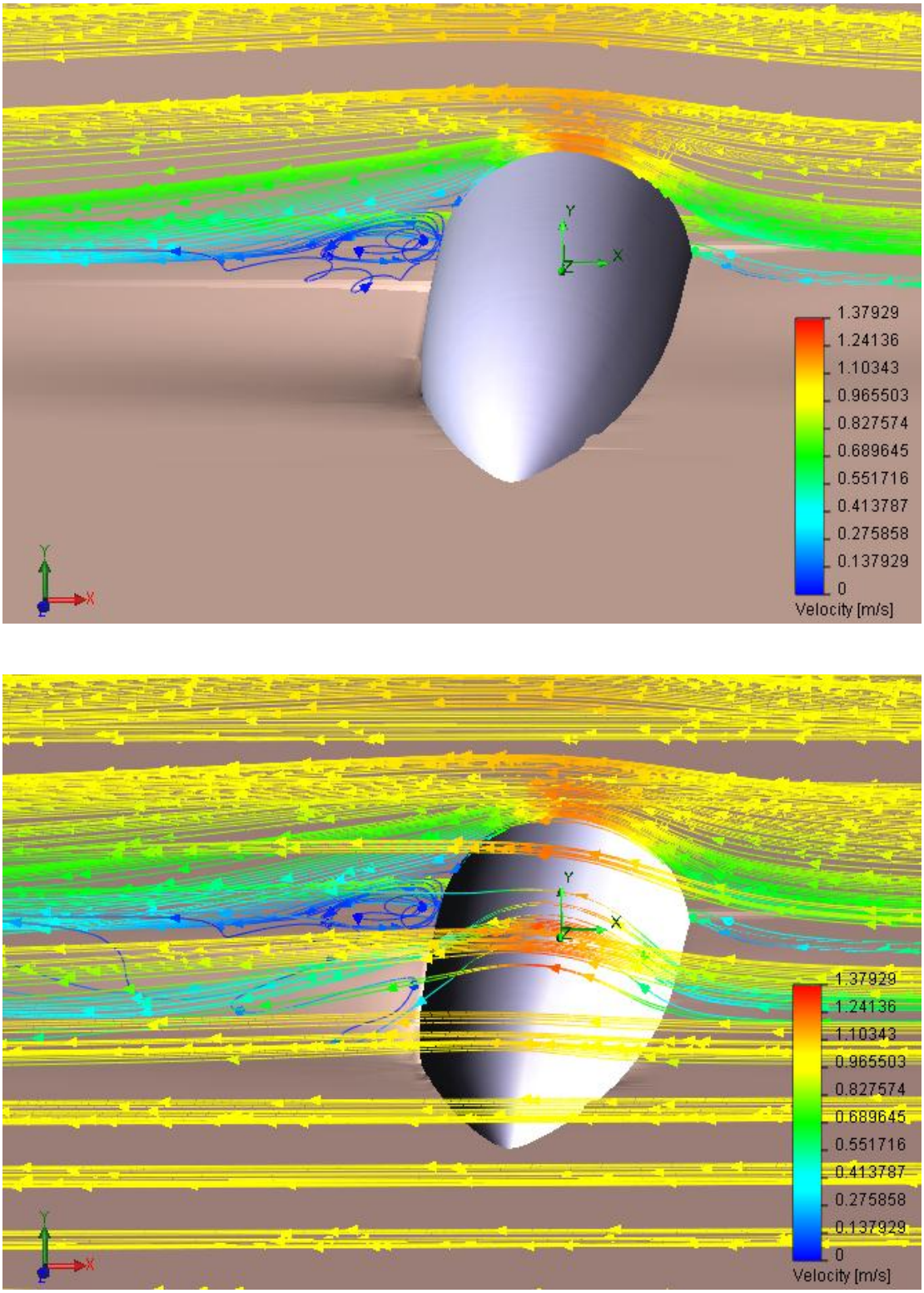

Figure 20. A simulation of the vortex and scour field around a 5”/38 UXO surrogate buried in the sediment cover along the floor of an awa channel.; 64% burial upper, 67% burial lower.

parameter indicate that very little movement of the UXO occurs because hydrodynamic moments associated with drag and lift are insufficient to overcome the restraining moments due to gravity. The reasons this condition occurred during the PMRF experiment are due to a combination of benign wave climate and vertical divergence of the wave induced surges and streaming over the reef channels.

Awa side wall influence on the nearfield flow dynamics are one of the most unique features of the biogenic reef environments that was not previously encountered at the other UXO MM field test and demonstration sites that took place on collision and trailing edge coasts. Both the LIDAR data in Figure 13 and its lofting from Fourier decomposition Figure 15b, as well as underwater photos of the demonstration site (Figure 17) reveal that the channels introduce both curvature effects and roughness effects on the flow of wave surges and wave induced streaming.

These flow disturbances undoubtedly produce eddies that could induce additional vortex scour to the nearfield of the UXO beyond that induced directly by the UXO shape. This increases the modeling challenge by forcing us to expand the nearfield grid to include the prominent features of awa side walls in the immediate vicinity of the UXO site. It is neither practical nor computationally efficient to extend the 3mm resolution of the shape lattice of the UXO across tens of meters of adjacent awa channel sidewalls. A coarser-scale lattice of the awa wall geometry was nested around the UXO shape lattice and embedded it inside the farfield grid of the reef platform. This merely required replication of existing code to create a secondary nested grid inside code module #13 of the model architecture. Grid resolution was set at 0.5 m for the secondary nested grid of the sidewall geometry around the UXO field.

The upgraded awa-cell MM using synthetic micro bathymetry is capable of predicting the same flow details in the awa channels that were simulated previously using the high resolution LIDAR data directly (Wilson, et. al., 2008b). Figures 22 & 23 shows an awa-cell upgraded MM simulation of the curvature effects of the awa in the neighborhood of the offshore UXO field. Vertical divergence of the flow field between the top of the reef and the bottom of the channel is accentuated over the UXO field because it is sited on the inside of the channel bend for onshore directed surges and wave-induced streaming. There is also a tendency for the near channel bottom flow to develop secondary meanders that can introduce cross-flow components over the UXO surrogates. The primary consequence of these secondary flows and vertical divergence phenomena is to promote sub-critical flow conditions over the UXO that retard migration while promoting burial.

The second major influence of the awa sidewalls comes from the encroaching shoulders of the sidewalls into the sand channel. These shoulders cause large scale disturbances along the major axis of the primary flow channel. These disturbances in turn can generate rather large scale eddies, much larger than those shed by the relatively small body radius of the UXO. In Figure 23, the nested secondary grid derived from the lofting the Fourier decomposition of the LIDAR micro-bathymetry was used to simulate these large-scale channel vortices near ten of the twelve UXO in the offshore field. This simulation is representative of the sub-critical channel surges recorded by the ADCP shown in Figure 18 for which $u \approx 0.4$ m/sec. In spite of the low velocities in the bottom of the channel, the encroaching sidewall is able to excite a large channel eddy with a high vertical velocity component, $w \approx 0.2$ m/sec.

Vertical velocities of this magnitude in the nearfield of the UXO are capable of excavating large scour depressions into which the UXO can readily roll. Thus, large external channel eddies can facilitate UXO migration even when the Shields parameter remains sub-critical.

Figure 21. The awa channel's sidewall intersects the carbonate seabed at the PMRF site; note the wall surface roughness and curvature of the lithofied reef structures (photo: SEI).

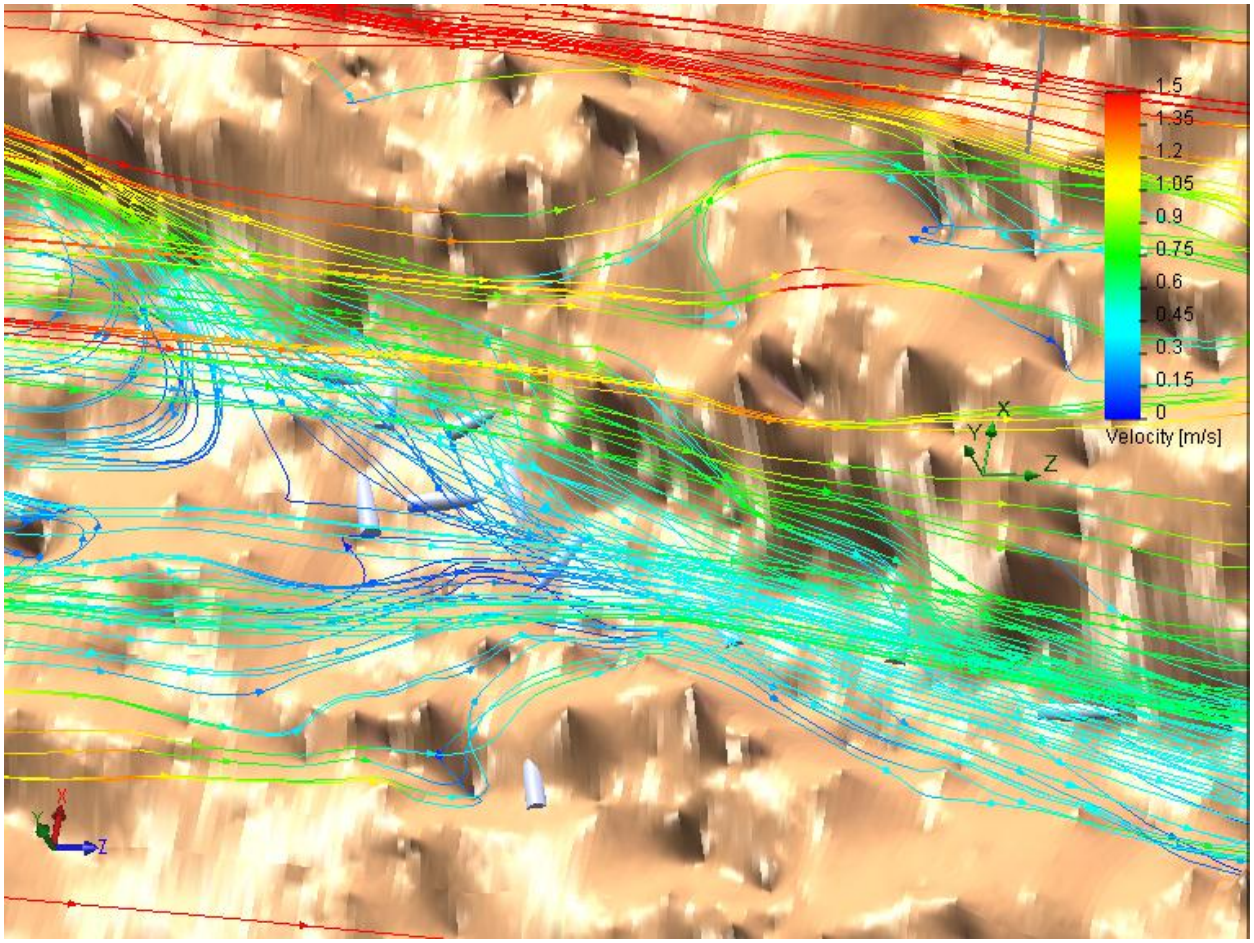

Figure 22. Upgrade awa-cell MM simulation of vertical divergence and secondary flows induced by the side walls of the awa channel in the vicinity of the demonstration site at PMRF, Kauai**.** Reef platform micro-bathymetry based on Fourier decomposition of LIDAR data.

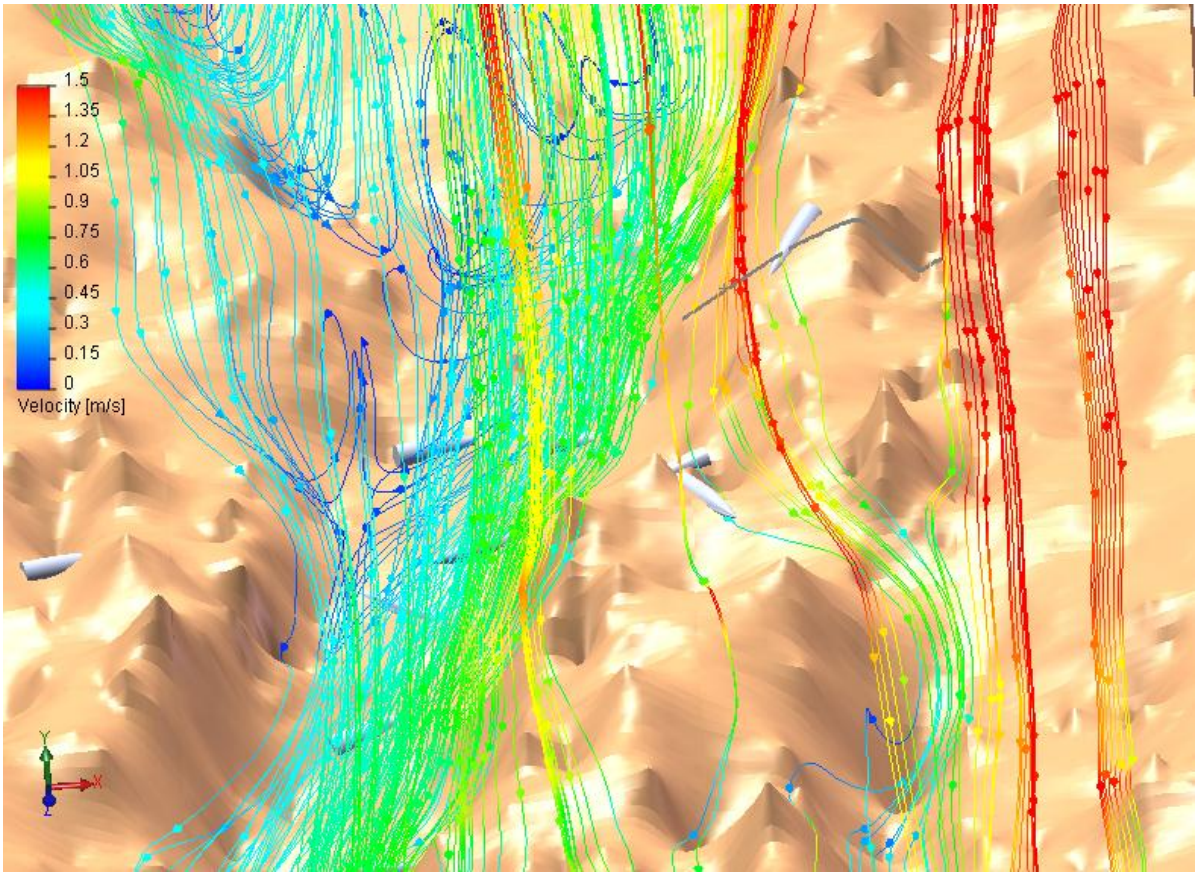

Figure 23. A simulation of the large-scale eddies induced over UXO by the expansion and contraction of encroaching shoulders of the awa sidewalls in the vicinity of the demonstration site at PMRF, Kauai. Reef platform micro-bathymetry based on Fourier decomposition of LIDAR data.

Migration and burial of each of the 24 UXO in the inshore and offshore sites at PMRF (Figures 9 & 10) were simulated by the awa-cell upgraded MM for the wave and current forcing measured by the ADCP and the grain size distribution. Wave forcing measured at the offshore site by the ADCP was corrected to the inshore site using refraction/diffraction analysis. The vertical divergence and large scale eddies induced by the awa side wall geometry was computed separately for the offshore and inshore sites. These simulations were based on the synthetic bathymetry generated by the Fourier decomposition of the high resolution LIDAR bathymetry (cf. Figure 7).

Figure 24 gives the awa-cell upgraded MM simulated migration and burial rates during the entirety of the PMRF experiment averaged over the 12 surrogates in the inshore test site. Blue crosses indicate the individual simulations of migration for each wave measurement in Figure 17 that caused some increment of migration to occur.

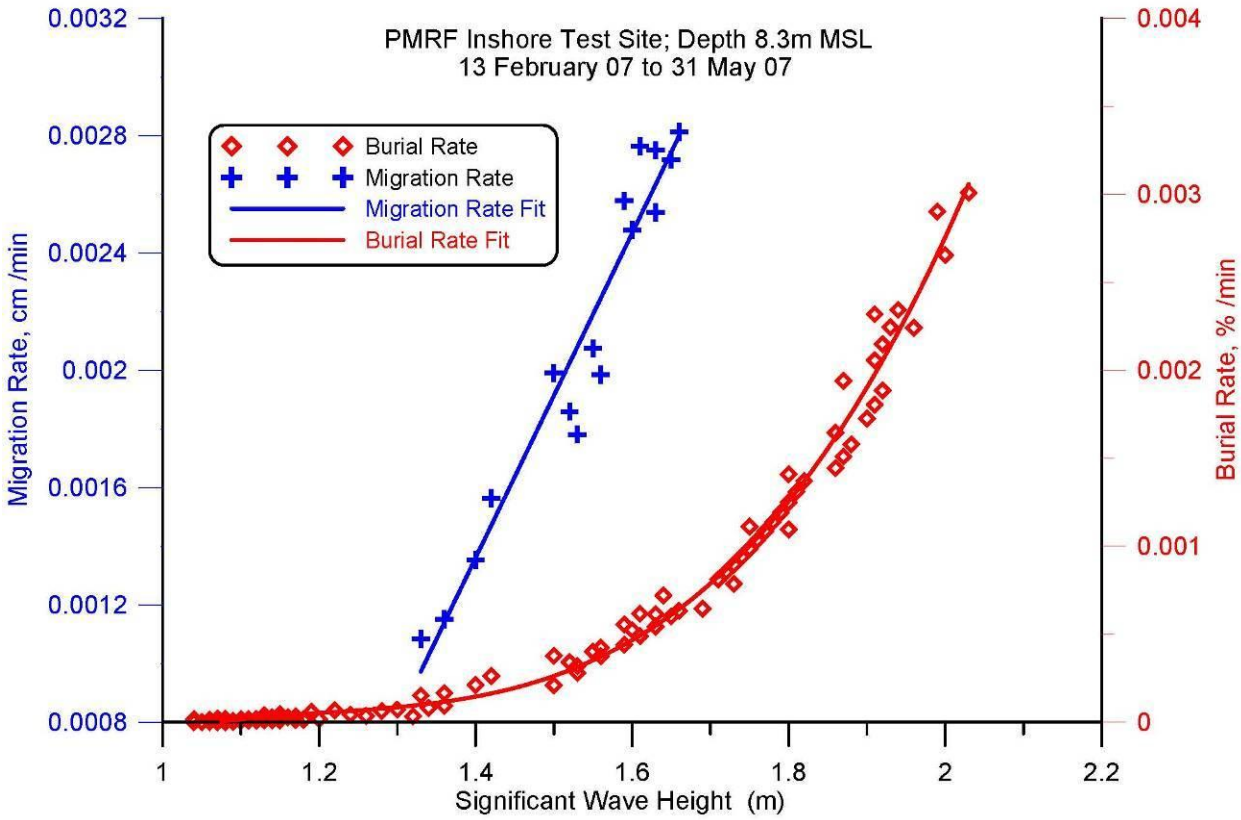

Figure 24. Upgraded awa-cell MM simulation of migration and burial rates of 5”/38 UXO surrogates at the inshore site at 8.3m depth as a function of measured wave heights.

Similarly, the red diamonds in Figure 24 give simulations of burial for each wave measurement that caused some increment of burial to occur. Here burial is expressed in terms of burial depth as a % of the diameter (caliber) of the round. The obvious difference in the numbers of blue crosses versus red diamonds indicates that relatively few wave events caused the rounds to actually move. This reflects the fact that the surrogates became completely buried under many centimeters (20-50 cm) of overburden, whereas migration is halted by lock-down that sets up while the surrogates are still only partially buried. The solid blue and red lines in Figure 24 are best-fit polynomials to the simulated points generated by the individual wave events. No model realizations are shown for waves heights less than 1m because smaller waves produce bottom velocities at 8.3m depth that are less than the threshold of motion of the median grain size of sediment. .

The scatter about each of the fit lines in Figure 24 is due to the wave period dependence of migration and burial rate, which for these shallow water conditions is second order relative to wave height dependence. From this outcome, the average threshold of migration for the 5”/38 UXO surrogates appears to be at a significant wave height of approximately 1.3 m at water depths of 8.3 meters. From this threshold, migration rates increase rapidly with increasing wave height, roughly tripling with an increase of only 0.3 m in wave height. While this process

occurs, burial rates increase at first slowly, from negligibly small rates at threshold of migration wave heights, to rapidly increasing rates as burial lock-down is approached, which takes place in the neighborhood of significant wave heights of 1.6 m. Maximum migration rates are approximately 0.0028 cm/min. Beyond burial lock-down, the burial rate continues to accelerate until total burial is achieved, when the scour burial mechanism vanishes and only farfield burial from bottom profile change can effect any subsequent burial. Scour burial maximums for the 5”/38 surrogates occur at significant wave heights of approximately 2m at a rate of 0.003 % per minute, though this result is somewhat controlled by the particular sidewall effects of the awa at the inshore site.

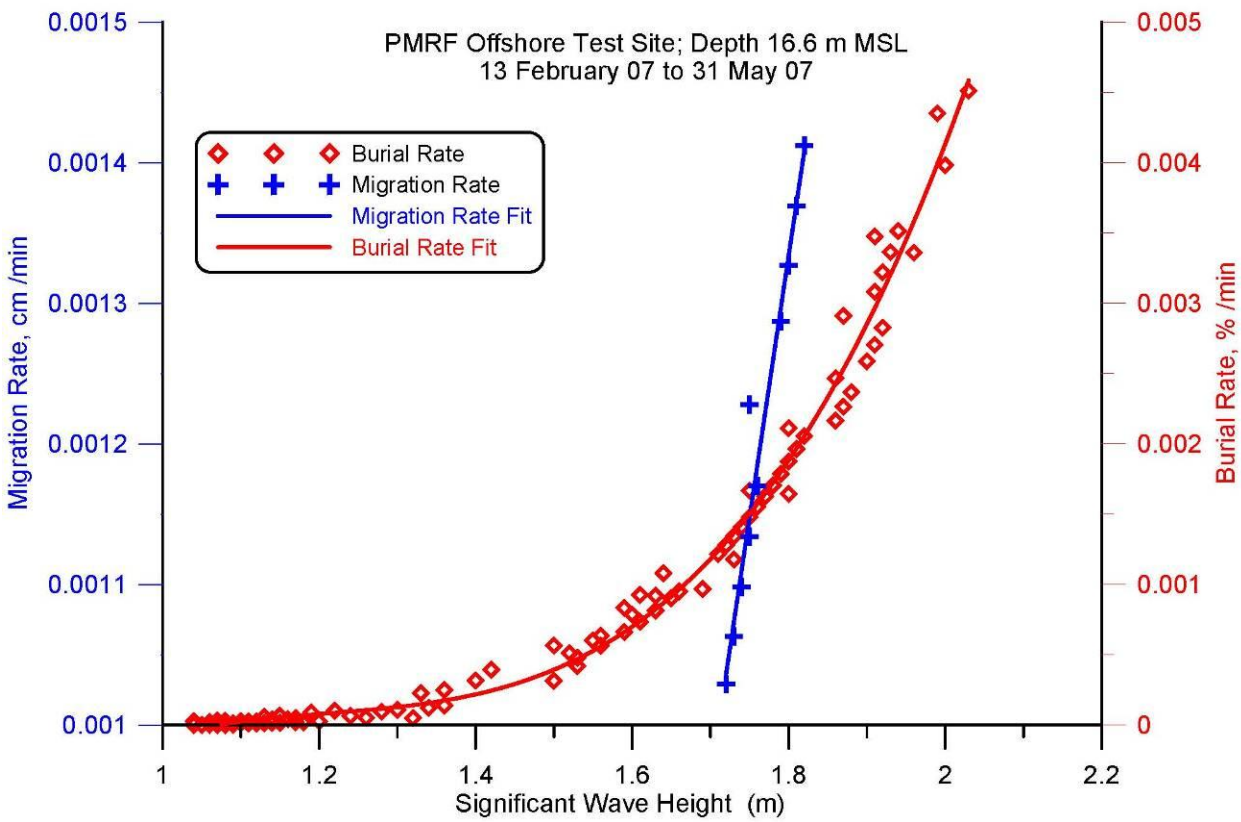

Figure 25. Upgraded awa-cell MM simulation of migration and burial rates of 5”/38 UXO surrogates at the offshore site at 16.6m depth as a function of measured wave heights

Figure 25 provides the average simulated migration and burial rates for the 12 surrogates in the offshore test site at PMRF at 16.6m mean depth. Again, blue crosses indicate the simulations of migration for each wave measurement that caused some increment of migration to occur; and, red diamonds give simulations of burial for each wave measurement that caused some increment of burial to occur; where burial is expressed in terms of burial depth as a % of the diameter of the round. For clarity, the axes in Figure 25 were re-scaled for the differences in dynamic range. Upon comparing Figure 25 with Figure 24, it is apparent that the threshold wave height for migration of the UXO surrogates in the offshore array is substantially higher (increasing to a significant wave height of 1.7m), primarily due to depth attenuation of the wave orbital velocity

in the deeper waters of the offshore site. For the same reason, there are fewer numbers of wave events that induce migration at the deeper offshore site; compare numbers of blue crosses in Figure 24 with those in Figure 25. However, once the UXO surrogates in the offshore array begin to move, their migration rate increases rapidly, increasing 140% with a 0.1m increase in wave height above threshold of migration and reaching a maximum migration rate 0.0015 cm per minute at significant wave heights greater than 1.8m. This maximum migration rate is approximately one half that of the surrogates in the inshore array and occurs at a substantially higher significant wave height (1.8 m vs. 1.6 m), again because of depth attenuation in orbital wave velocities. At their maximum migration rate, surrogates in the offshore array are burying at 0.0019 % per minute while surrogates in the inshore array are burying at approximately 1/3 that rate, or 0.0005 % per minute. Thus, surrogates in the offshore array reach burial lock-down sooner and thereby have less time to migrate off-station.

Maximum burial rates of surrogates in the offshore array are 0.0045 % per minute at a significant wave height of 2m, or about 50% faster than for surrogates in the inshore array. While this may be partly understood in terms of slower migration rates going hand-n-hand with higher burial rates, it is not intuitive when considering that burial rates tend to increase with orbital velocity while orbital velocity decreases with increasing depth. Our interpretation of this specific and somewhat paradoxical result is that the large scale eddies induced by the awa sidewalls are more active and well developed at the offshore site, and this action increases scour burial rates induced by relatively smaller orbital velocities.

7.0 PERFORMANCE ASSESSMENT

The awa-cell upgraded MM performance is tested against data from two separate UXO sites deployed in an awa in the nearshore of PMRF, Kauai, HI, between 13 February and 27 June 2007. The details of the lay-down pattern of 12 each UXO surrogates of a 5”/38 naval rounds that were deployed at each of the two test sites (24 surrogates in total) is shown in Figures 9 & 10. At both the offshore and inshore sites, surrogates were laid in two along-channel rows 30 ft apart at 30 ft spacing with six surrogates in each row. The surrogates were deployed on 13 February 2007 and thereafter the position and burial depths of some or all of the surrogates was measured on 22 February, 2 March, 21 March, 13 April, 9 May, 31 May, and 27 June 2007.

Two approaches are applied to assess the predictive skill of the quantitative awa-cell upgraded MM predictions of the magnitude of migration and burial of UXO surrogates at PMRF. With the first approach, probability density functions are produced for migration and burial magnitudes predicted by the model and compare them with the probability density functions assembled from the observed outcomes of the experiment. Because the experimental outcomes involve small ensemble statistics, we merge the results of all 24 surrogates from the inshore and offshore demonstration sites into a single set of probability density functions. By the second approach, we a compute predictive skill factor, R, is computed from the mean squared error between the predicted and measured outcomes.

To generate awa-cell upgraded MM predictions of migration and burial magnitudes from the rates in Figures 24 and 25, we integrate those rates (as computed for each surrogate) over the

duration of each migration or burial rate-inducing wave event. Figure 26a presents the probability density function (histogram) of the predicted UXO migration distances for all 24 surrogates at PMRF. A total of 312 realizations of migration distance were constructed from the rates (blue crosses) in Figures 24 and 25. These are contrasted with the 24 measured outcomes of migration distance that make up the measured probability density function in Figure 26b. The peak, spread and shape of the predicted and measured probability density functions of migration in Figure 26 are quite similar, although the granularity of the measured distribution is much coarser owing to the relatively small numbers of observations. The bin width for the migration distance histograms are 10 cm with a migration distance error of +/-5 cm. Generally, both distributions give a mean migration distance of a little more than 1 m and a maximum migration on the order of 3-4 m. In particular, the upgraded awa-cell MM predicted a mean migration distance of 1.25 m as compared to a measured mean migration of 1.45 m from the ensemble of 24 UXO surrogates. For the extremes, the both the measured and modeled minimum migration distance was 0 m, occurring at the offshore site, while the upgraded awa-cell MM predicted a maximum migration distance of 3.0 m as compared to a measured maximum migration of 4.0 m occurring at the inshore cluster of 12 UXO surrogates. In both the predicted and observed outcomes, migration almost exclusively occurred along the major axis of the awa channel.

Figure 27 compares the awa-cell upgraded MM predicted versus measured probability density functions for UXO burial at PMRF during the period 13 February to 27 June 2007. The larger numbers of burial-inducing wave events in Figures 24 and 25 produced nearly 10 times more realizations (3,806) of predicted burial in Figure 27a. The comparison with measured probability density function for burial in Figure 27b is quite satisfying, despite the small ensemble of measured statistics. Again, the peak of the measured distribution, its breadth, and shape are all faithfully mimicked by the modeled distribution in Figure 27. The bin width for the burial depth histogram is 1 cm with a burial depth error of +/- 5 cm. Mean burial depths are approximately 20 cm while maximum burial depths are 40-50 cm. The upgraded awa-cell MM predicted a mean burial depth of 17.5 cm as compared to a measured mean burial depth of 20.5 cm from the ensemble of 24 UXO surrogates. For the extremes, the both the measured and modeled minimum burial depths was on the order of 8 cm, occurring at the offshore site, while the upgraded awa-cell MM predicted a maximum burial depth of 50.0 cm as compared to a measured maximum burial depth of 40.0 cm occurring at the inshore cluster of 12 UXO surrogates.

Based on the predicted versus measured outcomes in Figures 26 & 27, the skill factor for migration (Equation 1, Sec 1.2) at PMRF was calculated at $R_\xi =$ 0.88 and $R_h =$ 0.90 for burial (from Equation 1, Sec 1.2). For coastal processes modeling and mine burial prediction in particular, any skill factor in excess of 0.8 is considered to be a good result (Gallagher et al. 1997).

The predictive skill factors achieved by upgraded awa-cell MM at PMRF using the synthetic micro bathymetry lofted from spatial Fourier decomposition LIDAR data are comparable to the predictive skill previously achieved using the high resolution LIDAR data directly on a relatively smaller area of reef (cf, Wilson et.al., 2008b) The upgraded MM is able to achieve this comparable performance at significantly greater numerical efficiency and stability, allowing it to model the fate and transport of significantly greater numbers of UXO over larger UXO fields.

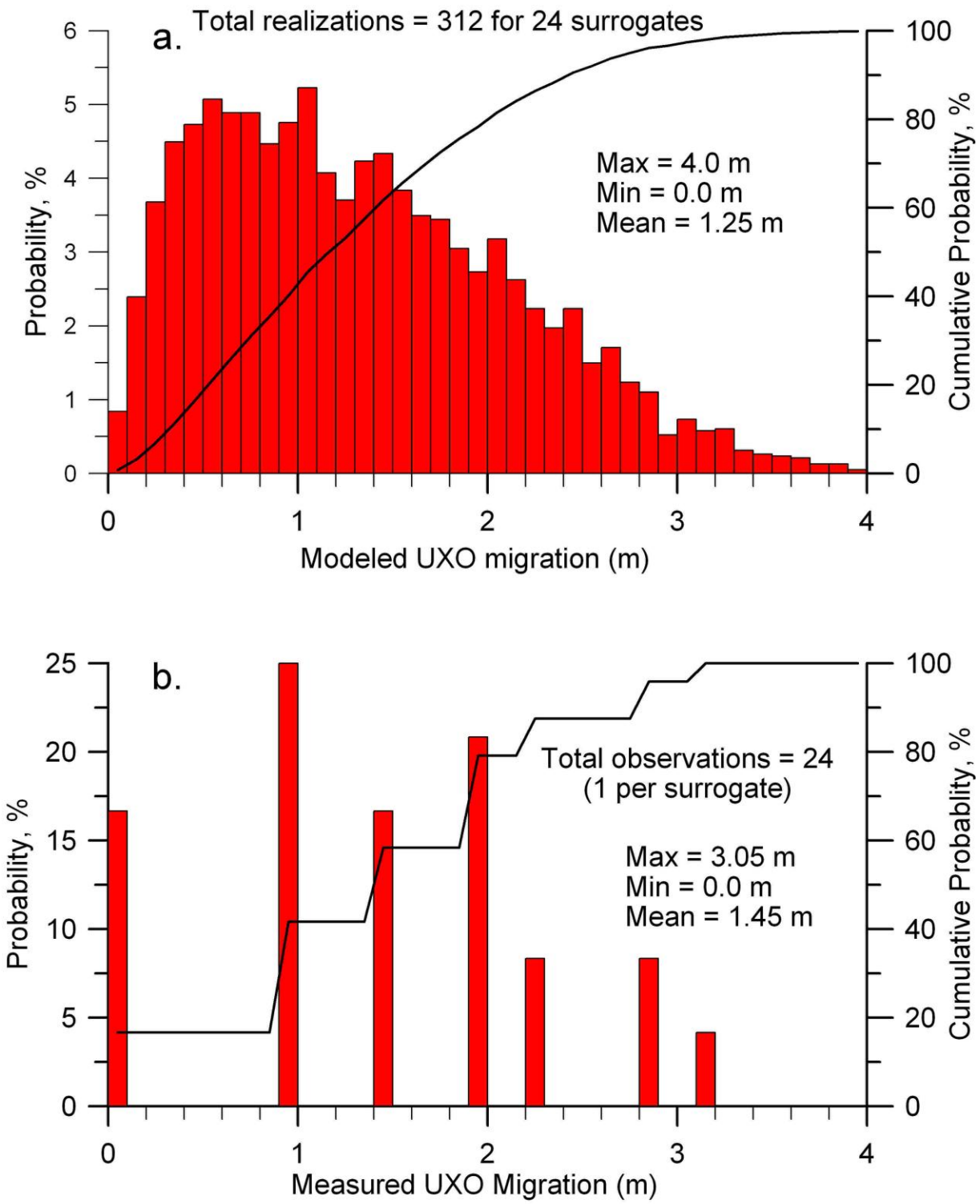

Figure 26. Comparing Upgraded awa-cell MM Modeled probability density functions for UXO migration in panel-a versus the measured probability density function of all surrogates during the demonstration in panel-b.

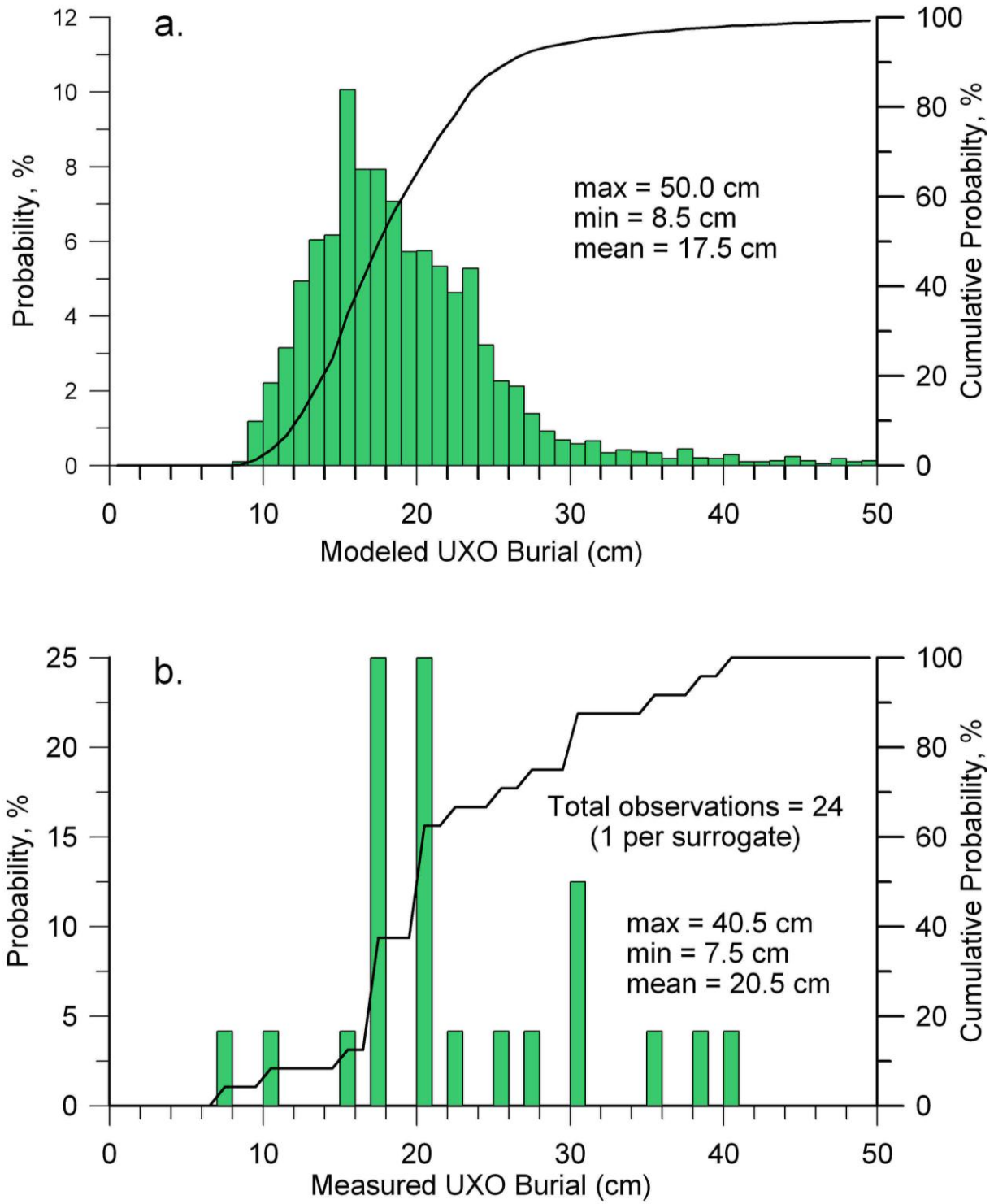

Figure 27. Comparing upgraded awa-cell MM modeled probability density functions for UXO burial in panel-a versus the measured probability density function for all surrogates during the demonstration in panel-b.

Whereas the early MM code reported in Wilson et al, 2008 modeled fate and transport of only 24 UXO surrogates, the upgrade awa-cell MM is capable of modeling the simultaneous migration and burial of as many as 500 UXO.

Alternatively, the accuracy of predictions from upgraded awa-cell MM based the Fourier reconstructed reef platform roughness (mode-2) versus the earlier approach using the high resolution LIDAR bathymetry after Wilson et al., 2008 can be quantified by the usual coefficient of determination, r^2, calculated by:

$$r^2 = \frac{SSe}{SSe - SSr} \tag{8}$$

where SSe is the residual sum of squares given by the sum of the squares of the difference between the predicted and observed values, and SSr is the regression sum of squares given by the sum of the differences between the average of all observed values and the predicted value at each time, i. Figure 28a shows that the numerically efficient Fourier-based mode-2, with its capability of resolving the behavior of larger numbers of UXO dispersed over larger areas, can replicate the mode-3 migration simulations (based on high resolution LIDAR inputs) with an $r^2 = 0.93$, and the burial within an $r^2 = 0.86$. Because the upgraded awa-cell MM can do better than $R > 0.8$ or $r^2 > 0.8$, it is considered to perform with sufficient accuracy that its results are comparable to the present ESTCP certified MM; while the cost savings derived from its reduced input rigor makes it attractive for remediation planning, both in terms of fiscal constraints and coverage requirements.

The level of validation achieved in the ESTCP tests is sufficient for bringing the upgraded awa-cell MM into widespread use at biogenic reef sites such as Vieques Island. Therefore the upgraded MM will not only directly benefits the individual program users but will also establish a DoD-wide base of experience. This process provides field experience for the widest possible range of site environmental conditions and UXO types. Such experience established relationships between site characteristics and controlling MM parameters that can subsequently be used to expedite calibration for all remaining sites. In turn, users are now able to interpolate MM results for future un-calibrated sites instead of initiating a new extrapolation

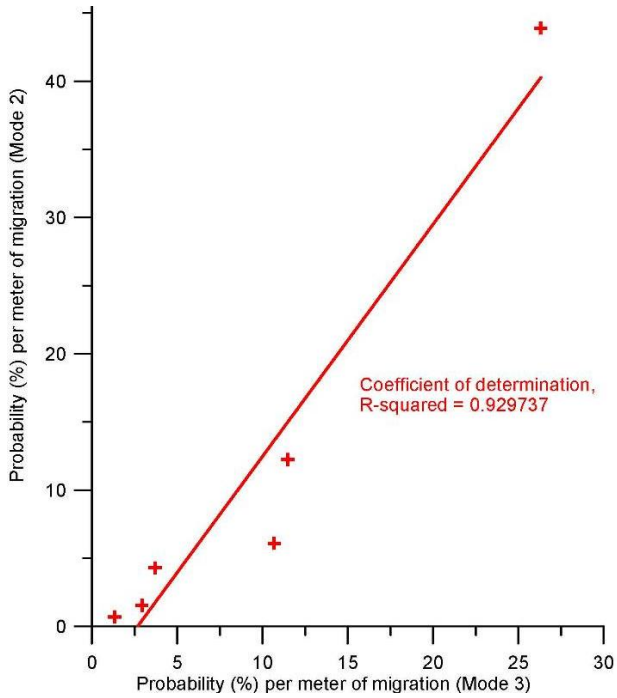

Figure 28a. Regression analysis of Mode 2 Fourier micro-bathymetric technique v. Mode 3 high resolution LIDAR supported migration predictions for 5’’/38 rounds, PMRF, HI

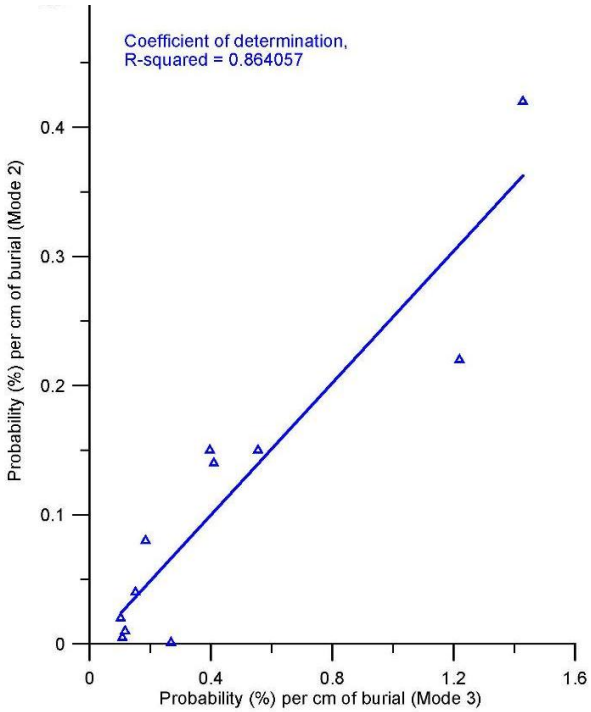

Figure 28b. Regression analysis of Mode 2 Fourier micro-bathymetric technique v. Mode 3 high resolution LIDAR supported burial predictions for 5’’/38 rounds, PMRF, HI

8.0 COST ASSESSMENT

Per the Federal Remediation Technologies Roundtable (FRTR) *Guide to Documenting and Managing Cost and Performance Information for Remediation Projects (EPA 542B 98-007, Oct 98*), "The total cost for an application should not include other project phases/activities, such as preliminary assessment/site investigation, remedial investigation/feasibility study, remedial design, or post-closure surveillance and long-term monitoring." Since the UXO Mobility Model is a basic tool to support all of the "other project phases/activities", the cost structure of this section will not include most of the items in the standard format that pertain to the actual remediation process.

The operational costs of using the MM and associated IM are substantially less than the costs that were required to develop and validate the two models. The primary cost elements for using the MM, in generally descending order, are:

- Data acquisition (climatology, bathymetry, seafloor conditions, human use activities, UXO history and distribution). The costs can be minimal if the site is already well documented, but can be as much as several hundred thousand dollars for each small site if in situ surveys are required.
- Data formatting and processing for use (gridding bathymetry, deriving UXO population – can be as much as a few months of labor)
- MM computer operations (typically less than a few weeks of labor)
- Report development
- Customer liaison

Since the MM is applied in steps (Mode 1, 2, 3 as required), the total cost of using the MM is controlled by the level of detail required, and by the site-specific results obtained as the analysis proceeds. The actual costs of the MM development and validation are provided here for reference. Then example estimates of costs for various levels of site analysis are provided.

8.1 COST MODEL

Per the Federal Remediation Technologies Roundtable (FRTR) *Guide to Documenting and Managing Cost and Performance Information for Remediation Projects (EPA 542B 98-007, Oct 98*), "The total cost for an application should not include other project phases/activities, such as preliminary assessment/site investigation, remedial investigation/feasibility study, remedial design, or post-closure surveillance and long-term monitoring." Since the UXO Mobility Model is a basic tool to support all of the "other project phases/activities", the cost structure of this section will not include most of the items in the standard format that pertain to the actual remediation process.

The Navy program that developed the UXO Mobility Model and provided the initial limited validation started in December 2002 and concluded in December 2005. The entire ESTCP UXO Mobility Model validation program started in June 2004 and concluded in June 2008. The program spanned 5 years and the total expenditure was approximately $1,795,750. The ESTCP investment was approximately $1,278,000.

Table 4 summarizes the program costs as adapted from Wilson, et al, (2008d). The investment was divided between the MM development work (28%) and the field validation effort (72%).

Table 4. UXO Mobility Model program cost summary.

	Navy	ESTCP	TOTAL
MOBILITY MODEL DEVELOPMENT			$498,375
FY02-FY04	$143,375		
FY05-FY08		$355,000	
MOBILITY MODEL VALIDATION			$1,297,375
Pt. Mugu Test	$119,188		
Measurement Method Field Test	$255,188		
FRF Duck, NC, Demonstration		$404,320	
PMRF Kauai, HI, Demonstration		$433,320	
Example Application Analysis		$85,360	
	$517,750	$1,278,000	*$1,795,750*

8.2 COST DRIVERS

As discussed above, the main cost drivers on the use of the MM and IM area the acquisition and processing of the environmental data required as inputs to the models. The best way to illustrate the range of those costs is by example.

The costs to apply the MM at full-scale sites are separated into three phases of analysis. The detailed process of applying the MM to a full-scale site is described in Wilson et al. [7], the Applications Guidance Document.

Mode 1 Screening Analysis

The first phase uses only Mode 1 of the MM. All of the inputs for this phase are composed of existing data available from a “desk-top” study. Default values are used for many of the MM inputs, based on the general coastal type. The primary purpose of the Mode 1 analysis is to determine areas that are *not* at risk of human exposure to UXO. Therefore, these are areas in which either (a) there are no UXO of concern or (b) the UXO is permanently entombed – buried at depths below any known or forecast human activities (i.e., fishing, dredging, etc.). The term “permanently” is limited by the worst-case storm activity ever recorded or forecast for the site. Table 5 shows an example cost estimate for a basic Mode 1 screening analysis of a typical UXO “site”.

The assumptions made in this cost estimate are as follows:

- UXO site manager liaison is provided via NAVFAC
- Analysis performed by support contractors (e.g., engineers/computer analysts)
- UXO site managers have Mode 1 level data available, including:
    - general estimate of history of UXO type and distribution
    - basic bathymetry (NOAA charts or past local surveys)
    - defined areas of responsibility (boundaries)
    - summary of type and location of human use (e.g., fishing, recreation, dredge, etc.)
- Initial analysis performed without travel (no site visits)
- Baseline "site" is a single section of coastline (e.g., small bay, offshore from firing range, etc.)
- Duration of Mode 1 phase is approximately 3-6 months.

Note that the word, “site”, in this context refers to a relatively small, contiguous area of UXO with dimensions on the order of a few kilometers, such as a small bay, firing range, etc. Estimates for larger “sites” such as an entire island, a major coastline, etc., are developed as multiples of single sites.

Table 5. Nominal cost of Mode 1 screening analysis of a single UXO site, (as adapted from Wilson, et al, 2008d)

MODE 1 SCREENING ANALYSIS	
Initial contact, problem definition, liaison	$20,000
Preliminary screening (set up ARCGIS, plot areas of use, define closure depth)	$20,000
Mode 1 analysis of UXO movement at selected points in risk areas (no Model modifications)	$30,000
Preliminary analysis of risk of human interaction	$8,000
Initial report & recommendations	$8,000
Program management	$10,000
Mode 1 Total	**$96,000**

Unless either (a) the desktop data for the Mode 1 are unusually complete and detailed or (b) the Mode 1 analysis clearly shows that even conservative estimates place virtually all the UXO at the site at very low risk of human interaction, it will be necessary to conduct a more detailed analysis, using additional site-specific data inputs (Mode 2).

Mode 2 Detailed Analysis

The Mode 2 analysis is only conducted on those parts of the site that are not clearly shown to be low risk by the Mode 1 analysis. Mode 2 requires input data for the local environmental conditions that are not normally available for UXO sites. However, the Mode 2 analysis does not involve any direct surveys of the UXO distribution itself. The assumptions for the Mode 2 Detailed Analysis phase are as follows:

- Mode 1 was previously completed
- UXO site manager liaison is provided via NAVFAC
- Analysis performed by support contractors (e.g., engineers/computer analysts)
- Environmental site surveys required (though a UXO survey is not)
    - bathymetry (LIDAR or multibeam backscatter (MBBS) for details of depth at 2-5m spacing, <1 m resolution)
    - bottom samples to determine sediment properties
    - on-site wave measurements are necessary to refine the REF/DIF model
    - on-site human use surveys are conducted to obtain fishing data, etc.
- Climate and human use studies cover one annual cycle
- Mode 2 phase lasts about 18 months after Mode 1.

Mode 2 will likely meet the analysis needs for most sites.

The costs to apply the MM at full-scale sites varies considerably with the size and location of the site (e.g., area to be modeled, cost of data to be collected), complexity of the bathymetry, level of human use, etc. The size of UXO sites ranges from as little as a square kilometer for one bay at Vieques, PR, 100 km^2 for the offshore area of Camp Perry on Lake Erie, 150 km^2 for the entire coastline of Kaho'olawe, HI, and 240 km^2 for the firing range off Ft. Monroe, VA. Each of those could be surveyed in a single day by aircraft at approximately $50,000 per day, plus mobilization costs. The subsequent post-processing of the data costs approximately $1000/$km^2$. Therefore, the total price for LIDAR survey of typical UXO sites range from about $90,000 for the Vieques area to as much as ≈ $310,000 for the Ft. Monroe area. For an example mid-sized site, the estimated cost is as shown in Table 6; note that the dominant costs are associated with the site surveys.

Table 6. Estimated cost of Mode 2 Detailed Analysis (as adapted from Wilson, et al, 2008d)

MODE 2 DETAILED ANALYSIS	
Detailed Mode 2 phase program plan	$10,000
Bathymetry survey (LIDAR or MBBS)	$200,000
On-site sediment sampling & ADCP (four seasons)	$95,000
Human use surveys (fishing, boating, diving, etc.)	$30,000
Update Mode 1 ARCGIS and data sets	$15,000
Mode 2 Analysis of UXO movement at selected points in risk areas.	$50,000
Updated analysis of risk of human interaction	$12,000
Mode 2 Report	$12,000
Program management	$35,000
Total	**$459,000**

Mode 3 Enhanced Analysis

Mode 3 adds the final input detail of enhanced estimates of the UXO initial distribution. Since obtaining this type of information is the most expensive, and potentially dangerous data to

collect, it is only added to the process when the desk-top data on UXO distributions are not credible due to such issues as age, inconsistencies, etc., and either (a) there is clear evidence of substantial risk of human interaction or (b) large-scale UXO movements are predicted that require more accurate estimates. The development of enhanced UXO distribution estimates involves several possible technologies and considerable on-site effort and cost. It begins with additional analysis of historical data to convert recorded UXO entry (e.g., air drops, gunnery, etc.) into expected impact with the seafloor and initial burial. This data is matched against more refined on-site surveys of the seafloor itself to locate and identify UXO that are not entirely buried. The final step is to locate buried UXO using sub-bottom profilers, magnetometers, diver, checks, etc.

The assumptions for a Mode 3 Enhanced Analysis cost estimate are as follows:

- Mode 1 and 2 were previously completed
- Mode 3 is only used for cases of high risk, or if UXO data are questionable
- UXO site manager liaison is provided via NAVFAC
- Analysis performed by support contractors (e.g., engineers/computer analysts)
- Mixture of means used to develop UXO distribution baseline:
    - impact analysis (historical firing records and physics of impact)
    - analysis of previous bottom imagery to detect surface UXO
    - new visual searches of seafloor (e.g., ROV, towed fish, divers)
    - new acoustic surveys (e.g., imagery, sub-bottom)
    - magnetometer surveys
- Costs vary considerably with size and location of site and type of UXO
- Mode 3 phase spans approximately 12 months beyond Mode 2 phase (6 months survey, 6 months analysis)

Table 7 shows an example estimate of the costs of this additional Mode 3 Enhanced Analysis phase.

Table 7. Mode 3 Enhanced Analysis cost estimate, (as adapted from Wilson, et al, 2008d)

MODE 3 ENHANCED ANALYSIS	
Detailed Mode 3 phase program plan	$5,000
Impact analysis (historical firing records plus physics of impact)	$8,000
Analysis of previous bottom imagery (for surface UXO)	$10,000
New visual searches of seafloor (ROV, towed fish, divers)	$200,000
New acoustic surveys (imagery, sub-bottom)	$200,000
Magnetometer surveys	$50,000
Run Mode 3 simulations (updates Mode 2 results at key points). Estimate half-life of UXO survey data v. remediation schedule	$30,000
Updated analysis of risk of human interaction	$12,000
Mode 3 Report	$12,000
Program management	$50,000
Total	**$577,000**

8.3 COST BENEFITS

8.3.1 COST COMPARISON

There are no other available computer models to which the MM can be compared to determine competitiveness. The most instructive comparison is the cost of applying the MM versus the potential savings in remediation efforts.

In any event, the cost of using the MM to define areas of high risk will be small compared to alternative approaches such as sweeping the total area of possible UXO contamination, which can easily cost many tens of $M per site. As of this writing, the MM is also the only tool that allows credible analysis of sites to be conducted to verify that risk either is already at an acceptably low level, and therefore does not require comprehensive clean up costs, or to set the depth and area of cleanup so that it covers the entire risk area and avoids the need to sweep the area again later if adjacent UXO migrate into the swept area after cleanup. Also, analysis at the Mode 1 level reduces the need for Mode 2 data collection, and, in turn, Mode 2 reduces need for Mode 3 to be conducted.

One way to quantify the value and compare the cost of using the MM is to estimate the Return On Investment (ROI). That is, compare the cost savings produced by the MM, less the investment costs, as a fraction of the investment costs. The equation for ROI is:

$$ROI = (Savings - Investment)/Investment$$

An ROI of 0 is the break-even point where the savings equals the investment.

Of course there are other non-economic benefits associated with using the MM, such as reducing risk, demonstrating good faith efforts, etc. However, this analysis solely focus on cost benefits.

The primary cost benefit from the UXO Mobility Model is to reduce the size of the area requiring cleanup and remediation. The MM shows where UXO are permanently entombed deeper than any human interaction will occur. It also provides the limits of UXO movement, so it bounds the need for “preventative” clearance measures.

The actual ROI depends heavily on the derived percent reduction in required cleanup, which will not be known until the MM is applied to specific sites. However, it is possible to bound the ROI.

For example, in 2004, the approximation of “best-possible” ROI was determined as follows:

- The estimated cost to clean up three major underwater UXO sites (Mare Island, Vieques, Kaho’olawe) was ≈ $2,764M.
- The estimated cost of the UXO Mobility Model development and validation program was $1.32M (note that no estimates for operational use were available at that time).
- IF the MM program then showed that NO cleanup was required at those three sites, which is unlikely, but a “best case” scenario, the ROI would then be equivalent to

$$\frac{(\$2{,}764 - \$1.32)}{\$1.32} = 2092$$

This value translates into savings that are 2092 times the cost of using the MM – a significant ROI.

Now that the development program is concluded, it is possible to develop a more realistic estimate of the ROI.

- First, there is now a better estimate of the cost to use the MM. A Mode 1 screening analysis can be performed for a single site for approximately $200k. However, if detailed *in situ* surveys of the UXO baseline population are required, it could cost as much as $1M per site. These two estimates range from $0.6M (minimum) to $3.0M (maximum) for the three sites. Also, the cost correction for inflation makes the 3-Site total cleanup cost equal to ≈ $3,233M.

- Second, the analysis can consider the example sites and how much cleanup area might actually be reduced by using the MM analysis to better estimate of savings.

- As a final step, the minimum amount of cleanup reduction required to equal the future investment costs, the break-even point, can be determined.

Note that the $1.5M development costs are sunk and not part ROI for future investments.

For the updated "Best Case" scenario (parallels the 2004 approach),

$$ROI = (\$3233M - \$3M)/\$3M = 1077$$

which translates into savings = 1077x MM use costs.

To refine the ROI further, consider the examples of Vieques Island (Figure 28a) and Waianae, HI (Figure 28b). In both Figures 28a & b, the maximum area requiring remediation is outlined, along with an example of the possible reduction in area allowed by the results of the MM. For these more realistic scenarios, the savings average ≈ 75% of the worst-case. Therefore,

$$ROI = [(0.75 \times \$3233)-\$3]/\$3 = 807$$

which still signifies that the savings is equivalent to 807 x MM use costs, a good investment by almost any standard.

The break-even point, or ROI = 0, occurs when MM usage saves just $3M, which is 000928 x worst case costs (less than 0.1%); this is only 0.06 km^2, or an area of seafloor approximately 245 x 245 m^2 (one football field per site).

Clearly, the cost to use the MM will virtually always be much less than the savings it produces in reduced area requiring survey and remediation.

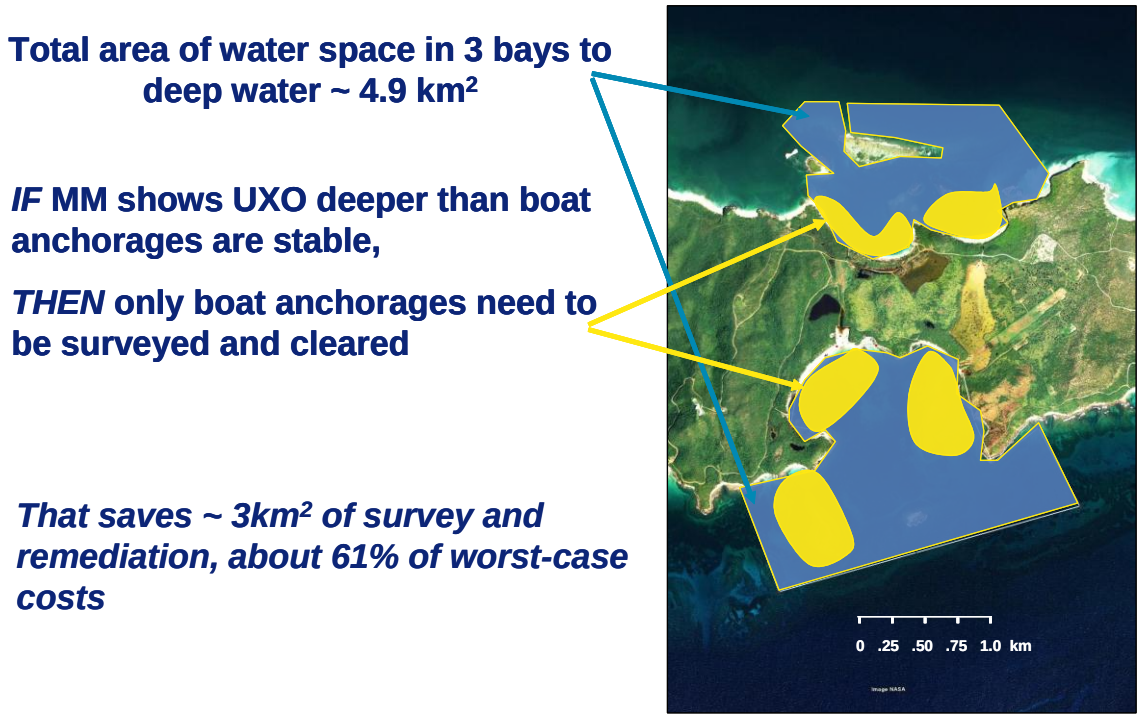

Figure 29a. Vieques range UXO remediation area comparison.

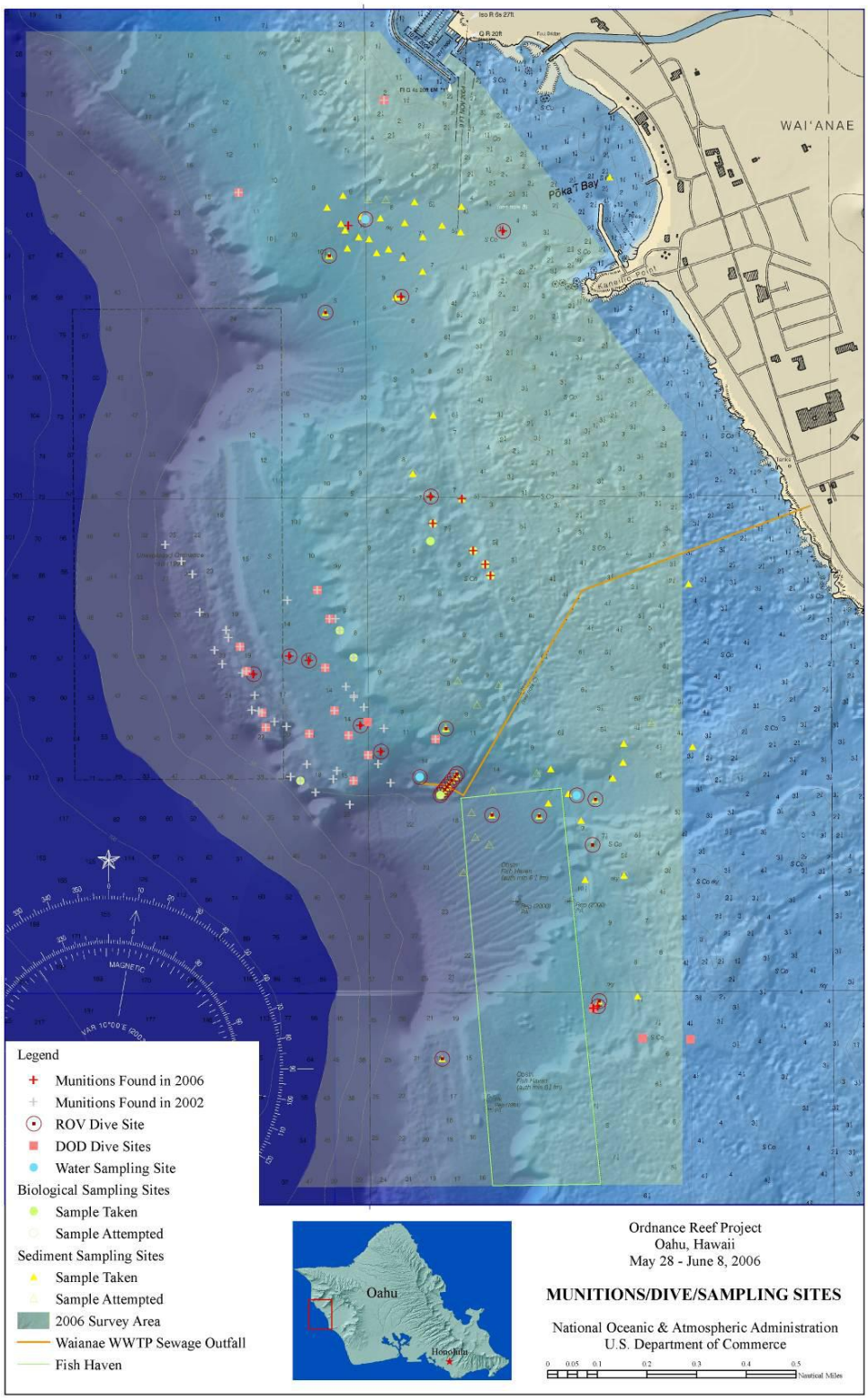

Figure 29b. Ordnance Reef, Waianae Oahu, HI UXO remediation area comparison. Total water space = 51 square km. MM calculates UXO immobile in an area of 40 square km reducing area requiring surveying and worst- case costs by 80%.

9.0 IMPLEMENTATION ISSUES:

The application of the UXO Mobility Model itself requires no environmental permits, as there is no field activity in the modeling process. The acquisition of survey data would require standard permits for operating aircraft or vessels with multi-beam sonars, but those are standard commercial operations with very low environmental impact. Bottom sample collection by divers, use of ADCP instruments, etc., for site monitoring would fall in the same general category.

All of the activities associated with the use of the MM are extremely low-impact environmentally. In fact, the overall result of use of the MM is to actually improve the environment by minimizing risk of human exposure to UXO.

9.1 IMPLIMENTATION AT VIEQUES ISLAND

In this section we implement the upgraded awa-cell MM in a modified mode-2 fate and transport assessment at Vieques Island (Figure 30a) based on reef platform roughness (micro-bathymetry) generated by the Fourier decomposition method described in Sections 2.2 and 6.1. An additional objective of this implementation is to demonstrate how the increased computational efficiency and numerical stability afforded by this MM upgrade allows simultaneous computations of the potential migration and burial of large numbers of UXO over large areas to be performed by a relatively inexpensive desktop computational mode in this most difficult and important coastal classification, namely the biogenic reef environment. Through this implementation effort, we will also show that a natural sorting mechanism of the UXO occurs in response to long term wave climate interacting with the unique features of the awa cell bathymetry which has important implications for remediation planning and to assessing potential risk of human contact with underwater UXO.

There are two underwater UXO fields located north and south of the impact area at the eastern end of Vieques Island (Figure 31). The North UXO field is known as Bahia Salinas, while the South UXO field is referred to as Bahia Salina del Sur. For both the North and South UXO Demo Areas, awa control cells were generated using high resolution aerial photographs to locate and geo-register the awa channels (Figures 32 and 33). These awa channels are highlighted in magenta Figures 32 and 33, and establish the boundaries and planar dimensions of the reef platform. Figure 30b gives an indication of the population density of UXO on the reef platforms in the South Demo Area at Vieques Island (cf. Figure 33).

The reef platforms at Vieques Island are specified in the awa-cell upgraded MM by filling in the regions between the awa channels in Figures 32 & 33 using the lofting developed for platform micro bathymetry derived from Fourier decomposition of the LIDAR data at PMRF. Figure 7 shows the auto spectra of reef platform roughness in terms of depth deviations about the 30 m depth contour. This procedure was repeated at 2 m depth increments between the 0 and 50 m depth contours, and the ensemble of the Fourier coefficients of these departures from the local mean depth were then lofted into a complete set of multiple/coupled awa cells, as shown in Figure 8 at PMRF, Kauai and Figure 36 for the South Demo Area at Vieques Island. When the

Figure 30a: Vieques Island Aerial Photograph

Figure 30b: Underwater UXO at North Impact Area (Bahia Salinas), Vieques Island

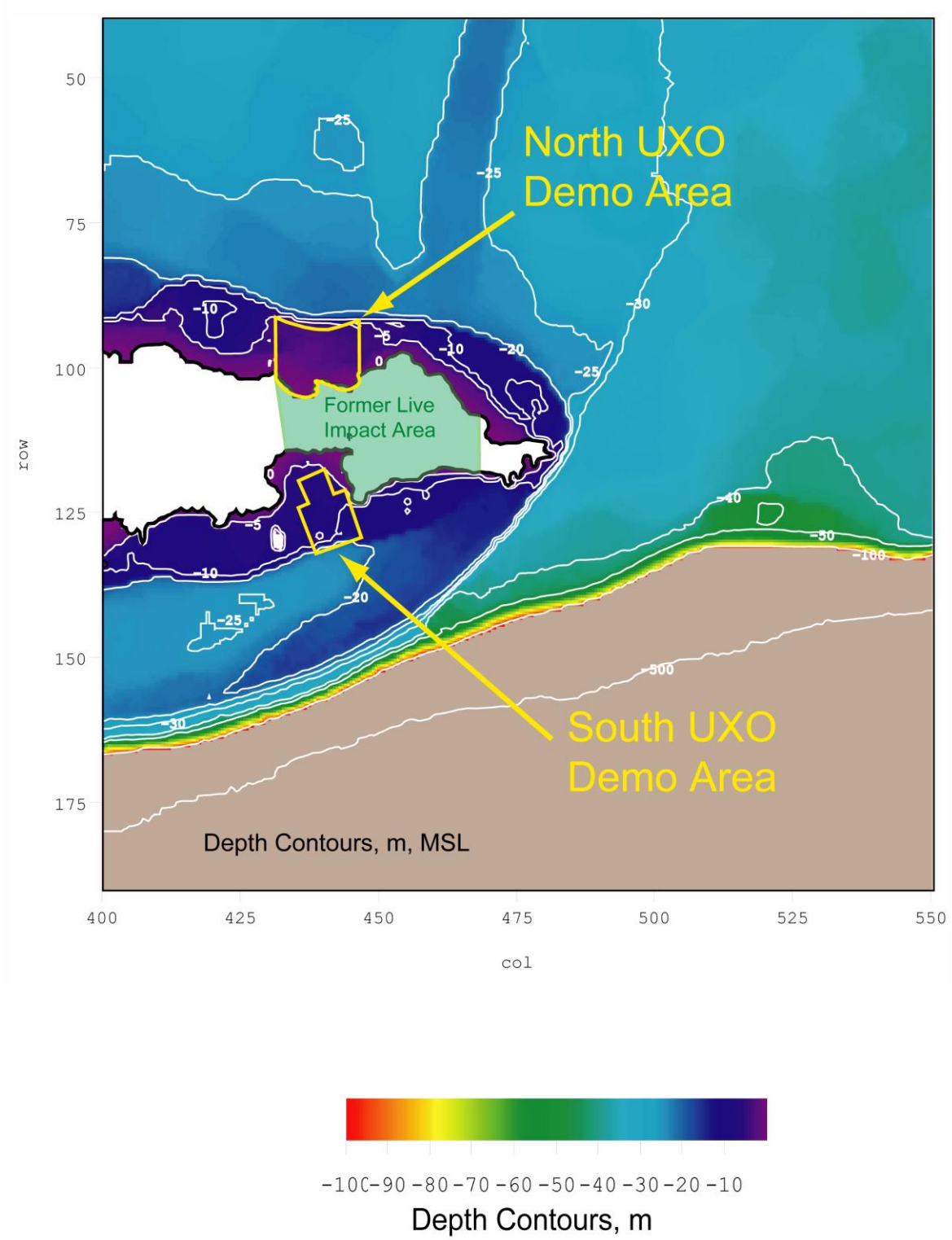

Figure 31: Vieques Island UXO Demonstration Areas

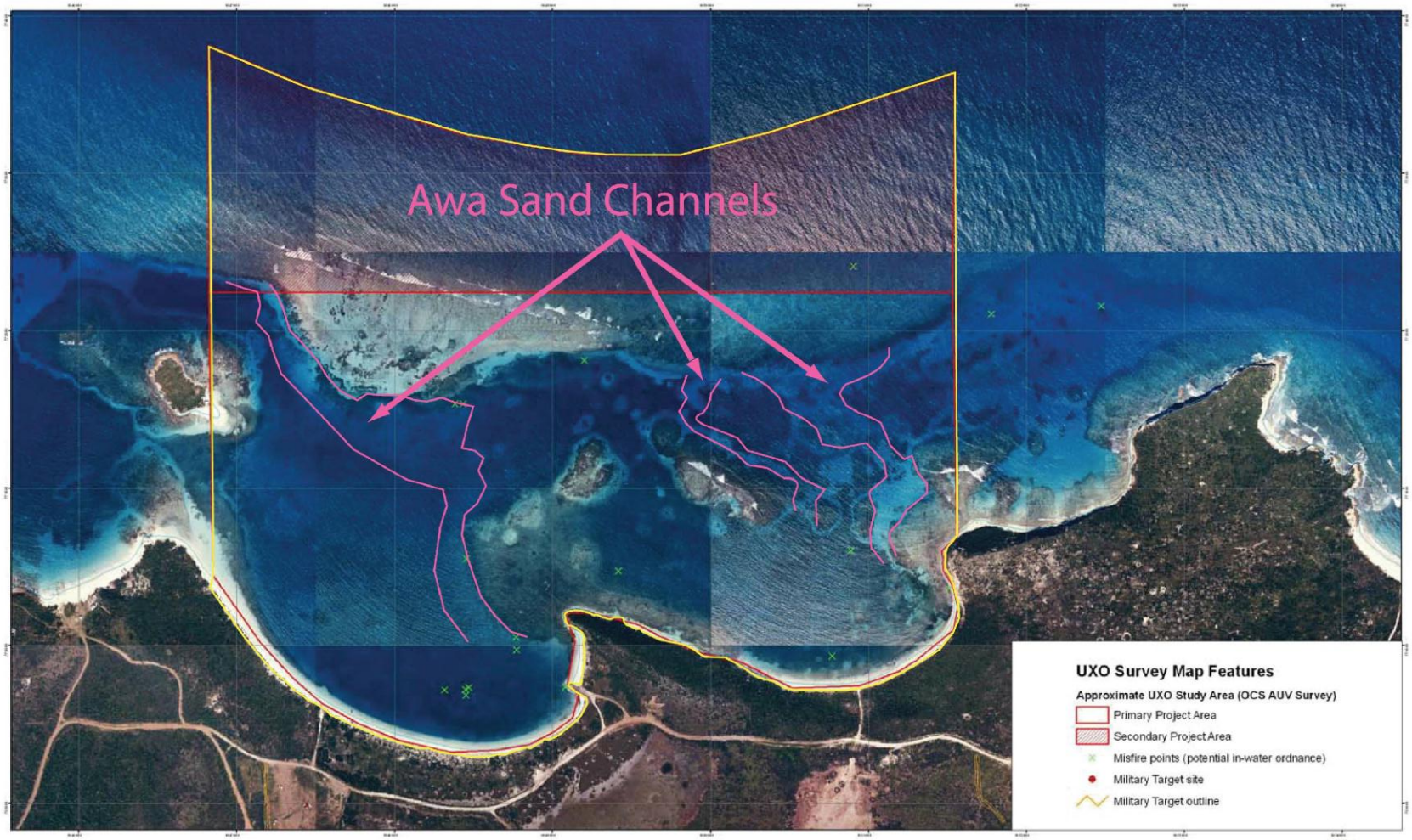

Project Study Area (North): Bahia Salinas

Vieques Underwater UXO Demonstration Project, Vieques Island, Puerto Rico

A joint project between -
NOAA's Ocean Service, University of New Hampshire Joint Hydrographic Center,
and the US Navy Munitions Response Program

Data note:
Aerial photography from US Navy 1999 survey. Military Targets, misfire points and target features from US Navy NAVFAC spatial data library for Puerto Rico. Map grid set to 1000' cells. All data in Puerto Rico State Plane Survey Feet

Figure 32: Vieques Island North Impact Area awa channels

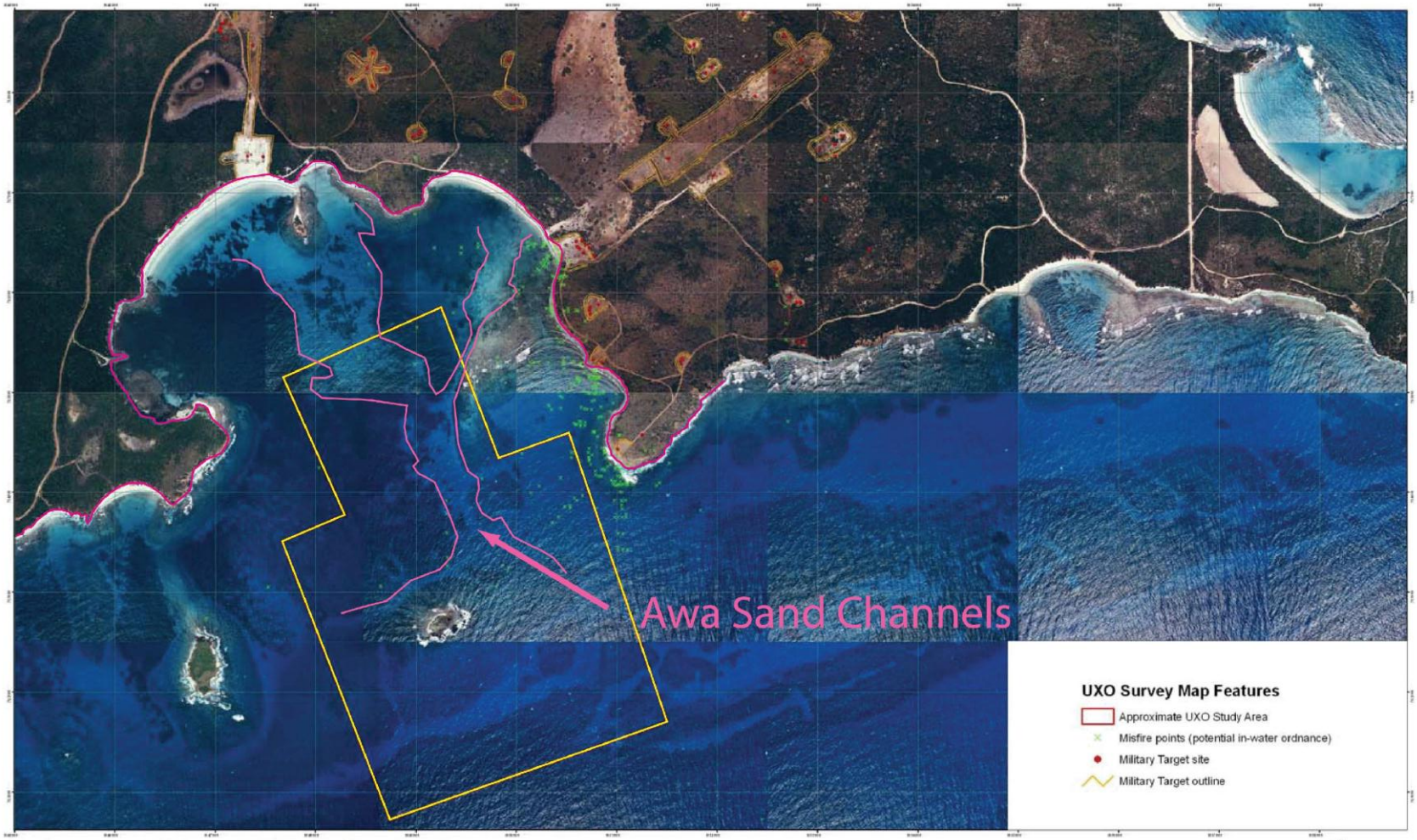

Project Study Area: Bahia Salina del Sur

Vieques Underwater UXO Demonstration Project, Vieques Island, Puerto Rico

A joint project between -
NOAA's Ocean Service, University of New Hampshire Joint Hydrographic Center,
and the US Navy Munitions Response Program

Data note:
Aerial photography from US Navy 1999 survey, Military Targets, misfire points and target features from US Navy NAVFAC spatial data library for Puerto Rico. Map grid set to 1000' cells. All data in Puerto Rico State Plane Survey Feet

Figure 33: Vieques Island South Impact Area awa channels

reef platform micro-bathymetry from PMRF is applied to the areas between the awa channels at Vieques Is.(Figures 32 and 33) , we are making the implicit assumption that reef platforms at Kauai are geomorphically similar to those at Vieques Island.

To derive model input for the sediment cover along the floor of the awa channels, sediment grain size distributions are derived from Wilson, et al. 2008c; while bottom elevation changes along the non-stationary profiles of the shorerise and bar-berm are computed by thermodynamic equilibrium profile algorithms after Jenkins and Inman (2006). The stationary and non-stationary sediment profiles are interpolated to 0.5 m resolution to resolve the sediment cover along the floor of the awa channels.

Wave forcing for long term UXO transport and burial simulations using the awa-cell upgraded MM at Vieques Island was derived from 30 years of wave measurements at NOAA Buoy #41046 at Lat/Long 23.99^0 N; 70.99^0 W (Figure 34). Note that this wave record contains one very significant extreme event, Hurricane Earl in 2010, producing a 14m deep water significant wave height. Spatial variation in wave forcing over the multiple awa cell systems of the North and South Demo Areas at Vieques Island are resolved by refraction/diffraction analysis over the far field grid by modules #6 and #8 in Figure 2, producing regional wave height distributions like those shown in Figure 35, as calculated for discrete events of directional wave measurements from Figure 34. (In this particular example, we show the shoaling and refraction/diffraction effects from a Hurricane wave tracking into the region from the tropical wave regime of the trade wind belt, with a deep water significant wave height of 2m incident on the South Demo Area from 225 degrees with 12 second period.) While the shelf rise along the south coast of Vieques Island produces bright spots in the refraction pattern at several locations along the south shore of the island (Figure 35), the refracted waves display relatively small alongshore variations inside the North and South UXO Demo Areas.

Hypothesis of Natural Sorting of UXO in Awa Cells: The absence of local alongshore gradients in shoaling wave heights in the farfield (Figure 35) allows the depth variations between the reef platform and the awa channels to dominate the nearshore circulation. Shoaling wave heights are locally greater over the reef platform than in the adjacent awa channel at any given distance offshore of the fringing reef system. Consequently there exists an alongshore divergence of drift between the reef platform and the awa channel, producing alongshore currents that flow away from the reef platform and converge at the awa channel, producing nearly perpetual rip currents flowing seaward through the awa channels (cf. figure 3). This assures that the predominant net long-term drift will be along shore over the reef platform, converging on the awa channels; and up/down channel along the cross-shore axis of the awa channels. It is this general circulation mechanism (resolved by module #7 in Figure 2) that motivates the hypothesis tested herein that, over time, UXO will ultimately migrate off the reef platform and concentrate in the awa channels. This general circulation model, as diagrammed schematically in Figure 3, is also fortified by the second law of thermodynamics, that in this context requires that the UXO will ultimately arrive at a state of minimum potential energy, as stored in the gravitational force field, and seek an equilibrium associated with minimum elevation. The analogue is natural systems in which heavy objects subjected to random disturbance ultimately come to rest in depressions in the topography, where their equilibrium is in the well of the potential energy minimum (Fermi, 1936).

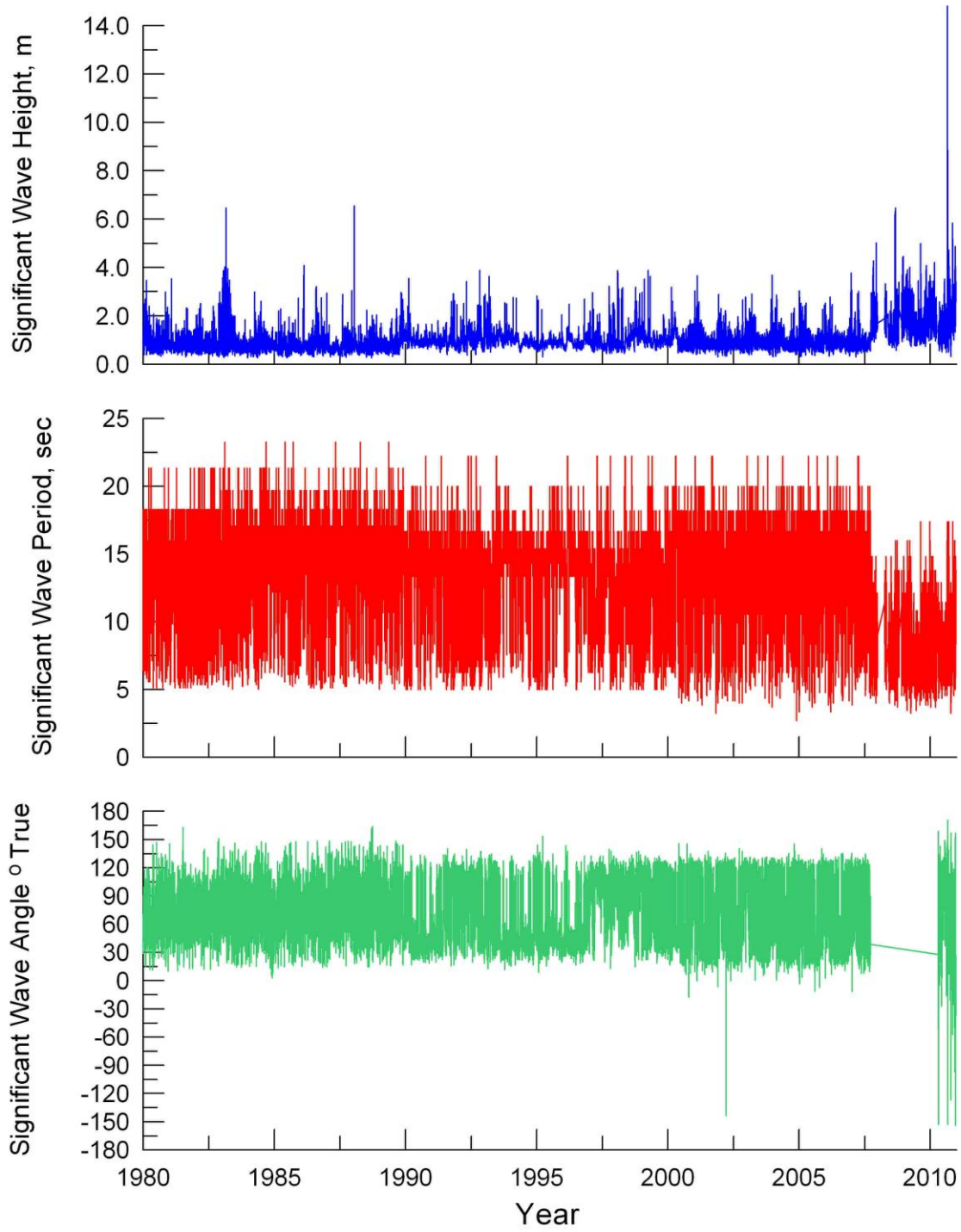

Figure 34: Long-term Wave Climate for UXO Migration and Sorting Simulation at Vieques Island South Impact Area. Wave data derived from forward refraction of wave measurements at NOAA Buoy #41046 at Lat/Long 23.99^0 N; 70.99^0 W. The extreme wave event is due to Hurricane Earl in 2010.

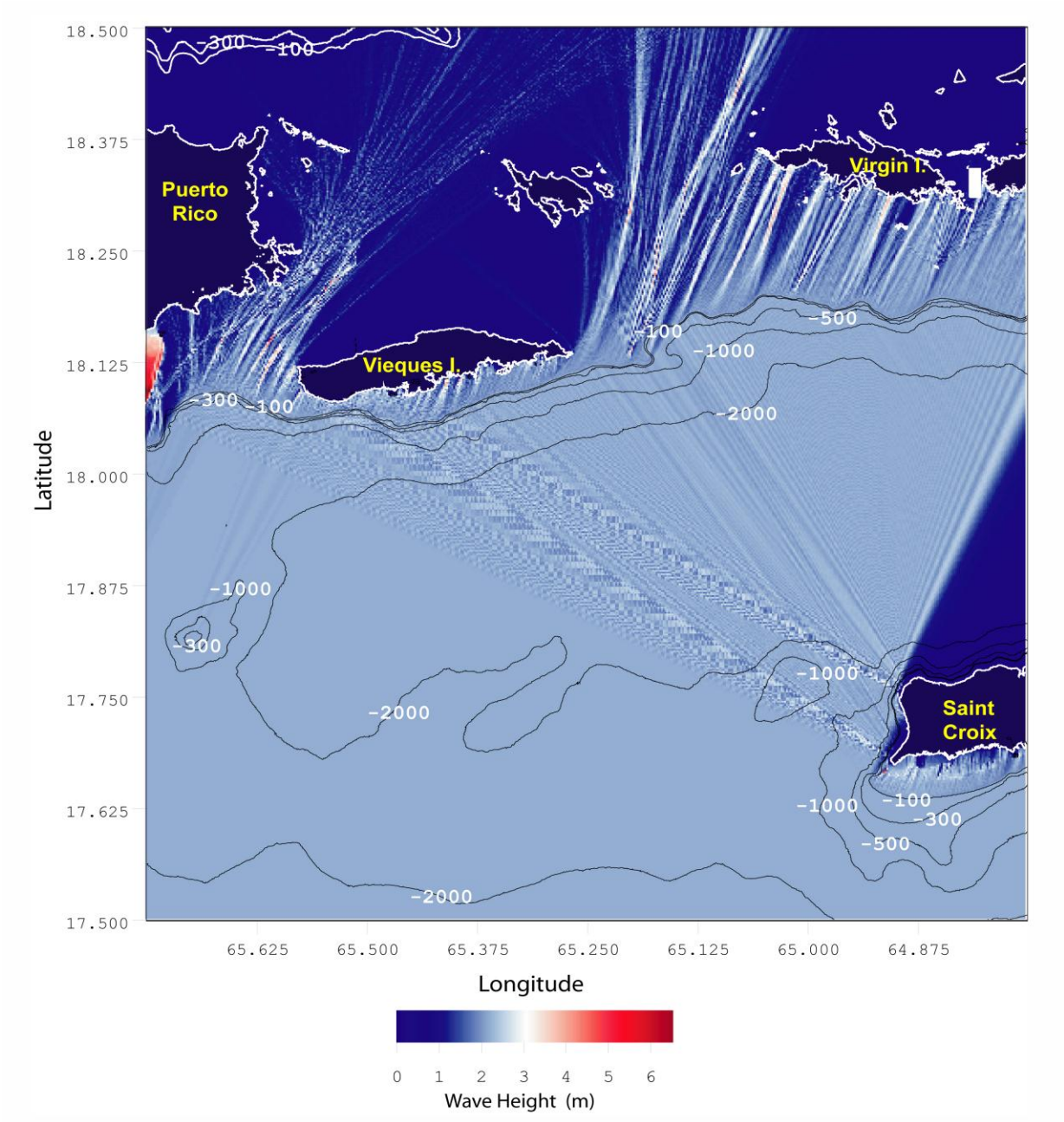

Figure 35: Vieques Island Wave Refraction/Diffraction Pattern. Bathymetry contours (white), m MSL; Deep water wave height, 2 m; period, 12 sec; direction, 225 degrees.

To examine the natural sorting mechanism hypothesis for UXO in biogenic reef environments, we conduct a numerical experiment, 30 years in duration, using the South Demo Area at Vieques Island as a test bed. With the upgraded awa-cell MM initialized using Fourier decomposed micro-bathymetry, the coupled, multiple awa cells of the South Demo (Impact) Area after Figure 32 were populated with a hypothetical, uniformly distributed ensemble of five hundred 5”/38 naval projectiles, as shown in Figure 36. Here, the UXO are rendered in silver, and are more discernable if the reader uses the zoom tool when viewing this figure. The uniform initial population distribution is believed to be representative of the initials results of live firing exercises intended to hit the designated impact area on land (green area in Figure 31); but because of random over or under shoots, the actual impacts occurred in the waters of the South Demo Area (Figure 31). With this uniform initial distribution, 6% of the 500 UXO are in awa channels while 94% are on the reef platform. In Figure 36 the shoreward (shallow) end of the reef system is along the upper edge of the figure, while the deeper seaward facing end is along the lower edge. Between the shallow and deep edges of the figure, depths range from 2m MSL to 30m MSL. This convention and view angle is used throughout all renderings of the long term simulation in Figures 36-43.

Figure 37 shows the general flow pattern from the awa-cell upgraded MM over a subset of the initial UXO population and resident awa cells in the South Impact Area, as rendered by a sheet of instantaneous streamlines under a wave trough. The wave used in this simulation is nearly normally incident (wave direction 080 degrees) and has a 1 m wave height and 12 second period, (typical of a mild swell propagating into the region from the trade wind belt). Under the wave trough the general circulation is offshore producing both bathymetric divergence and large scale eddying over portions of awa channels having either expansion or contraction sections or which exhibit longshore turning in the axis of the channel, similar to what was found in the PMRF simulations (cf. Figures 22 & 23). These types of non-uniformities in the general flow field create significant variation in the intensity of the nearfield flow disturbances acting on any given UXO, (and hence differences in onset of motion among individual UXO). However it is likely that these bathymetric-induced variations tend to average out in over a long term (30 year) simulation due to variations in wave direction. The eddying and flow divergence over the multiple awa cell system of the South Impact Area is highly directionally dependent.

Figure 38 shows the instantaneous vertical velocity profiles in five separate vertical plains oriented in the on/off shore direction, as derived from the same general flow pattern in Figure 37. In all five plains, the highest velocities appear along the shallow shoreward edge of the reef system (upper edge of the figure) as a consequence of wave shoaling. When comparing the vertical velocity distribution over the reef platform (eg. first plain on the right hand side of Figure 38) with the vertical velocity distribution in an awa channel (eg. first plain on the left hand side of Figure 38) it is apparent that near-bottom velocities are significantly greater over the reef platform that in the awa channel. Thus, onset of motion and subsequent migration of UXO on the reef platform is more likely for any given wave condition than for UXO in the awa channel, where near bottom velocities and wave induced stress is less. This flow feature is general to all simulations performed with the awa-cell upgraded MM, and is the principle mechanism that drives the UXO sorting hypothesis; namely, if UXO are more mobile on the reef platform due to velocity intensification, then they are more likely to eventually fall into the

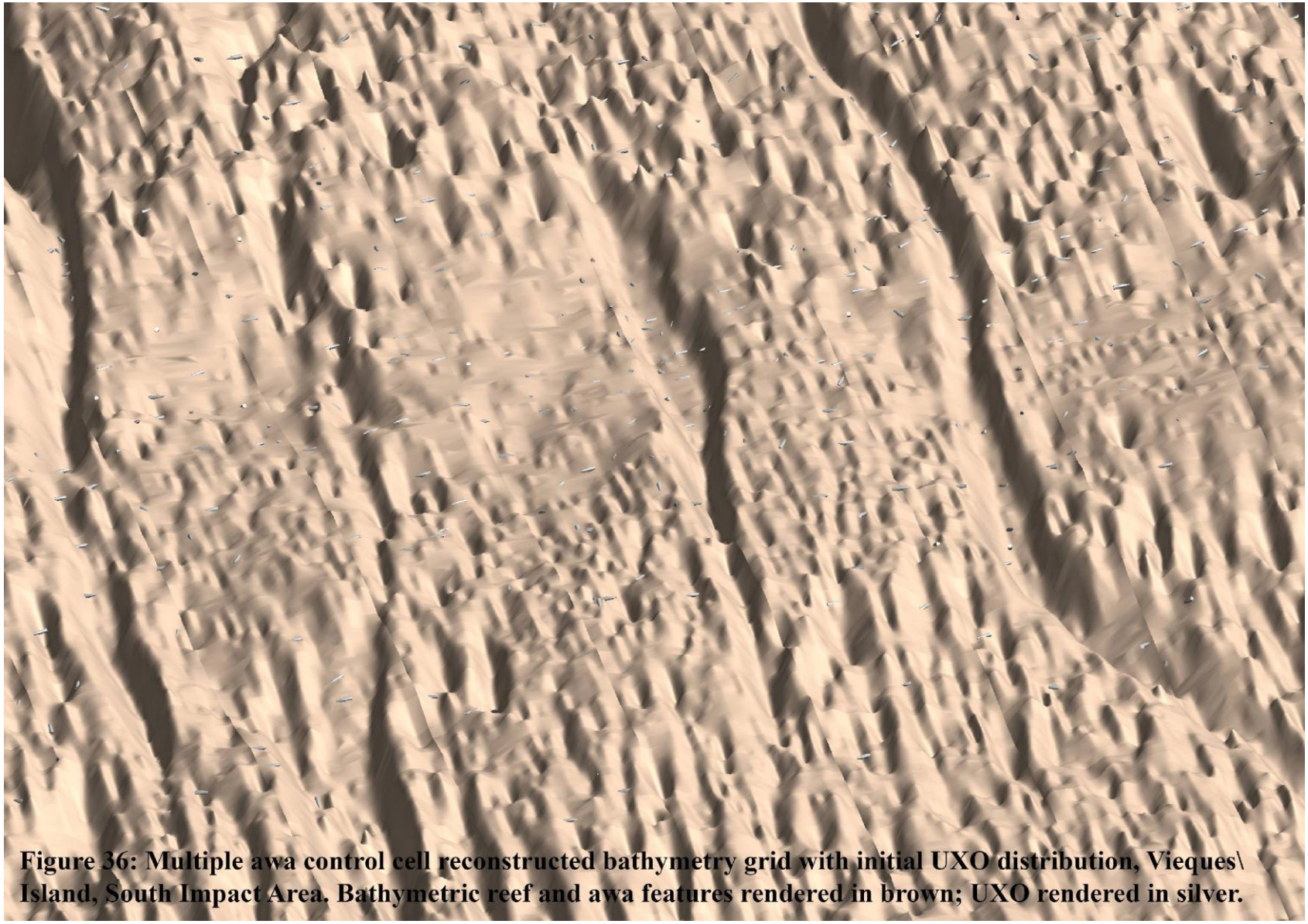

Figure 36: Multiple awa control cell reconstructed bathymetry grid with initial UXO distribution, Vieques\ Island, South Impact Area. Bathymetric reef and awa features rendered in brown; UXO rendered in silver.

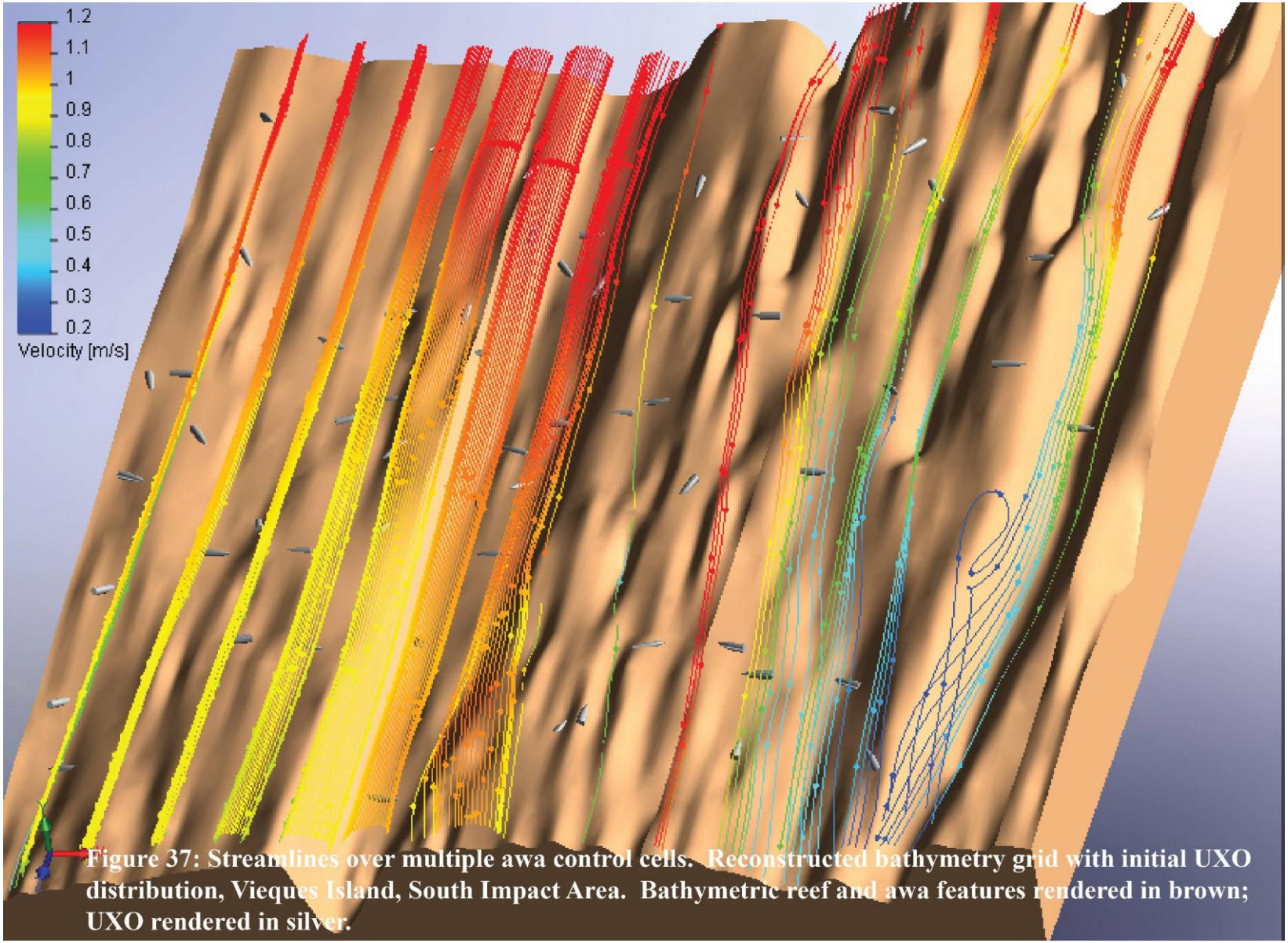

Figure 37: Streamlines over multiple awa control cells. Reconstructed bathymetry grid with initial UXO distribution, Vieques Island, South Impact Area. Bathymetric reef and awa features rendered in brown; UXO rendered in silver.

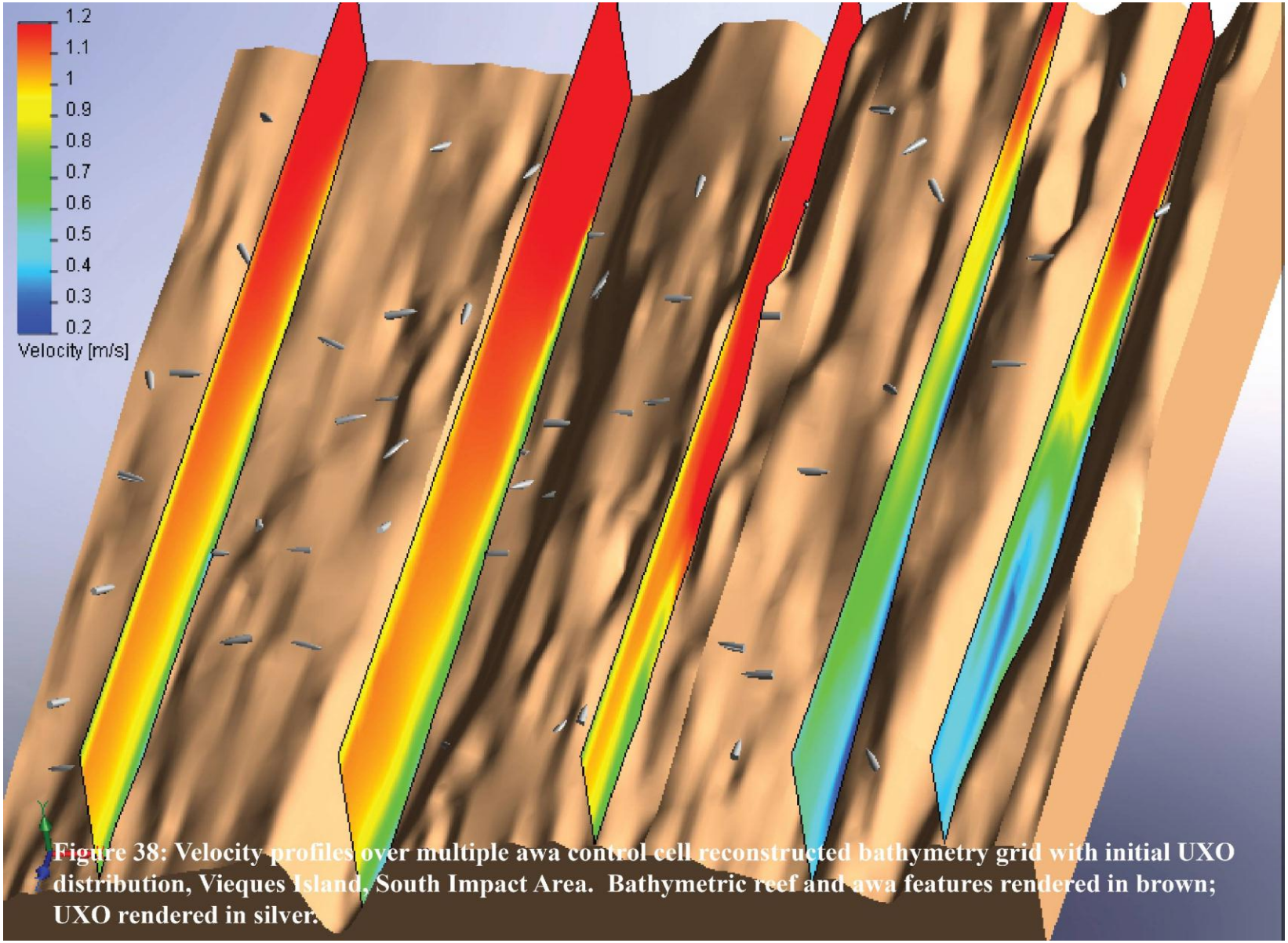

Figure 38: Velocity profiles over multiple awa control cell reconstructed bathymetry grid with initial UXO distribution, Vieques Island, South Impact Area. Bathymetric reef and awa features rendered in brown; UXO rendered in silver.

depressions formed by the awa channels where their mobility is significantly diminished in the presence of weaker near-bottom flow. Velocity shadowing from near-bottom flow separation is also apparent in the awa channels and further reduces the mobility for UXO in these channels. In first plain on the left hand side of Figure 38 and in the second plain on the left hand side, we see where a region of retarded near bottom flow originates at the top of a UXO protruding from the floor of the awa channel, and forms a near bottom wake that persists downstream and offshore from the original UXO disturbance. This is a feature of flow separation that reveals how UXO can interact with one another.

We now turn on the awa-cell upgraded MM and let it time step through the 30years of wave forcing in Figure 34 and calculate the migration and changes of position of each of the 500 UXO of the initial population at the South Demo (Impact) Area from Figure 36. Figure 39 shows the new population distribution at 10 years into the simulation. Upon inspection of Figure 39 with the zoom tool, we find there is an apparent increase in the numbers of UXO in the awa channels. By actual count, the numbers of UXO on the reef platform has decreased from 94% to 58%, while the numbers of UXO in the awa channels has increased from 6% to 42%. There is also a noticeable increase in the numbers of UXO on the reef platform in the immediate neighborhood of the awa channels, as the more mobile UXO atop the reef platform move away from the center of the platform and follow the shallow bottom gradients that slope toward the awa channels. After 20 years of wave excitation, the initial UXO population in the South Demo area has redistributed to the more concentrated arrangement shown in Figure 40. Now the numbers of UXO on the reef platform has decreased from the initial population percentage of 94% to 25%, while the numbers of UXO in the awa channels has increased from the initial 6% to 75%. And finally, in Figure 41, after 30 years of simulated wave forcing, the numbers of UXO on the reef platform has decreased from the initial population percentage of 94% to only 5%, while the numbers of UXO in the awa channels has increased from the initial 6% to 95%. The burial states of the UXO population that ultimately sorted into the awa channels after 30 years of simulation was distributed as follows: 7% of the population was buried between 9% and 20% of total burial; 14% of the population was buried between 20% and 40% of total burial; 38% of the population was buried between 60% and 80% of total burial; 32% of the population was buried between 80% and 100% of total burial; 4% of the population was buried more than 100% of total potential burial. None of the 95% population percentile that eventually wound up in the awa channels was buried less than 9% total burial. The concentration rates of UXO in the awa channels was fairly constant during the first 20 years of the simulation, with a 36 % increase in the first 10 years (+3.6% per year), and an increase of an additional 33 % increase in the second 10 years (or +3.3% per year). This is due to the relatively uniform wave climate during the first 20 years of the simulation, with a handful of slightly higher wave energy events occurring during the first 10 years (cf. Figure 34). As the population on the reef platform became depleted in the last ten years of the simulation, concentration rates of UXO in the awa channels slowed to only 20%, or +2.0% per year, despite the occurrence of the extreme event wave from Hurricane Earl in the final year of the 30-year long simulation. Had the Hurricane Earl event occurred early in the simulation, the concentration rates of UXO in the awa-channels would probably have been initially much greater. Thus the wave climate history is a controlling mechanism of concentration in the awa-cell UXO sorting mechanism.

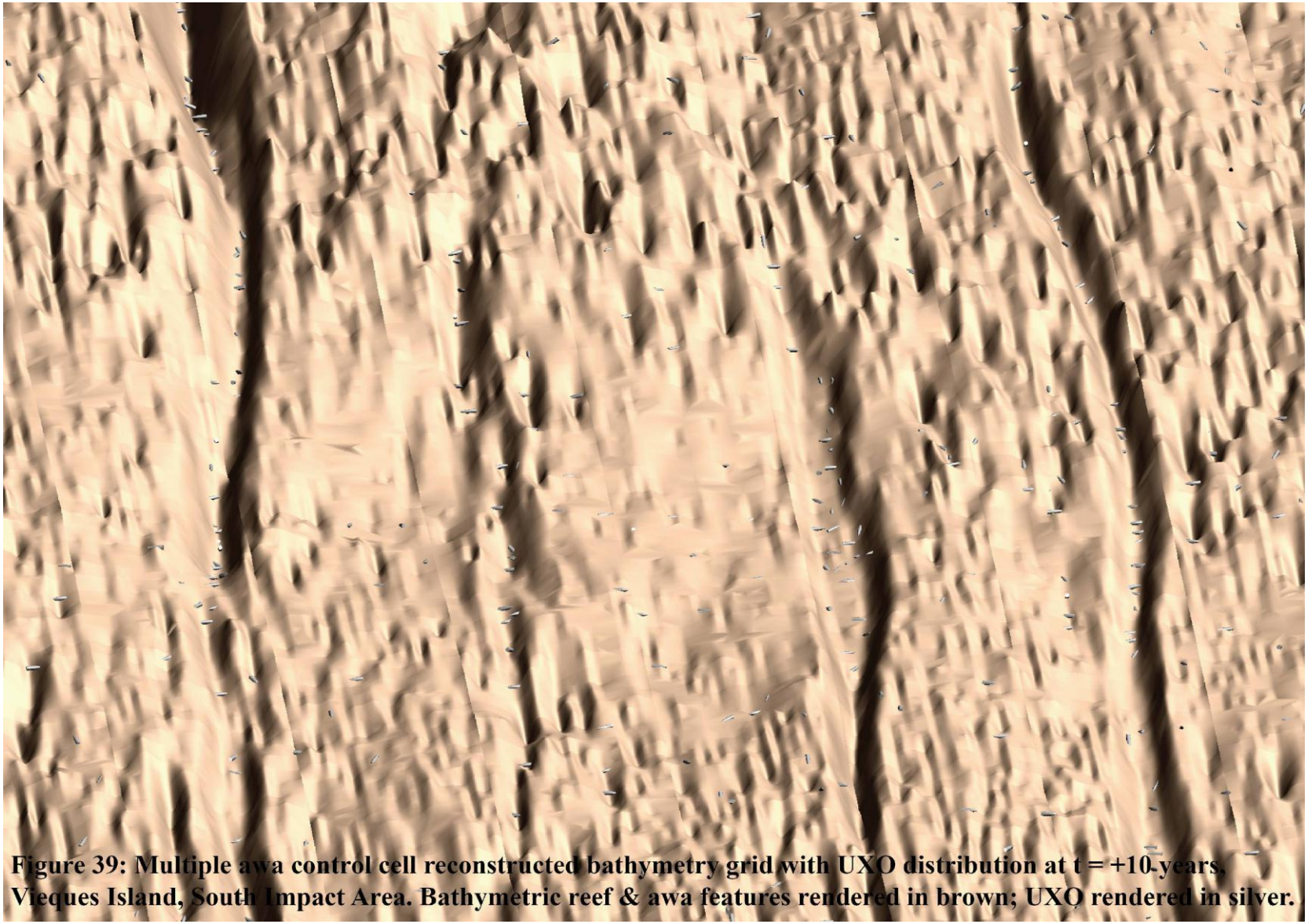

Figure 39: Multiple awa control cell reconstructed bathymetry grid with UXO distribution at t = +10 years, Vieques Island, South Impact Area. Bathymetric reef & awa features rendered in brown; UXO rendered in silver.

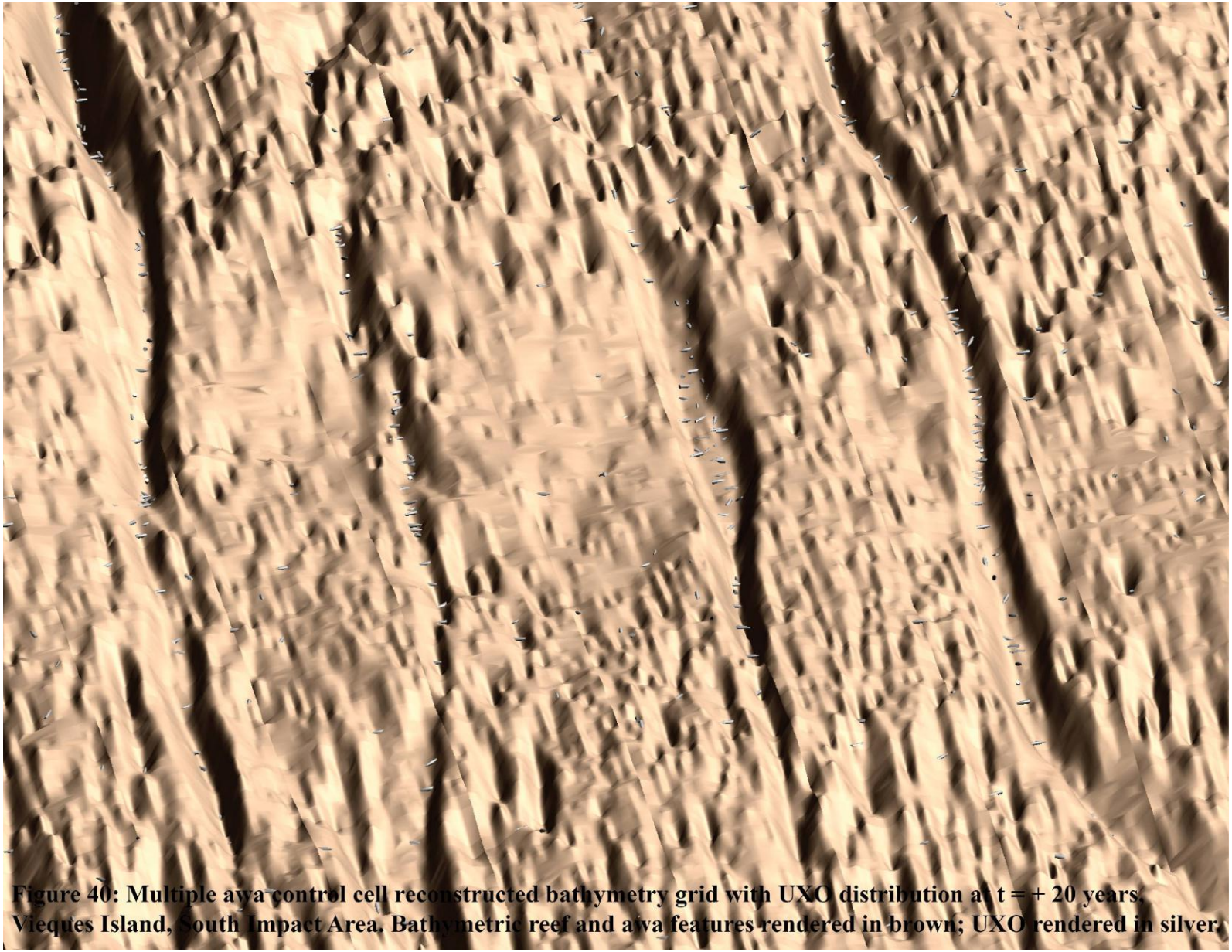

Figure 40: Multiple awa control cell reconstructed bathymetry grid with UXO distribution at t = + 20 years, Vieques Island, South Impact Area. Bathymetric reef and awa features rendered in brown; UXO rendered in silver.

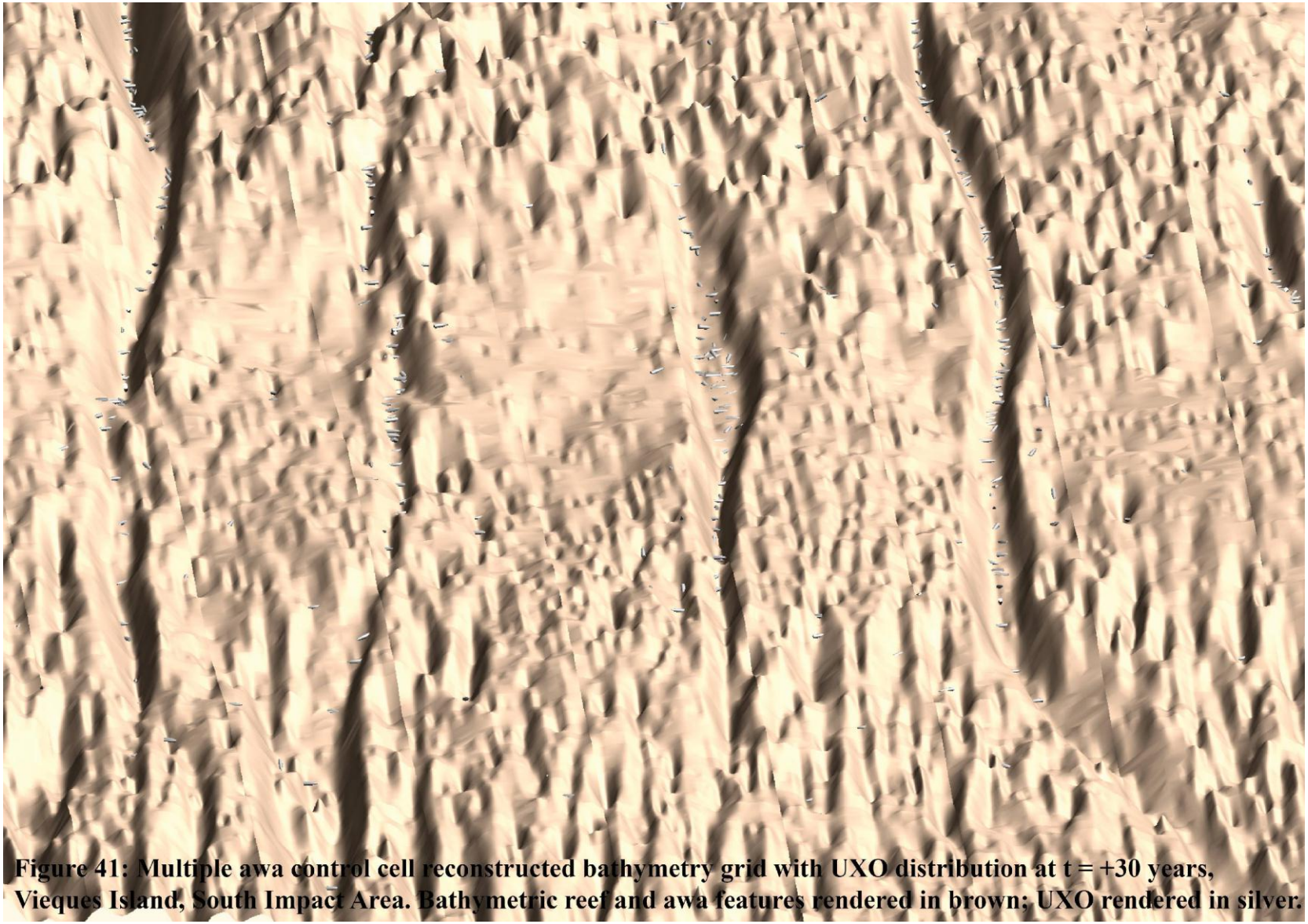

Figure 41: Multiple awa control cell reconstructed bathymetry grid with UXO distribution at t = +30 years, Vieques Island, South Impact Area. Bathymetric reef and awa features rendered in brown; UXO rendered in silver.

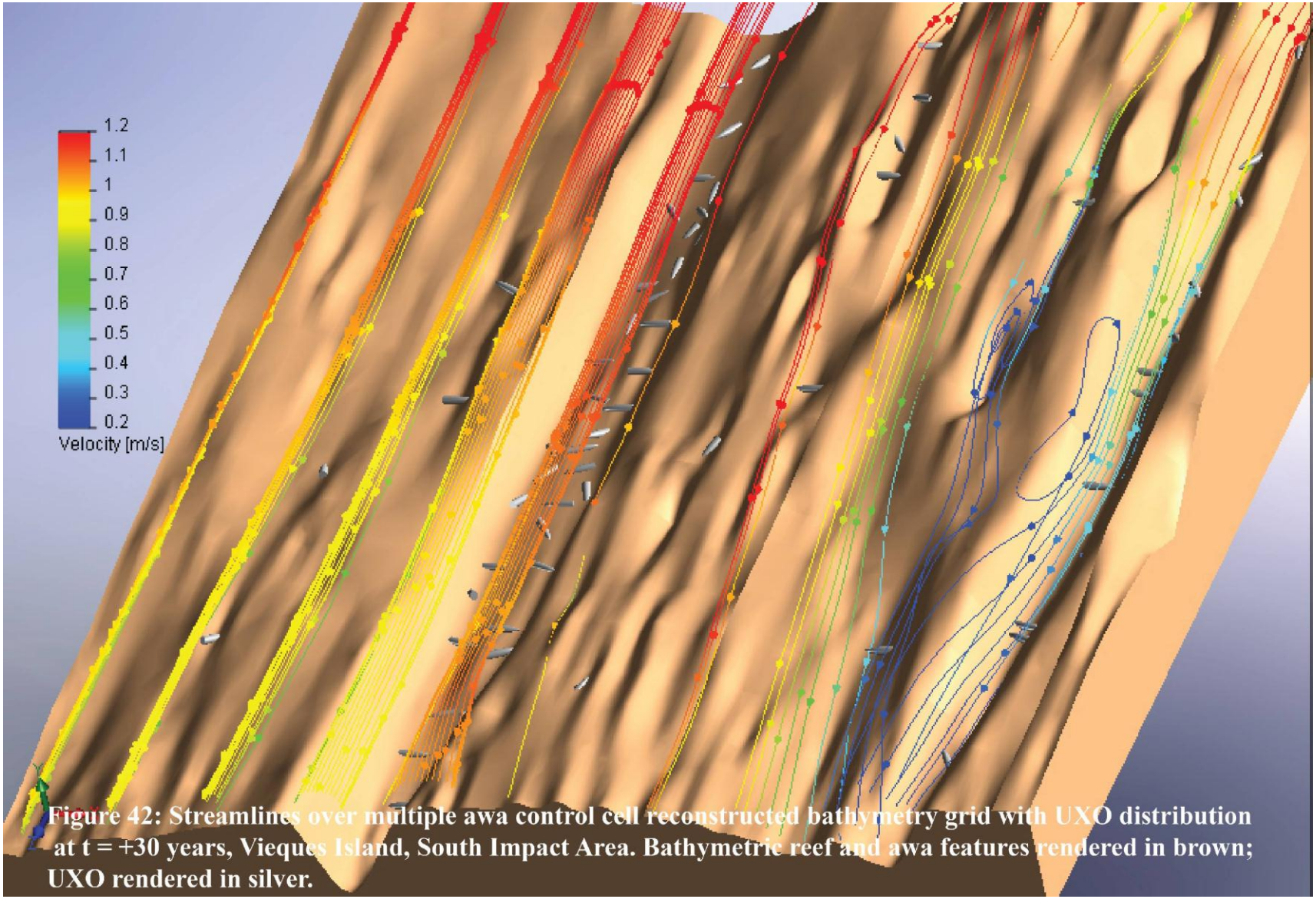

Figure 42: Streamlines over multiple awa control cell reconstructed bathymetry grid with UXO distribution at t = +30 years, Vieques Island, South Impact Area. Bathymetric reef and awa features rendered in brown; UXO rendered in silver.

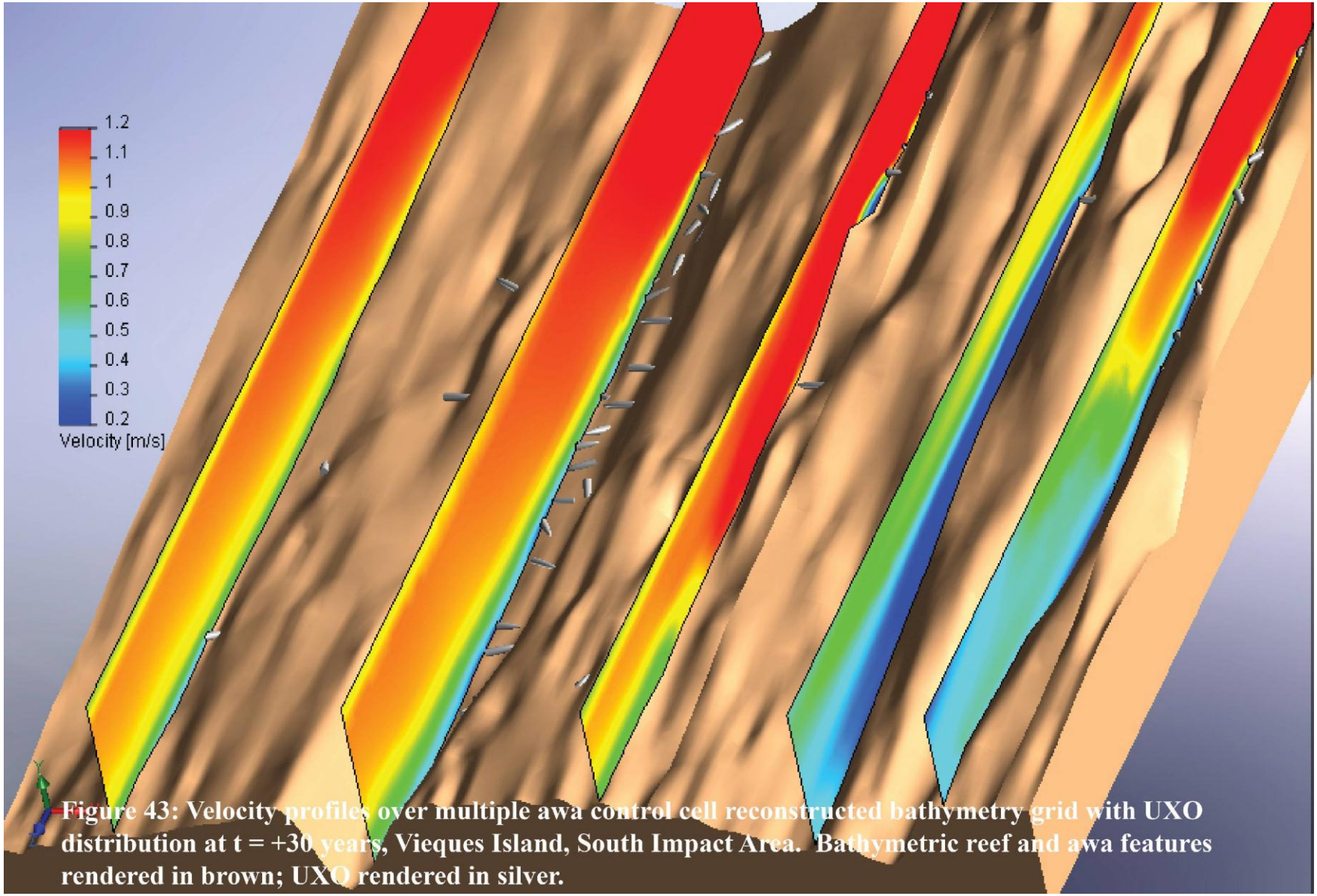

Figure 43: Velocity profiles over multiple awa control cell reconstructed bathymetry grid with UXO distribution at t = +30 years, Vieques Island, South Impact Area. Bathymetric reef and awa features rendered in brown; UXO rendered in silver.

There are several notable features in the velocity field over the concentrated UXO population at the end of the 30-year long simulation. Figure 42 shows similar bathymetric divergences and large scale eddying still exist with the final UXO population state, occurring over portions of awa channels having either expansion or contraction sections or which exhibit longshore turning in the axis of the channel. But, in Figure 43, velocity shadowing from near-bottom flow separation over the UXO in the awa channels has intensified. As UXO fall into and accumulate in the awa channels, their presences increase the bottom roughness of the channel, forming a thick bottom boundary layer that isolates UXO in the channel from the higher shear stresses in the stronger flow above that bottom boundary layer.

There is one additional mechanism that drives the sorting mechanism by increasing mobility of UXO on the reef platform and reducing their mobility in the awa channels. That mechanism is due to the differences in rolling resistance for UXO on the reef platform vs. those in the awa channels. In the awa channels, onset of motion and migration is constrained by partial burial (cf. Figure 20 a & b). As a result there is resistance to motion by the gravitational and granular force moments in Figure 6c associated with the burial depth. These rolling resistance forces require additional drag and added mass forces from the fluid motion to both raise the UXO out of its scour hole and then push it against the granular shearing forces and dispersive pressures of the sedimentary bed. However, for UXO perched on the reef platform, there are no such rolling resistance forces because there is no burial, as the UXO rests on hard lithofied substrate. Without burial, the fluid motion is able to get under the UXO, as shown in Figure 44, that produce lift forces, and consequently larger fluid dynamic drag associated with those lift forces (induced drag). (The induced drag is associated with the complex vortex structure in the lower panel of Figure 44). With no rolling resistance and enhanced fluid dynamic forces, UXO becomes more mobile on hard substrate such as the reef platform. This enhanced mobility on hard substrate also allows the UXO to migrate under the influence of even the most mild slope gradients. Figure 45 shows an awa-cell upgraded MM simulation of a UXO migration pathway following the slope gradients from the reef platform to the bottom of the awa channel. While a rolling cone would roll in a closed circle on a flat plane surface, a paraboloid of revolution such as a UXO will roll in a series J-shaped trajectories directed down-slope, with each J-shaped trajectory (numbered 1-8 in Figure 45) resembling elliptic cycloids of varying eccentricity depending on the local slope (Jenkins and Inman, 2006). This rolling behavior was observed in the field as reported in Wilson and Jenkins (2005). Lithification effects acting to cement UXO in place on the reef platform (as illustrated in Figure 30b) were not explicitly treated by the model physics herein. However, the presence of reef debris on the beach after major storms such as Hurricane Earl suggests that extreme events can dislodge lithofied objects and render them mobile during subsequent forcing events.

We have tested and proved the hypothesis (through long-term, extreme-event simulations) that at biogenic reef environments like Vieques Island South Impact Area the UXO will eventually concentrate in the reef awa channels. This has important cost savings and remediation planning implications. When concentrated over time in the awa channels, UXO are amenable to recovery by conventional sand dredging methods. Also, it is generally infeasible to search 100% of a known underwater UXO field with 100% probability of detection using present platform and sensor technology. Therefore, it would appear advantageous and cost effective to integrate these models at the outset of a survey with detection systems to guide those assets into the most problematic areas of a given underwater UXO field. By using models to develop an initial Wide

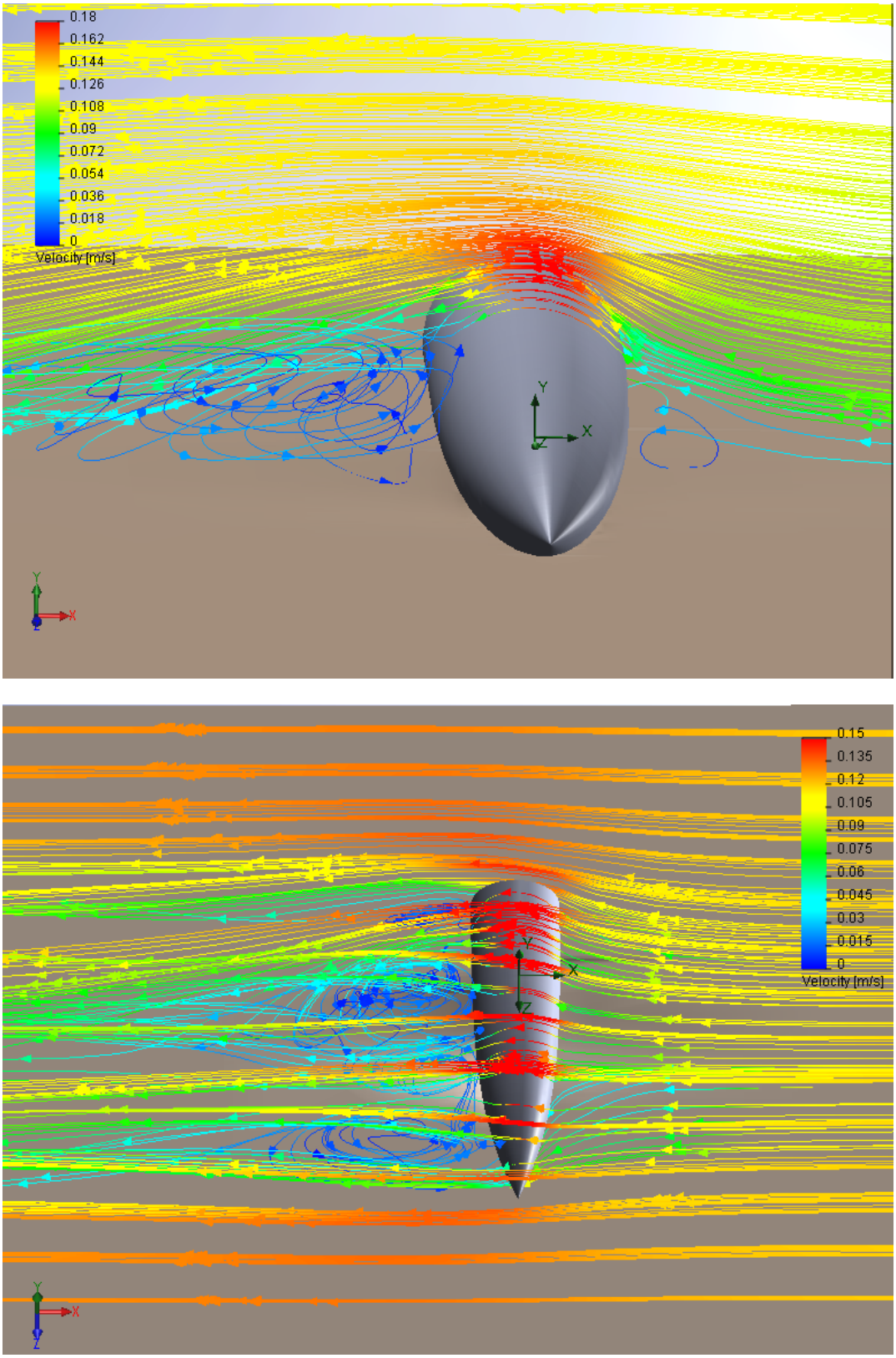

Figure 44: Upgraded MM simulation of local flow field around a UXO resting on hard substrate with no burial.

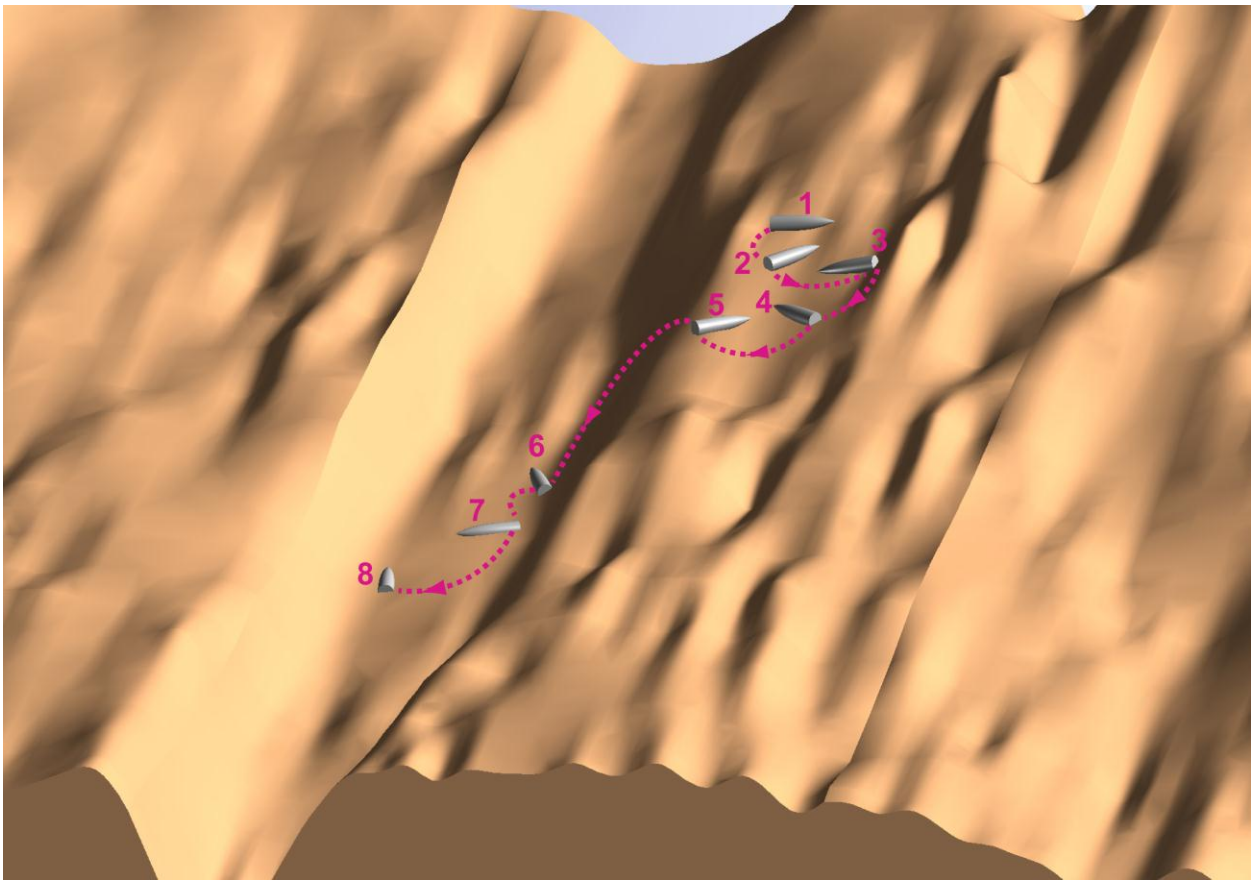

Figure 45: Mechanics of UXO Downslope Migration Progression. Bathymetric reef and awa features rendered in brown; UXO rendered in silver.

Area Assessment (WAA), that subdivides a UXO field into stable and unstable areas, one can avoid wasting unproductive deployment of detection resources in areas where UXO remain a non-factor in a state of permanent entombment beneath a stable seabed.

Predictive fate and transport models can be used to conduct an analysis of the risk and cost impact of UXO at a coastal site. Given an area of UXO locations and the required input data for one model predictions, the model output can be used to clearly define: a) areas outside of human contact and b) areas where UXO are fully stabilized and pose little risk to humans. Further consideration of the risks presented by the UXO can lead range management to make recommendations for site remediation and assessment of the hazard presented to humans and wildlife. There are substantial benefits to remediation planners that can be obtained from using these models to:

- Determine (and minimize) the scope of any required remediation efforts, minimize both survey and removal efforts, and thus realize potential savings of millions of dollars.
- Ensure that any remediation effort covers enough distance from protected sites that UXO will not move back into areas of concern (to avoid recurring clean-up efforts)
- Aid in planning the sampling survey by predicting (a) the conditions under which the most UXO would be unburied (visible) and (b) the effective *half-life of the survey data*. This predictive capability enables survey efforts or remediation efforts to be scheduled, with respect to making a determination of how long UXO will remain where they are

found. Often considerable mobilization time is required for UXO clearance efforts. Post survey model predictions can provide guidance to remediation planners of the effects of intervening storms on already located UXO positions during the period between UXO surveys and site mobilization of clearance assets.

- Provide an inexpensive, rapidly implemented method of demonstrating good-faith effort to assess risk to public health from UXO.

10.0 REFERENCES

Almquist, B, et al., 2007, *"Final Report Specialist Team for Sea Mine Burial Expert System"*, Maritime Capability Group 3 (MCC/3), NATO.

Bagnold, R.A., 1956, "The flow of cohesionless grains in fluids, Philos. Trans. R. Soc. London Ser. A, 249(964), 235–297.

Bagnold, R.A., 1963, "*Mechanics of Marine Sedimentation"* in The Sea, v. 3, The Earth Beneath the Sea, edited by M.N. Hill, p. 507-528, Wiley Interscience, New York, London, 963 pp.

Connor, J.J. and J. D. Wang, 1973, *"Finite element modeling of two-dimensional hydrodynamic circulation"*, MIT Technical Report #MITSG 74-4, p. 1-57.

R. A. Dalrymple, J. T. Kirby, and P. A. Hwang, 1984, "Wave diffraction due to areas of energy dissipation", J. Waterway Port, Coast, and Ocean Engineering., vol. 110, p. 67-79.

DeVisser, A., 2004, *"Environmental Security Technology Certification Program (ESTCP) Demonstration Plan 200417 Predicting the Mobility and Burial of Underwater Unexploded Ordnance (UXO) Using the Modified VORTEX Model",* Technical Report.

Elmore, P.A., M.D. Richardson, and C.T. Friedrichs, 2005, *"A model for predicting scour shows promise toward forecasting mine burial in sandy bottoms",* Sea Technology, 46(3), p. 10-12.

Fermi, E., 1936, *Thermodynamics*, Dover, New York.

Friedrichs, C.T., 2001, *"A review of the present knowledge of mine burial processes"*, Report to Office of Naval Research Coastal Geosciences Program, ONR Code 322, Award N00014-01-1-0169, 44 pp.

Friedrichs, C.T., 2007, *"Reformulation of mine scour equations using observations from MBP field sites"*, Report to Office of Naval Research Coastal Geosciences Program, ONR Code 322, Award N00014-05-1-0112, 9 pp.

Friedrichs, C.T., 2011, *"Simple Parameterized Models for Predicting Mobility, Burial and Re-exposure of Underwater Munitions",* SERDP pre-proposal #12 MR02-0024, 7 pp.

Gallagher, E. L., S. Elgar, and R. T. Guza (1998), Observations of sand bar evolution on a natural beach, *J. Geophys. Res.*, *103*(C2), 3203–3215.

Garrood, D., 2008, *"UXO Mobility Model Users' Manual",* NAVFAC ESC Technical Report, Revision 8.4, ESTCP 200417, 79 pp.

Inman, D. L., and R. Dolan, 1989, *"The Outer Banks of North Carolina: Budget of Sediment and Inlet Dynamics Along a Migrating Barrier System"*, J. Coastal Research, vol. 5, n. 2, p. 193–237.

Inman, D. L. (1987), Accretion and erosion waves on beaches, *Shore & Beach*, *55*(3/4), 61–66.

Inman, D., L., and S. A. Jenkins, "Scour and Burial of Bottom Mines, A Primer for Fleet Use," Scripps Institution of Oceanography: Univ. of California, San Diego, SIO Reference Series 02-8, 2002. Available: http://repositories.cdlib.org/sio/reference/02-8/

Inman, D., L. and S. A. Jenkins, "Accretion and Erosion Waves on Beaches," in *Encyclopedia of Coastal Science*, M. Schwartz, Ed. Dordrecht, Netherlands: Kluwer Academic Publishers, 2005, pp. 1–4. Available: http://repositories.cdlib.org/sio/cmg/6/

Jenkins, S.A. and J. Wasyl, 1990, *"Resuspension of estuarial fine sediments by tethered wings"*, J. Coastal Res., vol. 6, n. 4, p. 961-980.

Jenkins, S.A. and D.L. Inman, 2002,*"Model for Mine Scour and Burial: An Illustrated Abstract with Technical Appendix*", University of California, San Diego, Scripps Institution of Oceanography, SIO Reference Series 02-2, 42 pp.

Jenkins, S.A. and J. Wasyl, 2005, *"Model for Prediction and Updates For UXO Transport during MMFT 1 & 2, Ocean Shores, WA"*, submitted to Sound and Sea Technologies, 170 pp.

Jenkins, S.A. and D.L. Inman, 2006, *"Thermodynamic solutions for equilibrium beach profiles"*, J. Geophysical Res., 111, C02003, doi:110.1029/2005JC002899.

Jenkins S. A. , D.L. Inman, M. D. Richardson, T. F. Wever, and J. Wasyl , 2007, *"Scour and Burial Mechanics of Objects in the Nearshore"*, IEEE J. Ocean Eng, vol. 32, no. 1, p. 78-90.

Johnson, C.J., Sugiyama, B., Wild, B., Lin, S. and A. Pedersen, 2002, *"Environmental effects of underwater ordinance",* Navy Internal Tech Report, SPAWAR, San Diego Code D362 and NAVFAC ESC Point Hueneme, EV45, 302 pp.

Kirby, J.T. 1986, *"Higher-order approximations in the parabolic equation method for water-waves"*, J. Geophysical Res., vol. 91, n. C1, p. 933–952.

NFESC, (2008), "Applications Guidance Document: Predicting the Mobility and Burial of Underwater Unexploded Ordnance (UXO) using the *UXO Mobility Model*," Naval Facilities Engineering Service Center, Ocean Engineering Division, OP51 Port Hueneme CA , ESTCP Project 200417, Contract N62473-06-D-3005, 82pp

Rennie, S. and A. Brandt, 2002, *"An Expert Systems Approach for predicting Mine Burial"*, Fifth International symposium on Technology and the Mine Problem. Naval Post Graduate School, Monterey.

Rennie, S. E., Brandt, A. and Plant, N., 2007, *"A Probabilistic Expert System Approach for Sea Mine Burial Prediction",* IEEE J. of Oceanic Eng., 32(1), p. 260-272.

Richardson, M.D., E.F. Braithwaite, S. Griffin, J. Bradley, C.T. Friedrichs, and A.C. Trembanis, 2004, *"Real-time characterization of mine scour burial at the Martha's Vineyard Coastal Observatory",* Proceedings of the 6th International Symposium on Technology and the Mine Problem, Naval Postgraduate School, Monterey, Ca, 6 pp.

Trembanis, A.C., C.T. Friedrichs, M.D. Richardson, P. Traykovski, P.A. Howd, P.A. Elmore, and T. Wever, 2007, *"Predicting seabed burial of cylinders by wave-induced scour: application to the sandy inner shelf off Florida and Massachusetts"*, IEEE Journal of Oceanic Engineering, vol. 32, p. 167-183.

Wilson, J.V. and S.A. Jenkins, 2002, ***"****VORTEX / Lattice mine burial model modification for predicting transport of munitions of concern (MEC)",* submitted to NAVFAC ESC, Code ESC51, 4 pp.

Wilson, J. V., 2004, *"UXO Migration Field Test Point Mugu Lagrangian Drifters, final report",* Sound and Sea Technology, Report 04-13.

Wilson, J.V. and S.A. Jenkins, 2005, *"UXO Measurement Method Field Tests (MMFT1&2) and Mobility Model Modification, final report",* Sound & Sea Technology Report 05-07.

Wilson, J.V.; DeVisser, A; Sugiyama, B., 2008a, *"(ESTCP) 200417 Predicting the Mobility and Burial of Underwater Unexploded Ordnance (UXO) Using the UXO Mobility Model, field test report, (FRF Duck, NC)"*, NAVFAC ESC Technical Report.

Wilson, J.V.; DeVisser, A; Sugiyama, B., 2008b, *"(ESTCP) 200417 Predicting the Mobility and Burial of Underwater Unexploded Ordnance (UXO) Using the UXO Mobility Model, field test report (PMRF Barking Sands, Kauai, Hawaii)",* NAVFAC ESC Technical Report.

Wilson, J.V.; DeVisser, A; Sugiyama, B., 2008c, *"(ESTCP) 200417 Predicting the Mobility and Burial of Underwater Unexploded Ordnance (UXO) Using the UXO Mobility Model, final report",* NAVFAC ESC Technical Report.

Wilson, J.V.; DeVisser, A; Sugiyama, B., 2008d, *"(ESTCP) 200417 Predicting the Mobility and Burial of Underwater Unexploded Ordnance (UXO) Using the UXO Mobility Model, cost & performance report",* NAVFAC ESC Technical Report.

Wilson, J.V.; DeVisser, A; Sugiyama, B.,, 2008e, "*TO-2008-09-16-T061, Example Applications Analysis Using the UXO Mobility Model: Lake Erie Impact Range Analysis",* NAVFAC ESC Technical Report, 53 pp.

Wolfson, M.L., D.F. Naar, P.A. Howd, S.D. Locker, B.T. Donahue, C.T. Friedrichs, A.C. Trembanis, M.D. Richardson, and T. Wever, 2007. Comparing predicted mine scour and burial to multibeam observations offshore of Clearwater, Florida. IEEE Journal of Oceanic Engineering, 32: 103-118.

APPENDICES

APPENDIX A: HEALTH AND SAFETY PLAN (HASP)

No field work of any kind will be required by this demonstration plan. The software modification / validation will use data collected at PRMF, Barking Sands, Kauai, Hawaii, 2007.

APPENDIX B: POINTS OF CONTACT

POINT OF CONTACT Name	ORGANIZATION Name Address	Phone Fax E-mail	Role in Project
Gerald D' Spain, Ph. D.	Marine Physical Laboratory, Scripps Institution of Oceanography, 291 Rosecrans Street, San Diego, CA 92106	(858) 534-5517 (858) 534-5255 gdspain@ucsd.edu	Principal Scientist
Scott A. Jenkins, Ph. D.	Marine Physical Laboratory, Scripps Institution of Oceanography, 291 Rosecrans Street, San Diego, CA 92106	(858) 822-4075 (858) 534-5255 sjenkins@ucsd.edu	Principal Research Engineer
Joseph Wasyl	Marine Physical Laboratory, Scripps Institution of Oceanography, 291 Rosecrans Street, San Diego, CA 92106	(858) 534-5809 (858) 534-5255 jwasyl@ucsd.edu	Numerical Scientist Programmer

ADDITIONAL APPENDICES